

UNIVERSITY OF NAPLES FEDERICO II

Department of Structures for Engineering and Architecture

PH.D. PROGRAMME IN INDUSTRIAL PRODUCT AND PROCESS

ENGINEERING

XXXIV CYCLE



MARTINA SCALVENZI

PH.D. THESIS

**Role of material properties and retrofitting
systems in structural robustness of reinforced
concrete frame buildings**

TUTOR PROF. FULVIO PARISI

2021

ABSTRACT

Catastrophic consequences of progressive collapse of structures, particularly under extreme events, have produced a growing interest in structural robustness by different actors of construction industry (*e.g.*, regulators, designers, construction companies, facility managers, homeland security agencies). Research programmes have been funded to simulate progressive collapse and to quantify structural robustness, both experimentally and theoretically. Significant research outcomes have thus allowed the development of advanced simulation methods for structural response analysis under abnormal loading, as well as different methods for robustness quantification and design, which are presented in several guidelines at both national and international levels. Nonetheless, a number of open issues still need to be deeply investigated, particularly regarding existing structures that were designed only to gravity loads according to past technical codes, design procedures, and practice rules.

This PhD thesis deals with progressive collapse performance and structural robustness of existing reinforced concrete (RC) frame buildings, which are a significant fraction of worldwide built heritage. Special emphasis is given on the role of mechanical properties of structural materials used for construction and retrofitting of RC frame buildings. Both cast-in-place and precast buildings are considered, simulating their large-displacement nonlinear response to both single- and multi-column loss scenarios. Structural response analysis was carried out using incremental static (pushdown) analysis and incremental dynamic analysis (IDA). Among direct approaches, the alternate load path (ALP) analysis method was extensively implemented both deterministically and probabilistically, in the latter case by modelling and propagating uncertainties in material properties that are often an important uncertainty source in existing buildings. Possible catastrophic effects of improper structural retrofitting operations were also addressed, to provide a contribution to knowledge on robustness during retrofitting.

The PhD thesis consists of seven chapters, starting from Chapter 1 that provides the objectives of this study and the outline of the thesis.

Chapter 2 provides a state-of-the-art review to support understanding of methodologies implemented in this study. After concepts regarding extreme actions, progressive and disproportionate collapses, and structural robustness are delineated, robustness-oriented design methods and progressive collapse simulation are briefly reviewed. In the final part of Chapter 2, the role of robustness in disaster resilience of structures, infrastructures and urban systems is discussed.

In Chapter 3, the role of material properties in progressive collapse resistance and robustness of cast-in-place RC frame buildings is investigated through sensitivity analysis, in order to identify the most influencing parameters. The reduction of yield strength of steel reinforcement and longitudinal reinforcement ratio of primary beams is found to have a fatal effect consisting in the progressive collapse of the framed structure. The same result comes out when the span length of primary and secondary beams is increased. The material property that least influences the progressive collapse resistance is the compressive strength of concrete. The sensitivity of the load capacity corresponding to five limit states defined for progressive collapse is also investigated in this study and all nonlinear analyses evidence a sequential occurrence of the performance limit states proposed. Tornado diagrams clearly indicate that span length of primary and secondary beams and yield strength of steel reinforcement are the capacity model properties that mostly influence the limit state load capacity. In this chapter the progressive collapse capacity of European RC framed buildings through a set of nonlinear dynamic analyses, considering multiple-column loss scenarios and alternative removal times is also investigated. This choice is due to the presence of many studies that have focused their attention on progressive collapse of building structures subjected to notional removal of single components at the ground floor. It is also noteworthy that multiple columns can be heavily damaged or totally destroyed in different time instants, for instance under events like impact of heavy objects on several parts of the structure or bomb detonation occurring at different distances from column. This study highlights that the failure removal of consecutive columns produce the lowest levels of load capacity against progressive collapse. In addition, under a scenario that involves first a corner column and afterwards a nearby column, at a time one order of magnitude higher than that of the first column, the maximum reduction in peak load is obtained.

Chapter 4 deals with the ability of existing reinforced concrete structures to prevent progressive collapse during structural retrofitting. The novelty of this study lies in the nonlinear analysis of a real existing building structure that suffered a partial progressive collapse during structural retrofitting interventions. Indeed, the majority of studies investigated the structure during its operation, assessing the progressive collapse capacity, robustness, vulnerability and risk under either abnormal load. It is worth noting that other stages of the building lifetime such as construction and retrofitting can notably undermine structural safety, frequently resulting in either the need for evacuation/demolition or even progressive collapse with huge impact on economy and people. Pushdown analysis with displacement control was performed on two different models of the structure, evidencing that the removal of concrete cover, (that is a typical retrofit measure) from an internal column results in a collapse capacity drop that is greater than that predicted for the same scenario involving a perimeter or corner column. The progressive collapse capacity of the structure reaches its maximum reduction in the case of simultaneous soil excavation at the base of three columns.

Linking to structural retrofitting, chapter 5 presents a numerical study on the impact that carbon fibre reinforced polymers (CFRPs) may have on the structural robustness of low-rise RC frame buildings. The sensitivity of progressive collapse resistance to structural and material properties, is evaluated through parametric analysis. This multi-hazard assessment study outlines that robustness enhancement can be effectively driven by seismic retrofitting based on CFRP strengthening, highlighting the importance of multi-hazard approaches for design, assessment and retrofit of structures. Significant beneficial effects of local seismic strengthening on robustness (in terms of load bearing capacity and, in some cases, inelastic deformation capacity) can result from 10%–20% amplifications in shear strength at beam ends.

Structural robustness of typical European precast concrete frame buildings is probabilistically assessed through a fragility analysis procedure in Chapter 6. Fragility analysis is performed to propagate the uncertainty in material properties of beam-column connections. The estimation of progressive collapse capacity is characterized by low levels of uncertainty, even degenerating into a deterministically predicted value of load capacity associated with the attainment of slight damage to the earthquake-resistant

building. Seismic detailing increases the median load factor at collapse, demonstrating some effectiveness in the mitigation of progressive collapse risk.

Based on the outcomes of this study, further studies in the field might be carried out to investigate the following open issues: (i) the beneficial contribution by secondary beams, floor systems and connections in 3D capacity models, particularly in case of precast RC buildings; (ii) the influence of aging and deterioration processes, as well as the extension of this kind of safety assessments in case of historical constructions that are often subjected to restoration and structural retrofitting; and (iii) the impact of other seismic retrofit methods (e.g., steel braces, RC walls, steel caging) on progressive collapse resistance.

Keywords: Progressive collapse, structural robustness, reinforced concrete buildings, incremental dynamic analysis, pushdown analysis, probabilistic assessment, structural retrofitting

ACKNOWLEDGEMENTS

TABLE OF CONTENTS

ABSTRACT	III
ACKNOWLEDGEMENTS	VII
TABLE OF CONTENTS	IX
LIST OF TABLES	XII
LIST OF FIGURES	XIV
CHAPTER 1 – INTRODUCTION	19
1.1. OBJECTIVES OF THE STUDY	19
1.2. OUTLINE OF THE THESIS	21
CHAPTER 2– STATE-OF-THE-ART REVIEW	23
2.1 EXTREME ACTIONS ON STRUCTURES	23
2.2 PROGRESSIVE AND DISPROPORTIONATE COLLAPSES.....	24
2.3 DEFINITION OF STRUCTURAL ROBUSTNESS.....	29
2.3.1 ROBUSTNESS IN EUROCODES.....	31
2.3.2 ROBUSTNESS IN NATIONAL BUILDING CODES	31
2.3.3 ROBUSTNESS WITHIN INTERNATIONAL GUIDELINES.....	32
2.4 DESIGN FOR ROBUSTNESS	33
2.4.1 INDIRECT DESIGN METHODS	34
2.4.2 DIRECT DESIGN METHODS	35
2.4.2.1 THREAT-DEPENDENT AND THREAT-INDEPENDENT APPROACHES.....	36
2.4.2.2 PROBABILISTIC VERSUS SEMI-PROBABILISTIC APPROACHES	37
2.5 ROBUSTNESS QUANTIFICATION	38
2.5.1 RESISTING MECHANISMS IN REINFORCED CONCRETE STRUCTURES.....	38
2.5.2 LOAD MODELLING	41
2.5.3 STRUCTURAL MODELLING	43
2.5.4 STRUCTURAL RESPONSE ANALYSIS METHODS	45
2.5.5 ROBUSTNESS MEASURES	47
2.6 FROM ROBUSTNESS TO DISASTER RESILIENCE	48
2.6.1 RESILIENCE OF URBAN SYSTEMS	49
2.6.2 RESILIENCE OF INFRASTRUCTURES AND STRUCTURAL SYSTEMS	53

CHAPTER 3 – INFLUENCE OF MATERIAL PROPERTIES ON PROGRESSIVE COLLAPSE RESISTANCE OF RC BUILDINGS UNDER DIFFERENT COLUMN LOSS SCENARIOS56

3.1 CHARACTERISTICS, MODELLING AND ANALYSIS OF CASE-STUDY STRUCTURE..... 56

3.2 CAPACITY AND LOAD MODELLING 57

3.3 COMPUTATIONAL PROCEDURE FOR SINGLE-COLUMN REMOVAL SCENARIOS 59

3.3.1 SENSITIVITY OF PROGRESSIVE COLLAPSE MEASURES TO CAPACITY MODELLING PROPERTIES..... 60

3.3.1.1 INFLUENCE OF ULTIMATE STEEL STRAIN 61

3.3.1.2 INFLUENCE OF MATERIAL STRENGTHS AND GEOMETRIC PROPERTIES 68

3.4 PROPOSAL OF PERFORMANCE LIMIT STATES FOR PROGRESSIVE COLLAPSE ANALYSIS ... 69

3.4.1 DEFINITION OF PERFORMANCE LIMIT STATES 70

3.4.2 SENSITIVITY ANALYSIS OF LIMIT STATE CAPACITY 72

3.5 COMPUTATIONAL PROCEDURE FOR MULTIPLE-COLUMN REMOVAL SCENARIOS 77

3.5.1 STRUCTURAL RESPONSE TO SIMULTANEOUS REMOVAL SCENARIOS..... 80

3.5.2 STRUCTURAL RESPONSE TO SEQUENTIAL REMOVAL SCENARIOS..... 84

CHAPTER 4 – PROGRESSIVE COLLAPSE RESISTANCE OF A REAL RC BUILDING COLLAPSED DURING STRUCTURAL RETROFITTING OPERATIONS97

4.1 PROBLEM STATEMENT..... 97

4.2 DESCRIPTION OF CASE-STUDY BUILDING 98

4.3 METHODOLOGY OF THE STUDY 101

4.3.1 DEFINITION OF STRUCTURAL RETROFITTING SCENARIOS 101

4.3.2 SIMULATED DESIGN PROCEDURE 103

4.4 PROGRESSIVE COLLAPSE ASSESSMENT THROUGH PUSHDOWN ANALYSIS 112

4.4.1 CAPACITY AND LOAD MODELLING CONDITIONS 112

4.4.2 SIMULATION OF RETROFITTING OPERATIONS 114

4.5 EFFECT OF STRUCTURAL RETROFITTING OPERATIONS 117

4.5.1 IMPLICATIONS OF CONCRETE COVER REMOVAL FROM GROUND-FLOOR COLUMNS.. 117

4.5.2 IMPACT OF SOIL EXCAVATION AROUND COLUMN BASES 123

CHAPTER 5 – INFLUENCE OF SEISMIC RETROFITTING WITH FRP SYSTEMS ON STRUCTURAL ROBUSTNESS: MULTI-HAZARD ANALYSIS 126

5.1 CASE-STUDY STRUCTURE AND MODELLING..... 126

5.1.1 CHARACTERISTICS AND MODELLING OF THE STRUCTURE 126

5.1.2 ASSESSMENT OF DYNAMIC AMPLIFICATION FACTOR 130

5.2 PROGRESSIVE COLLAPSE CAPACITY EVALUATION 133

5.2.1 INFLUENCE OF DESIGN LOADS AND ULTIMATE STEEL STRAIN ON PROGRESSIVE COLLAPSE CAPACITY 133

5.2.2 SHEAR SAFETY CHECKS 137

5.3 SEISMIC SAFETY ASSESSMENT 140

5.4 STRUCTURAL RETROFITTING WITH CARBON FIBRE-REINFORCED POLYMERS 145

5.4.1 DESIGN OF FRP SYSTEMS 145

5.4.2 IMPACT OF FRPS ON SEISMIC RETROFITTING AND STRUCTURAL ROBUSTNESS..... 147

5.4.3	SENSITIVITY OF JOINT SEISMIC-ROBUSTNESS PERFORMANCE TO BEAM SPAN LENGTH AND SHEAR STRENGTH OF STRENGTHENING SYSTEM	149
CHAPTER 6 – PROBABILISTIC ROBUSTNESS ASSESSMENT OF PRECAST RC BUILDINGS		155
6.1	OBJECTIVES OF THE WORK	155
6.2	CASE-STUDY STRUCTURE.....	156
6.2.1	MATERIAL AND GEOMETRIC PROPERTIES	157
6.2.2	STRUCTURAL MODELLING	161
6.2.3	BEAM-COLUMN CONNECTION MODELLING	162
6.3	DEFINITION OF PERFORMANCE LIMIT STATES	165
6.4	PROGRESSIVE COLLAPSE ANALYSIS OF PC BUILDINGS WITH MEAN VALUES OF PROPERTIES	167
6.5	FRAGILITY ANALYSIS	173
6.5.1	RANDOM VARIABLES.....	173
6.5.2	DISCUSSION OF RESULTS	174
6.5.2.1	EARTHQUAKE-RESISTANT BUILDING WITH TYPE 2 CONNECTION	174
6.5.2.2	EARTHQUAKE-RESISTANT BUILDING WITH TYPE 3 CONNECTION	175
CHAPTER 7 - CONCLUSIONS AND POTENTIAL FUTURE DEVELOPMENTS.....		177
REFERENCES.....		181

LIST OF TABLES

Table 2.1: Typical maximum values of dynamic increase factor for concrete and reinforcing steel

Table 2.2: Summary of literature review on resilience quantification [57]

Table 3.1: Mean and coefficient of variation of capacity model properties

Table 3.2: Progressive collapse measures of the case study structure under varying ultimate steel strain and column-removal scenario

Table 3.3: Sensitivity analysis results

Table 3.4: Items, variables and thresholds of performance limit states

Table 3.5: Limit state load multiplier under varying column-removal scenario

Table 3.6: Progressive collapse capacity measures for simultaneous column-loss scenarios

Table 3.7: Progressive collapse capacity measures for sequential column-loss scenarios

* **

Table 4.1: Material properties

Table 4.2: Design of beam reinforcement and evaluation of material stresses

Table 4.3: Size and steel reinforcement of columns sections

Table 4.4: Maximum load multiplier and its variations related to CCR scenarios on complete capacity model, with and without consideration of infill walls.

Table 4.5: Maximum load multiplier and its variations related to CCR scenarios on partial capacity model, with and without consideration of infill walls.

Table 4.6: Maximum load multiplier and its variations related to SE scenarios on complete capacity model, with and without consideration of infill walls.

Table 4.7: Maximum load multiplier and its variations related to SE scenarios on partial capacity model, with and without consideration of infill walls.

Table 5.1: Steel and concrete mechanical properties

Table 5.2: Demand-to-capacity ratios corresponding to the first occurrence of shear failure in structural elements for scenario A1*

Table 5.3: Demand-to-capacity ratios corresponding to the first occurrence of shear failure in structural elements for scenario A2

Table 5.4: Seismic hazard parameters for the case-study structure

Table 5.5: Beams and columns shear checks: demand-to-capacity ratios corresponding to mass profile

Table 5.6: Beams and columns shear checks: demand-to-capacity ratios corresponding to mode profile

Table 5.7: Properties of selected CFRPs

Table 5.8: Shear demand-to-capacity ratios of structural elements after retrofitting for mass profile

Table 5.9: Shear demand-to-capacity ratios of structural elements after retrofitting for mode profile

Table 5.10: Load multiplier and vertical drift values corresponding to the achievement of the first brittle failure

Table 5.11: Arrangement of CFRP along columns: plies distribution for structure levels

Table 5.12: Influence of CFRP shear strength variation on the achievement of first brittle failure

Table 6. 1: Mechanical properties of concrete, steel, and beam-column connections

Table 6.2: Nonlinear links properties for different types of beam-column connections

Table 6.3: Value of load multiplier corresponding to the achievement of PLSs under different column removal scenarios

Table 6.4: Median, dispersion and coefficient of determination of fragility curves for earthquake-resistant building with Type 2 connection

Table 6.5: Median, dispersion and coefficient of determination of fragility curves for earthquake-resistant building with Type 3 connection

LIST OF FIGURES

Figure 2.1: Categories and consequences of events

Figure 2.2: Progressive collapse examples: (a) Ronan Point (London, 1968), (b) World Trade Center (New York, 2001), (c) A.P. Murrah Federal Building (Oklahoma, 1995).

Figure 2.3: Components of disproportionate collapse risk and corresponding mitigation measures

Figure 2.4: Fragility functions of the RC framed buildings [34]

Figure 2.5: 3D RC beam-column sub assemblage

Figure 2.6: Schematic of (a) compressive arch action and (b) tensile catenary action [37]

Figure 2.7: Progressive collapse response curve of frame sub-structure

Figure 2.8: Trend of dynamic amplification factor

Figure 2.9: Load amplification under varying position of removed column

Figure 3.1: (a) Reference frame model of the case-study structure; cross sections and reinforcement arrangements of (b) beams and (c) columns

Figure 3.2: Column designation involved in single removal scenarios

Figure 3.3: Drift time histories under column-removal scenario A1: (a) $\epsilon_{su} = 4\%$, (b) $\epsilon_{su} = 10\%$, (c) $\epsilon_{su} = 20\%$

Figure 3.4: Drift time histories under column-removal scenario A2: (a) $\epsilon_{su} = 4\%$, (b) $\epsilon_{su} = 10\%$, (c) $\epsilon_{su} = 20\%$

Figure 3.5: IDA curves under varying column-removal scenario

Figure 3.6: Definition of performance limit states

Figure 3.7: Tornado diagrams for scenario A1

Figure 3.8: Tornado diagrams for scenario A2

Figure 3.9: Designation of columns and frame nodes (control points) involved multiple column removal scenarios

Figure 3.10: Flowchart of progressive collapse evaluation under multi-column loss scenarios

Figure 3.11: Drift time histories corresponding to: (a) scenario A1-A2, (b) scenario A1-A4, (c) scenario A1-A7

Figure 3.12: IDA curves corresponding to the simultaneous loss of either a corner column and an internal column or opposite corner columns

Figure 3.13: IDA curves corresponding to the simultaneous loss of two internal columns

Figure 3.14: Scenarios corresponding to different column deactivation times

Figure 3.15: IDA curves corresponding to the sequential removal scenario A1-A2, by varying control point and deactivation time

Figure 3.16: IDA curves corresponding to the sequential removal scenario A1-A3, by varying control point and deactivation time

Figure 3.17: IDA curves corresponding to the sequential removal scenario A1-A4, by varying control point and deactivation time

Figure 3.18: IDA curves corresponding to the sequential removal scenario A1-A5, by varying control point and deactivation time

Figure 3.19: IDA curves corresponding to the sequential removal scenario A1-A6, by varying control point and deactivation time

Figure 3.20: IDA curves corresponding to the sequential removal scenario A1-A7, by varying control point and deactivation time

Figure 3.21: Labelling of model elements

Figure 3.22: Maximum tensile strain/stress in steel fibres and minimum compressive strain/stress in concrete fibres under varying time and drift corresponding to the scenario A1-A2: strains in model elements: (a) B8-9a and B8-9b, (b) B9-10a and B9-10b

Figure 3.23: Maximum tensile strain/stress in steel fibres and minimum compressive strain/stress in concrete fibres under varying time and drift corresponding to the scenario A1-A2: stresses in model elements: (a) B8-9a and B8-9b, (b) B9-10a and B9-10b.

Figure 3.24: Maximum tensile strain/stress in steel fibres and minimum compressive strain/stress in concrete fibres under varying time and drift corresponding to the scenario A1-A4: (a) strains in model elements: (a) B8-9a and B8-9b, (b) B9-10a and B9-10b

Figure 3.25: Maximum tensile strain/stress in steel fibres and minimum compressive strain/stress in concrete fibres under varying time and drift corresponding to the scenario A1-A4: stresses in model elements: (a) B8-9a and B8-9b, (b) B9-10a and B9-10b.

Figure 3.26: Maximum tensile strain/stress in steel fibres and minimum compressive strain/stress in concrete fibres under varying time and drift corresponding to the scenario A1-A7 (model elements B8-9a and B8-9b): (a) strains; (b) stresses

Figure 4.1: Building corner (a) after collapse and (b) after reconstruction (black hatching indicates the portion built after the collapse)

Figure 4.2: Steel rebar details in a ground-floor column specimen extracted from the residual structure.

Figure 4.3: Corner building after debris removal: (a) overlapped floor slabs, ejected columns and staircase; (b) detail of ground-floor columns subjected to concrete cover removal and soil excavation at the base

Figure 4.4: Typical floor plan of case-study structure with identification of span length of beams, spanning direction of floor joist slabs and staircases (dimensions in m). [In red the building corner that collapsed during retrofitting interventions].

Figure 4.5: Definition of CCR and SE scenarios for progressive collapse analysis.

Figure 4.6: Steel use percentages for different categories as the year of construction [99]

Figure 4.7: Labelling of beam-column joints

Figure 4.8: Longitudinal sections of beams with longitudinal and transverse reinforcement: (a) x-direction and (b) y-direction (dimensions in mm)

Figure 4.9: Beam cross sections (dimensions in mm)

Figure 4.10: Columns sections (dimensions in mm)

Figure 4.11: Complete capacity model (CM) of the structure: (a) frontal view, (b) lateral view. (In red the building corner that suffered collapse).

Figure 4.12: Demand-to-capacity ratios of columns in terms of axial loading produced by gravity loads: (a) model without infill walls, (b) model with infill walls

Figure 4.13: Pushdown capacity curves of complete capacity model under CCR scenarios: (a) with infill walls; (b) without infill walls.

Figure 4.14: Pushdown capacity curves of partial capacity model under CCR scenarios: (a) with infill walls; (b) without infill walls.

Figure 4.15: Computational time of complete and partial capacity models with infill walls

Figure 4.16: Pushdown capacity curves of complete and partial capacity models under SE scenarios: (a) with infill walls; (b) without infill walls.

Figure 5.1: Elevation view of case-study structure

Figure 5.2 : Constitutive model: (a) Kent-Scott-Park constitutive model, (b) uniaxial bilinear model

Figure 5.3 : Discretization of structural elements

Figure 5.4 : Comparison between pushdown analysis (PDA) and incremental dynamic analysis (IDA): (a) Scenario A1; (b) Scenario A2

Figure 5.5 : Structure-specific DAF assessment for the case-study frame system

Figure 5.6: Influence of design gravity loads on progressive collapse capacity: (a) scenario A1, (b) scenario A2

Figure 5.7: Influence of ultimate steel strain on pushdown capacity curves: (a) scenario A1, (b) scenario A2

Figure 5.8: Beam behaviour under scenario A1: (a) beams denomination, (b) axial force under varying drift and ultimate steel strain.

Figure 5.9: Beams behaviour under scenario A2: (a) beams denomination, (b) axial force under varying drift and ultimate steel strain.

Figure 5.10: Denomination of columns line and beams span

Figure 5.11: Shear failures location: (a) scenario A1, (b) scenario A2

Figure 5.12: Global seismic performance assessment of case-study structure: (a) mode force profile; (b) mass force profile

Figure 5.13: Identification of frame members failing I shear for each orientation of lateral forces

Figure 5.14: Impact of retrofit measure on structural robustness: (a) scenario A1, (b) scenario A2

Figure 5.15: Impact of beam span length variation on structural robustness

Figure 5.16: Pushover of case study structure under variation of beam span length: (a) mode force profile, (b) mass force profile

Figure 5.17: Influence of retrofit measure under varying beam span length

Figure 5.18: Influence of CRFP shear strength variation on brittle failures

Figure 6.1: Geometry of case-study PC building: (a) plan and orientation of one-way floor slabs with identification of column removal scenarios; (b) elevation (dimensions in mm).

Figure 6.2: Beam-column connections: (a) Type 1, (b) Type 2, (c) Type 3 and (d) simplified structural model to design tying reinforcement.

Figure 6.3: Tying reinforcement size: (a) edge and corner column removal scenarios; (b) interior column removal scenario

Figure 6.4: Modelling of case-study PC building: (a) 3D FE model and connections; (b) Type 1 connection; (c) Type 2 connection; (d) Type 3 connection.

Figure 6.5: Performance limit states definition: (a) PC buildings with Type 2 connection and (b) PC buildings with Type 3 connection

Figure 6.6: Type 2 connection: (a) initial configuration; (b) collapse due to loss of support

Figure 6.7: Drift time histories of substandard building with Type 1 connection under varying column loss scenario.

Figure 6.8: Drift time histories under varying load factor for earthquake-resistant building with Type 2 connection: (a) internal scenario; (b) edge scenario; (c) corner scenario.

Figure 6.9: Drift time histories under varying load factor for earthquake-resistant building with Type 3 connection: (a) internal scenario; (b) edge scenario; (c) corner scenario.

Figure 6.10: IDA curves under varying column removal scenario: (a) earthquake-resistant building with Type 2 connection; (b) earthquake-resistant building with Type 3 connection.

Figure 6.11: Near-collapse deformed shapes of earthquake-resistant building with Type 2 connection: (a) corner scenario, (b) edge scenario, (c) internal scenario

Figure 6.12: Earthquake-resistant building with Type 2 connection: (a) IDA curves; (b) fragility curves.

Figure 6.13: Earthquake-resistant building with Type 3 connection: (a) IDA curves; (b) fragility curves

CHAPTER 1 – INTRODUCTION

1.1. Objectives of the Study

The awareness of what progressive collapse of both iconic and public buildings can cause in terms of losses of life and property has triggered significant interest in structural analysis and design under abnormal loads, promoting robustness as a structural measure to mitigate the catastrophic impact of low-probability/high-consequence events (e.g., blast, impact, fire). Nonetheless, structural behaviour under progressive collapse still needs to be deeply investigated, using advanced simulations with proper consideration of materials' mechanical behaviour and impact of strengthening solutions on existing constructions. To this aim, the main objective of this thesis is to investigate the parameters that mostly influence the progressive collapse resistance and robustness of reinforced concrete (RC) frame buildings, both from the point of view of materials behaviour and that of structural components. Four key issues were addressed as follows:

1. Quantification of structural robustness through nonlinear dynamic analysis according to the alternate load path (ALP) method. In the framework of threat-independent approaches, progressive collapse resistance and robustness were assessed under notional member loss by varying location and removal times of columns involved in the local damage scenario, which could trigger a progressive collapse mechanism. Different column-removal scenarios were considered, in order to identify the worst one for a case-study benchmark structure representative of existing RC buildings. Scenarios involving a single column or two columns were considered. In the latter case the influence of column removal time on progressive collapse capacity of the structure was assessed; to this aim simultaneous removal and sequential removal of two columns were identified. Specifically, first of all the same removal time was

assigned to the couple of columns. Then, different column removal time instants were considered, variables in a range from 0.01 s and 1s.

2. Sensitivity of RC frame building structures to the nonlinear mechanical behaviour and properties of structural materials, including concrete and steel reinforcement. A simple method that relies upon statistics of selected structural properties was delineated and implemented to investigate their influence on structural performance. Primary properties varied according to their mean value and standard deviation, resulting into a significant number of progressive collapse analyses. The output of the analysis made it possible to identify which properties mostly influenced the capacity of the structure, hence isolating properties with negligible impact.
3. Structural robustness to structural retrofitting. The progressive collapse assessment a real RC frame building that suffered a partial collapse during structural retrofitting operations at the ground floor. Based on forensic investigations, conditions that really made possible the progressive collapse of the building were reconstructed. The analysis of that case study highlights how much structural retrofitting can be a critical transient stage of the structure's lifetime, as improper interventions can produce major damages or even collapse.
4. Multi-hazard structural assessment under both earthquake actions and column loss, which is a major topic for optimal design and resource allocation allowing safety and sustainability requirements to be jointly met. The above-mentioned benchmark structure was analysed to assess the possible interaction between seismic resistance and structural robustness, in both as-built and retrofitted conditions. The impact of a local retrofitting method based on fibre reinforced polymers (FRPs) on seismic performance and structural robustness was assessed. More specifically, the use of FRPs and variations in their mechanical properties were evaluated as an effective solution to increase both seismic resistance and structural robustness. Advantages and limitations of local strengthening based on FRPs were thus outlined.

1.2. Outline of the Thesis

Structural robustness and its dependence on both material and geometric properties are presently hot topics in the field of structural engineering. This thesis aims to investigate the ability of both new and existing RC structures to avoid progressive collapse under varying characteristic factors of the structure. The thesis consists of five chapters, in addition to this Chapter 1 that summarises motivations and main contents of the study.

Chapter 2 provides main definitions and shows links between some key concepts, which are of primary importance to understand the work presented herein.

Chapter 3 focuses on the influence of material properties on progressive collapse resistance of a RC building when this is subjected to single or multiple column loss. Incremental dynamic analysis was performed to investigate the sensitivity of global capacity features (*i.e.*, ultimate resistance and vertical drift capacity) to material properties and location of notionally removed column. The innovative aspect of this work was the definition of performance limit states explicitly defined for progressive collapse analysis of RC framed structures, and on the other, the characterization of the corresponding limit state capacity.

Chapter 4 deals with the ability of existing reinforced concrete structures to avoid progressive collapse, when subjected to retrofit interventions. There are many real cases in which incorrect structural retrofit interventions have led to the collapse of structures, which may even be of historical and artistic value. In this context, a real structure with typical features of RC buildings constructed in the 1950s, which collapsed in 2001 during retrofitting, was investigated. Specifically, the effects of concrete cover removal from ground-floor columns on progressive collapse resistance were assessed.

Chapter 5 aims to investigate the impact of local seismic retrofitting with FRP systems on structural robustness. Indeed, FRPs are often externally bonded to the end parts of columns and/or beams in RC frame structures, to avoid brittle shear failures that might be caused by earthquake ground shaking. However, the effectiveness of such innovative building materials in increasing also the structural robustness is of great importance to avoid the installation of further strengthening systems. Based on nonlinear static analysis

with displacement control, a benchmark RC frame was first assessed under seismic actions and then analysed under notional column removal at the ground floor. The seismic capacity of the building was undermined by the potential occurrence of brittle shear failure at both beam and column end sections. Thus, FRP strengthening systems were designed to avoid those undesired failure modes, allowing their effectiveness assessment under column loss. A parametric analysis was also performed, in order to assess the impact of variations in structural geometric properties and shear strength of FRP systems.

The study of a precast RC frame structure, representative of low-rise commercial buildings, was addressed in chapter 6. It was analysed under different column loss scenarios, which can produce the partial or total collapse of the structural system. A fragility analysis procedure was used to evaluate the structural robustness in a probabilistic way. In particular, in this study, the role of different beam-to-column connections were investigated for different column removal scenarios and the impact of the variability of material properties through a Monte Carlo simulation.

Chapter 7 outlines the main findings of the PhD thesis, providing a basis for potential future developments that might allow a better understanding of structural robustness of RC frame buildings.

CHAPTER 2– STATE-OF-THE-ART REVIEW

2.1 Extreme actions on structures

During the structure’s lifetime, different types of actions can affect structural safety and these are distinguished according to their probability of occurrence and their consequences (Figure 2.1). Hazardous events can be classified as follows:

- *Frequent events*, which are characterized by high probability of occurrence and low consequences (e.g., loss of operation).
- *Rare events*, which are expected to produce moderate-to-significant consequences in case of their occurrence (e.g., collapse of single structural components).
- *Exceptional/extreme events*, which are marked by low probability of occurrence and high levels of consequences and are not usually considered in design and assessment of structural systems.

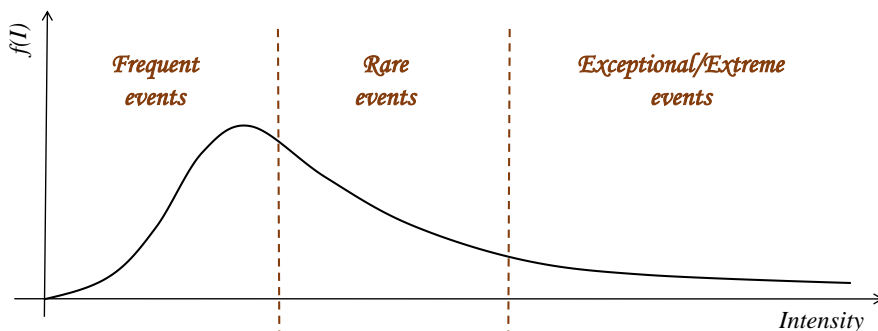


Figure 2.1: Categories and consequences of events

Low-probability/high-consequence (LPHC) events are characterized by (i) a probability of occurrence significantly lower than that of normal events (e.g., wind, snow,

earthquakes), and (ii) an expectation of huge losses (*i.e.*, casualties, repair costs, downtime).

Eurocode 0 [1] (§1.5.3.5) and Italian technical code [2] (§2.5.1.3), here abbreviated as NTC 2018, define an exceptional/extreme action as “*action, usually of short duration but of significant magnitude, that is unlikely to occur on a given structure during the design working life*”, and as an action “*that occur only exceptionally during the nominal life of the structure*”, respectively.

Exceptional actions can be classified in three categories, as follows:

1. actions arising from either natural phenomena (*e.g.*, earthquakes, meteorological phenomena or landslides) or involuntary human activity (*e.g.*, explosions of hazardous material, fire);
2. actions intentionally caused by man (*e.g.*, vandalism and terrorist attacks);
3. consequences of errors in design, construction and maintenance.

Current codes provide useful guidance to design structures against ordinary actions, such as earthquakes, but they do not give accurate and specific indications against extreme actions. While for conventional/ordinary events there is the possibility to obtain their probability of occurrence through probabilistic approaches, the same does not apply to extreme actions. Therefore, traditional methods cannot be used to design structures in relation to this kind of action.

2.2 Progressive and disproportionate collapses

The importance of extreme actions in the structural field is given by their relation with progressive collapse. Indeed, these often cause local damage to the structure, which in turn may lead to progressive collapse of the entire structure or of a large part of it. Progressive collapse is characterized by a localised damage to a single or a few structural components, which is followed by damage propagation throughout the structural system. Progressive collapse is associated with the propagation of failure within the structure and may be proportionate in size if failure propagation is arrested by some elements. Several definitions of progressive collapse are available in literature. The American

Society of Civil Engineers/ Structural Engineering Institute (ASCE/SEI) [3] defined progressive collapse as “*the spread of an initial local failure from element to element, resulting eventually in the collapse of an entire structure or a disproportionately large part of it*”, while GSA guidelines [4] as “*an extent of damage or collapse that is disproportionate to the magnitude of the initiating event*”. This latter definition outlines another type of collapse, which is called disproportionate collapse and is marked by a disproportion in size between a relatively minor damaging event and the final collapse configuration that is a large part or the whole of the structural system. Disproportionate collapse is thus associated with a final size of damaged structure compared to the initial damage, hence delineating the possibility of disproportion in size even without failure propagation. Therefore, the term "disproportionate" refers to the extent of the area affected by the collapse, while "progressive" refers to a specific mode of collapse. According to Adam et al. [5], the interest of research in this issue has increased especially after a number of notorious progressive collapses (see Figure 2.2), that involved an important number of victims and produced an extensive damage and important social impact, *i.e.* the Ronan Point collapse in 1968, the attacks on the Alfred P. Murrah Federal Building in Oklahoma in 1995 and on the World Trade Centre in New York in 2001. As discussed by Kunnath et al. [6], the amount of research on disproportionate collapse of building structures has been increasing sharply in the past 20 years, allowing the research community to address several issues in modelling, numerical simulation and performance quantification. Experimental testing of structural subassemblages and small-scale framed prototypes has been more recently carried out [7-11], allowing the validation of methods for progressive collapse analysis of reinforced concrete (RC) framed buildings. The study and the analysis of an experimental work carried out on a full-scale RC cast-in-place building structure subjected to a sudden corner-column failure scenario was carried out by Adam et al. [12], in order to investigate the possible consequences of an extreme event by the simulation of sudden removal of columns. Another significant drawback of many existing constructions is related to their seismic vulnerability, as highlighted by several earthquakes worldwide (*e.g.*, [13]). On the one

hand, most of the existing structures were built according to past codes without modern design criteria, resulting in insufficient levels of seismic capacity; on the other, missing or inadequate maintenance of such constructions produces high levels of deterioration, further increasing their seismic vulnerability [14]. Nevertheless, in the last few decades, a large number of seismic retrofit strategies have been proposed and industrialised for their widespread implementation in practice (*e.g.*, [15-20]). In contrast to the extensive literature on seismic retrofitting, a very limited number of research studies focused on developing and investigating retrofit strategies to avoid the progressive collapse of structures. Regarding RC buildings, Li et al. [21] carried out an experimental study aimed at ensuring the sustainability of a structure prone to progressive collapse, using a rapid method for retrofitting RC frames with CFRP wraps. Shayanfar et al. [22] demonstrated that the combined use of additional steel rebar and CFRP sheets on beams could be an efficient strategy for structural retrofit of RC frame buildings against progressive collapse. Similarly, Orton et al. [23] proposed and investigated a strategy to protect RC structures from progressive collapse by providing continuity of reinforcement in concrete beams through CFRPs. Qian et al. [24] experimentally investigated the use of externally bonded glass fibre-reinforced polymer (GFRP) sheets to mitigate the progressive collapse resistance of precast concrete buildings. Recently, Qin et al. [25] experimentally and numerically investigated the behaviour of beam-column sub-assemblages with steel-FRP composite bars (SFCBs). The use of SFCBs showed higher performances with respect to the other solutions, allowing the development of flexural, compressive arch and catenary actions. Numerical simulations confirmed that the installation of SFCBs can be able to effectively reduce the progressive collapse vulnerability of RC frames. The likelihood of multiple hazards has sharply increased due to the rapid population growth and economic development. This leads to the importance of considering the interaction between different hazards in the design, assessment and retrofit of structures [26]. In this respect, the interaction between seismic and robustness designs is a matter of discussion because of the differences between the effects of earthquake ground motion and those of, for instance, the failure of a structural

component. Nonetheless, the outcomes of several studies indicate some interesting chances to meet multiple performance objectives through the structure's ability to develop different behavioural modes depending on the type of actions it is subjected to. The topics of disproportionate collapse and risk are directly related to each other. Risk has a probabilistic nature, as it is related to the probability that a hazardous event will happen at a given site within a given timeframe (hazard), the probability that a structure will suffer local heavy damage and subsequent progressive collapse (vulnerability), and the amount of damage to people and property (exposure). Given (i) a potentially damaging event, H , with low probability of occurrence but high expected consequences (case of extreme events), (ii) a state of local failure (LF) to the structure induced by H and (iii) the disproportionate collapse (C) caused by LF , the probability of collapse can be evaluated as follows:

$$P[C] = P[C | LF] \cdot P[LF | H] \cdot P[H] \quad (1)$$

where:

- $P[C]$ represents the annual probability of structural collapse C due to event H , which is related to the collapse resistance of the system.
- $P[C|LF]$ is the conditional probability of disproportionate collapse given the local failure, LF .
- $P[LF|H]$ represents the conditional probability of local damage, given H .
- $P[H]$ is the probability of occurrence of the event H , equal to the annual average rate of occurrence, λ_H , which does not depend on the design strategies, but is related to the different typologies of actions.

Based on Equation (1), the following strategies for disproportionate collapse risk reduction can be implemented:

- Hazard mitigation, reducing the probability of occurrence of exceptional events, *i.e.* the probability of occurrence of the event H , with social and political planning; possible strategies could be the isolation of the structural system from

exposure to these actions (*e.g.*, protective barriers outside critical structures) or limitations of using exterior/interior zones.

- Local vulnerability mitigation, reducing the direct consequences of an exceptional event on the structure, *i.e.* the probability of a local damage given the event H .
- Global vulnerability mitigation, reducing the final consequences, *i.e.* the probability of collapse after local failure; this could be achieved by, for example, compartmentalization of the structural system (*i.e.*, developing ALP) the definition of alternative escape routes, or other active and/or passive measures.

An optimal strategy may include a combination of the three actions described above.

Equation (1) can be generalized to the case of multiple hazardous events and initial states of damage, and it becomes:

$$P[C] = \sum_H \sum_{LF} P[C | LF] \cdot P[LF | H] \cdot P[H] \quad (2)$$

This Equation can be extended to define the concept of expected loss, using different metrics for risk assessment: risk of death, probability of collapse and cost-benefit assessment [27]. This leads to reformulating Equation (2) as follows:

$$P[C] = \sum_H \sum_{LF} \sum_C \sum_L P[L | C] \cdot P[C | LF] \cdot P[LF | H] \cdot P[H] \quad (3)$$

where L indicate an appropriate loss metric that quantifies, for example, direct or indirect economic losses, loss of life, or downtime.

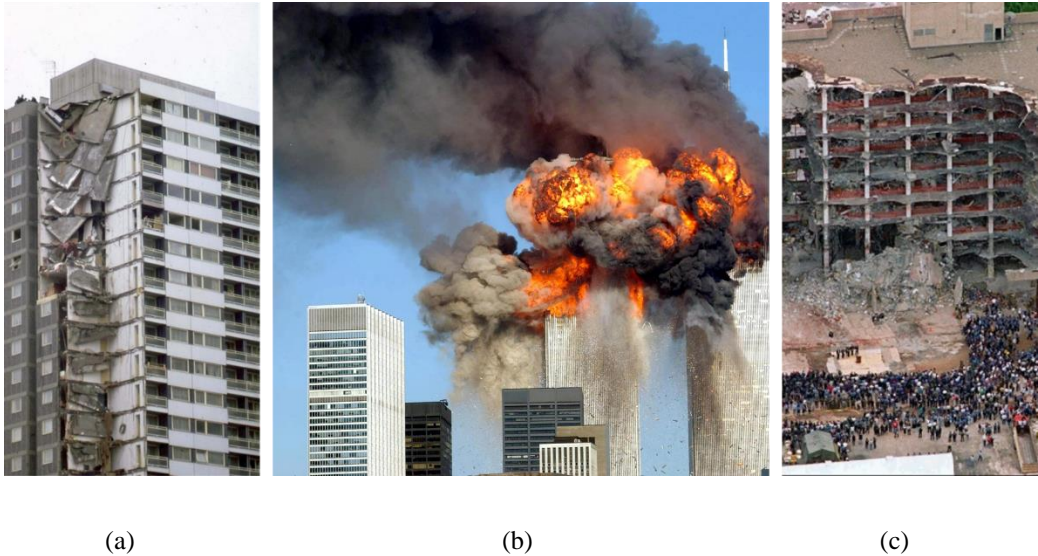


Figure 2.2: Progressive collapse examples: (a) Ronan Point (London, 1968), (b) World Trade Center (New York, 2001), (c) A.P. Murrah Federal Building (Oklahoma, 1995).

2.3 Definition of structural robustness

The ability of the structure to avoid disproportionate damage with respect to the magnitude of the action that triggers an initial damage can be expressed through the concept of structural robustness.

The probability of disproportionate collapse is directly related to the definition of structural robustness. Each term into Equation (1) is a contribution to its assessment, respectively in terms of the event, local damage and structural robustness. With the introduction of this concept, the progressive collapse resistance can be evaluated as illustrated in Figure 2.3. The majority of design codes require that structures have adequate robustness towards exceptional actions, both in relation to their intended use and to the consequences of a possible collapse.

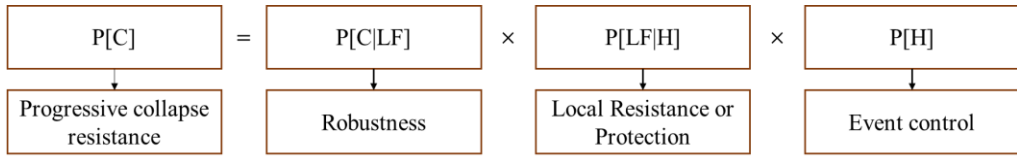


Figure 2.3: Components of disproportionate collapse risk and corresponding mitigation measures

In addition, the reduction of disproportionate collapse risk can be achieved by a correct design of the structure. The following structural features allow the limitation of damage propagation, increasing robustness:

- Redundancy: isostatic structures do not have any possibility to overcome the damage of a member by creating ALP. The increase in external and internal (two-dimensional structures) redundancy degree leads to a greater possibility of dealing with local damage.
- Ties: the presence of a three-dimensional tying system increases the capacity of the structure to exploit structural redundancy after the loss of key structural elements, in order to redistribute stresses and strains under large displacements.
- Ductility: materials must be able to withstand large displacements and/or rotations without excessive strength degradation.
- Structural regularity: structures with rather uniform distribution of stiffness, resistance and mass allow higher ability to redistribute loads in case of single member collapse.
- Adequate resistance to shear forces: shear strength of structural members should always exceed flexural capacity to activate a ductile response of the single members and of the structure.
- Ability to withstand load reversals: primary and secondary structural elements should have adequate resistance to load reversals that should occur during progressive collapse.

Design codes and standards provide specific verifications under exceptional actions for different types of construction, underlining how it is possible to ensure an appropriate

level of robustness, in relation to the expected use of the construction and the consequences of its possible collapse.

Currently, most of the building codes and guidelines deal with disproportionate collapse and integrity issues in a qualitative way, highlighting the general concepts of the problem and the need to obtain procedures for estimating and mitigating risk. Indeed, robustness can be interpreted and quantified differently. Different definitions of robustness and related regulatory requirements, provided by various codes, are discussed below.

2.3.1 Robustness in Eurocodes

Eurocode 1 [28], at §1.5.14, defines the robustness as “*the ability of a structure to withstand events like 'fire, explosions, impact or the consequences of human error, without being damaged to an extent disproportionate to the original cause*”. In addition, designing a structure with sufficient robustness is envisaged as a strategy to be adopted against exceptional actions. Sufficient robustness could be ensured through the adoption of one or more of the following approaches:

- Design of some key structural components, in order to increase the probability of structural survival after an exceptional event.
- Design of structural elements to have sufficient ductility, so as to absorb a significant deformation energy without breaking up.
- Design of the structure to get sufficient level of redundancy, so that ALP can develop after an exceptional event.

2.3.2 Robustness in National Building codes

NTC 2018 [2], at §2.1, defines robustness as the “*ability of the structure to avoid disproportionate damage to the extent of possible exceptional actions, such as explosions and impact*”. In addition, §2.2.5 provides design strategies to ensure an adequate level of robustness in relation to the intended use of the construction and the consequences of its possible collapse. The following design strategies are delineated by NTC 2018:

1. Design of the structure able to withstand exceptional actions of a conventional nature, combining nominal values of exceptional actions to other explicit design actions.
2. Prevention of the effects induced by exceptional actions which the structure may be subjected to or a reduction of their intensity.
3. Adoption of control systems, either passive or active, that are adapted to the actions and phenomena which the structure may be subjected to.
4. Adoption of a structural form and type able to tolerate localised damage caused by an exceptional action.
5. Adoption of a structural form and type with low sensitivity to the exceptional actions considered.
6. Construction of structures as redundant, resistant and/or ductile as possible.

Indeed, it is appropriate that constructions have an adequate degree of robustness, depending on the intended use of the construction, identifying risk scenarios and exceptional actions of relevance for its design.

2.3.3 Robustness within international guidelines

Another definition of structural robustness is given by Fib Model Code [29], which describes it as “*an indication of the ability of a structural system to mobilize alternative load paths around an area of local damage. It is related to the strength and form of the structural system, particularly the degree of redundancy (number of potential alternative load paths) within the structural system*”.

Therefore, structural robustness is related to ability of a system subject to accidental or exceptional loadings (such as fire, explosions, impact, or consequences of human errors) to sustain local damage to some structural components without experiencing a disproportionate/progressive collapse.

In addition, GSA guidelines [4] define structural robustness as the “*ability of a structure or structural components to resist damage without premature and/or brittle failure due*

to events like explosions, impacts, fire or consequences of human error, due to its vigorous strength and toughness”.

2.4 Design for robustness

As discussed above, there are different strategies to mitigate risk, particularly affecting three risk components as follows:

- Prevention of the occurrence of the event.
- Prevention of a disproportionate collapse from the development of local damage.
- Prevention of the development of a local damage into a disproportionate collapse of large parts of the building, i.e. the structure as a whole.

The first strategy can be achieved by reducing the probability of development of the risk and consequent collapse of the structure, so that it is necessary that the threat is individually identified. In this way, it might be possible to predict measures on the site of the building, on activities inside the building, or on the people authorized to enter the building. Under the occurrence of the risk scenario, robustness must be ensured through the design of the structural system.

Different design approaches can be distinguished according to analytical complexity level, depending on the level of risk accepted and the consequences of a possible collapse. Different design approaches were defined by ASCE [3], as follows:

- Prescriptive design process or performance-based design process, depending on the general approach taken to design.
- Direct and indirect method, depending on the method used for the design of the structural system.
- Specific threat or generic threat, depending on the definition of the risk scenario.

The definition of minimum characteristics of the structure is the feature of prescriptive approach, in order to increase its safety at a sufficient level with respect to disproportionate collapse. By contrast, performance-based engineering approaches assess the behaviour of the structure for a given set of risk scenarios. Therefore, a prior

definition of these scenarios and the expected structural performance associated with each of them is needed. In the first case, for example, minimum material strengths, minimum strengths and/or rigidity of the members and connections, construction details, or the limited use of certain structural systems may be prescribed.

In general, either a direct or indirect design method can be used in a performance-based design/assessment approach and the risk scenario can be identified through a definition of a specific threat or a generic threat. By contrast, a prescriptive approach always uses an indirect method of design.

2.4.1 Indirect design methods

This type of method aims to achieve robustness by ensuring a minimum level of connection between the various components of the structure; in this way the redundancy of the system and the ductility of the members are more effectively exploited. Through the use of these methods the choice of the structural system, the layout of the structural elements, the minimum resistance of the connections, their construction details and other structure characteristics are guided. They are easy to apply and lead to uniformity and standardization of the designs, but do not allow in any case a quantification of the structural robustness obtained. The ability of the structure to prevent local collapses and/or disproportionate collapses is not explicitly evaluated, and the designer's freedom is heavily penalized. The use of this approach requires a limited amount of additional calculation by the designer compared to the traditional project.

Indirect design methods include:

1. Tie force method, which is recommended in many codes [28,30,32] for structures with low risk of progressive collapse. It is characterized by an implicit consideration of resistance to progressive collapse. Code requirements vary according to the type of structure considered; in case of RC structures, the required level of robustness is achieved through continuous tying, while in steel and steel-concrete constructions, beam-to-column connections and secondary beam-to-primary beam connections are sized to

transfer not only bending and shear actions but also axial tensile forces. The following tying systems are suggested:

- Floor perimeter tying systems (in the two main directions).
- Internal plane tying systems (in the two main directions).
- Horizontal tying systems between columns or partitions.
- Vertical tying systems .

The aim is to increase the members' capacity so that the local collapse of an element can be absorbed through load redistribution, based on both arch and catenary effects under large deformations.

2. Key element design methods, in which key elements (i.e. structural members the failure of which activates a progressive collapse) are identified and designed to resist accidental loads. This method is characterized by the importance of combination of loads for accidental situation for its effects. The aim is to increase the system robustness by reducing the risk of disproportionate collapse through measures that reduce the probability of local damage. Key element design is often implemented when alternate load paths are complex to be identified.

2.4.2 Direct design methods

Opposed to indirect design approaches, direct design methods explicitly assess the capacity of the structure to prevent local failure or their possible evolution into disproportionate collapses due to exceptional actions. Direct methods require more complex analysis techniques compared to those used in traditional structural design. Therefore, the most suitable analysis tool should be identified with respect to the information required for modelling and computational skills of the analyst. The designer can follow two different approaches:

- To increase the resistance of main structural elements (key elements), the local damage of which could cause a disproportionate collapse. In this way, key elements are able to withstand exceptional design actions.

- To design the structure so that it is able to transfer loads after local failure.

Within the framework of direct design methods, one can distinguish between threat-dependent and threat-independent approaches, as described below.

2.4.2.1 Threat-dependent and threat-independent approaches

In a threat-dependent approach, extreme events and corresponding exceptional actions on the structure are quantified and considered explicitly. Structural analysis should identify the resulting initial damage and its possible evolution into a disproportionate collapse. The transition from defining the characteristics of the event to exceptional actions on the structure may also require multi-physics analysis methods. The specific threat can be represented by, for example, the amount of explosive, type of impact in terms of mass, speed and direction of the impacting vehicle, fire load, etc.

A general methodology in threat-dependent approaches consists of the following stages:

- 1) Definition of abnormal load scenarios.
- 2) Local analysis of single structural components under abnormal/exceptional loads, in order to identify initial damage cases.
- 3) Global analysis of residual structure under gravity loads, in order to assess safety and to identify critical scenarios and key structural elements.

In a threat-independent approach, exceptional actions and/or their effects are not defined nor quantified. If the actions cannot be modelled, notional actions (typically in the form of equivalent static loads) are defined and any initial damage and its possible evolution into a disproportionate collapse is assessed. If the effects of exceptional actions cannot be predicted, a notional initial failure is assumed regardless of its cause, assessing the potential evolution into a disproportionate collapse.

A general methodology for threat-independent approach can be described through two stages, as follows:

- 1) Notional removal of one or more structural components.
- 2) Global analysis of residual structure under gravity loads, in order to assess the safety and to identify critical scenarios and key structural elements.

A threat-independent approach is the alternate load path method (ALP), whereby the structure must be able to redistribute the loads carried by the collapsed element to the intact structural elements. This method can be implemented without the initial identification of threats and their quantification. It involves the removal of a structural element, typically a column, and verification through non-linear static or non-linear dynamic analysis that the residual structure is still able to transfer the actions in the combination of accidental load. If a structure owns ductility, structural regularity, redundancy and dissipation capacity, it is easier to establish ALP.

2.4.2.2 Probabilistic versus semi-probabilistic approaches

In order to obtain a correct assessment of disproportionate collapse risk, the presence of multiple damaging events and initial states of damage should be considered. In this case, Equation (2) may be generalized as follows, if the events are mutually independent:

$$P[C] = \sum_H \sum_{LF} P[C | LF] \cdot P[LF | H] \cdot \lambda_H \quad (4)$$

where λ_H , the average annual occurrence rate, replaces $P[H]$ if the accident rates are below 10^{-2} /year.

Sufficient data is needed to quantify λ_H , so that engineering decisions can be supported and taken on an unconditional risk basis. When the assessment of the annual occurrence rate may be critical, it is appropriate to proceed with analysis of risk based on S scenarios, thus assuming the event as deterministic. This kind of approach, also known as scenario analysis, is utilized when the type of event that can affect the structure is known, but there is no possibility to probabilistically model its occurrence and intensity.

On the other hand, if the occurrence of an event in a given site and reference period can be probabilistically modelled, a full probabilistic approach, also known as quantitative risk analysis, can be used to assess robustness. The evaluation in probabilistic terms should involve the use of advanced analysis methodologies, such as nonlinear dynamic analyses on detailed numerical models [33-35]. For example, Brunesi et al. [34] carried

out fragility analyses on RC framed buildings, in order to propose a set of fragility models that could be used for probabilistic assessment and management of progressive collapse risk. The fragility models proposed were optimally fitted to discrete fragility estimates provided by IDA combined with Monte Carlo simulation (Figure 2.4). Lognormal fragility functions described the conditional probability of exceeding a prescribed performance limit state given the intensity of gravity loads (see Equation (4)).

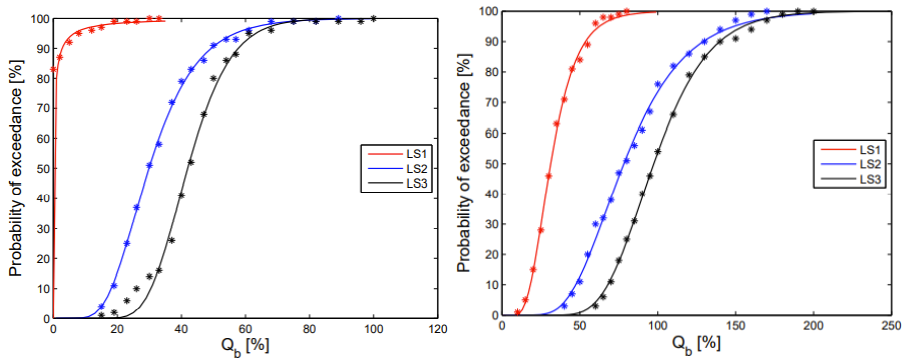


Figure 2.4: Fragility functions of the RC framed buildings [34]

2.5 Robustness quantification

An essential aspect for effective assessment and mitigation of disproportionate collapse risk is the quantification of robustness by appropriate measures. This quantification is influenced by some factors related to structural modelling under extreme conditions, which are described below.

2.5.1 Resisting mechanisms in reinforced concrete structures

The structural behaviour of a RC framed building subjected to an extreme event can be described through three different resisting mechanisms. Figure 2.5 illustrates an RC double-span frame sub-system under vertical point load at the location of central column. In case of column loss due to an extreme event, progressive collapse might be resisted by the following mechanisms that involve the connected beams: beam mechanism stage,

arch transient stage, and catenary mechanism stage, according to previous studies [36, 37] and illustrated in Figure 2.6. Such mechanisms produce a nonlinear relationship between the concentrated load applied at the column removed point (P) and the vertical deflection at the location of the removed column (D_v), as shown in Figure 2.7. Three different phases are illustrated and can be classified as follows:

- Beam stage (OB): bending behaviour of the beams and characterized by plastic hinging at the end sections of the column-beam connections.
- Transient arch stage (BD): the beam is subjected to a compression action with a consequent increase in the plasticization moment. As the displacement increase, a diagonal compression field occurs leading to an arch formation. The force–displacement relationship is thus characterized by a softening stage that describes a gradual decrease in the resisting force as the vertical displacement of the control point increases.
- Catenary stage (DE): resisting mechanism marked by a new growth in resisting force under increasing vertical displacement of the control point. This catenary action is related to ultimate elongation and strain hardening of longitudinal steel reinforcement, which relies on the anchorage of bars within beam-column joints.

The catenary effect vanishes when reinforcing bars suffer tensile rupture.

Based on such mechanisms, the frame sub-system is able to experience large deformations with increasing strength depending on the ultimate elongation and bond strength of longitudinal steel bars. A very large deformation capacity then develops due to both arch and catenary actions of beams. A continuous reinforcement between side columns is required for the catenary effect to be developed. Otherwise, the maximum load resisted by the structure are limited to that corresponding to the bending behaviour.

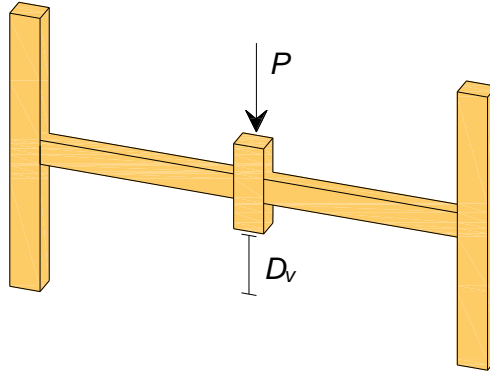


Figure 2.5: 3D RC beam-column sub assemblage

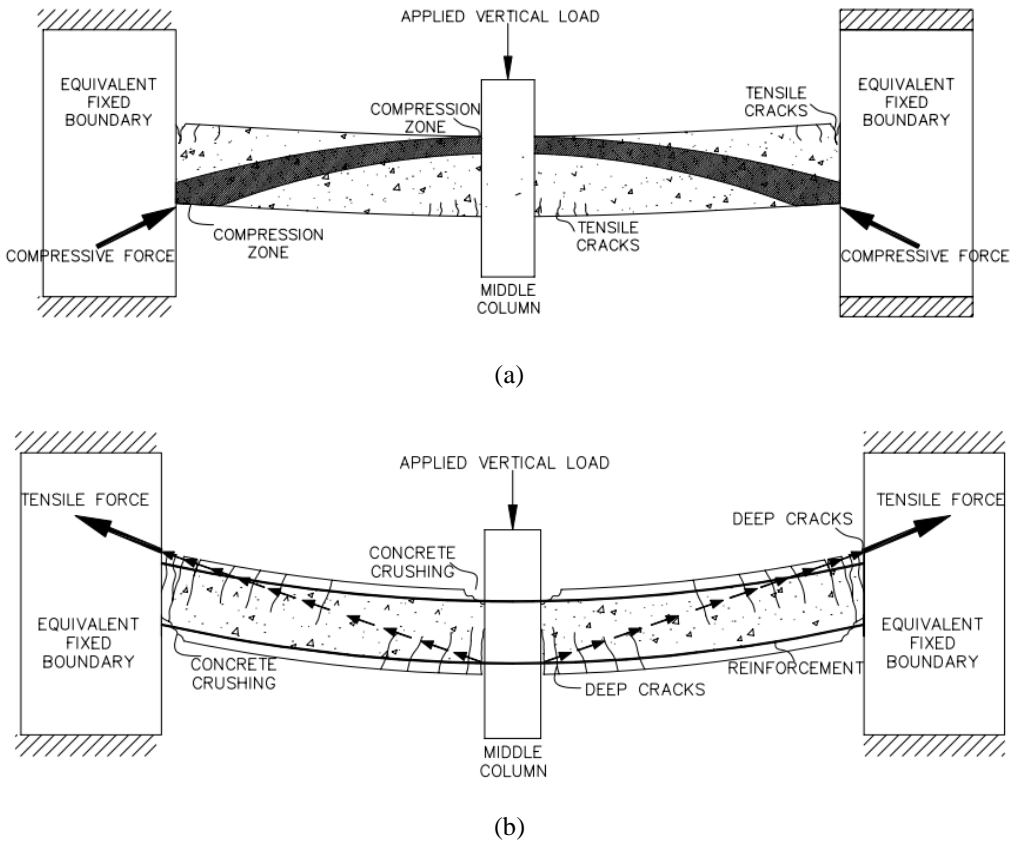


Figure 2.6: Schematic of (a) compressive arch action and (b) tensile catenary action [37]

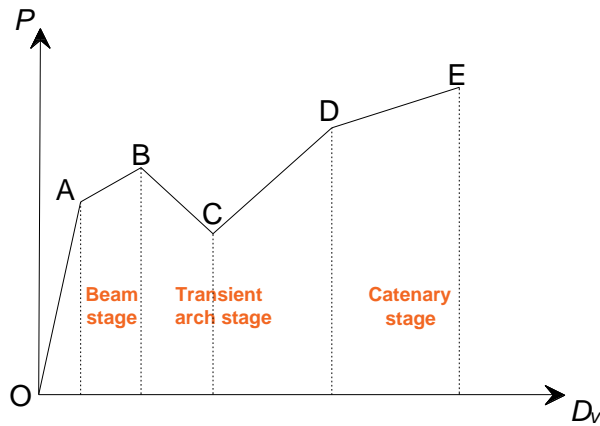


Figure 2.7: Progressive collapse response curve of frame sub-structure

2.5.2 Load modelling

When a structure is subjected to an extreme event that led to the removal of a vertical element, the beam-column joint on top of the removed column will move downward, afterwards experiencing vertical vibration if collapse is not reached. Gravity loads applied on the floor system become falling loads in a few moments, so their intensity will no longer be equal to that predicted in static conditions due to a dynamic amplification. In other words, inertia masses corresponding to gravity loads are subjected to vertical acceleration, resulting in total loads the intensity of which depends on the type of structural response. In the framework of static response analysis methods, this load amplification motivated the need to consider a dynamic amplification factor (Ω_N), the formulation of which varies according to the structural typology under consideration.

In case of a reinforced concrete framed structure and a steel framed structure, Ω_N can be predicted through Equations 3 and 4, respectively, according to Unified Facilities Criteria (UFC-04-023-03) [30]:

$$\Omega_N = 1.04 + \frac{0.45}{\frac{\theta_p}{\theta_Y} + 0.48} \quad (5)$$

$$\Omega_N = 1.08 + \frac{0.76}{\frac{\theta_p}{\theta_Y} + 0.83} \quad (6)$$

where θ_p is the plastic rotation capacity of the element, component, or connection, and θ_Y is the corresponding yield rotation. As regards reinforced concrete, masonry and timber wall structures, the dynamic amplification factor can be set equal to 2. The trend of Ω_N is shown in Figure 2.8; its maximum value is 2 and then it decreases as the plastic rotation of the plastic hinges increases.

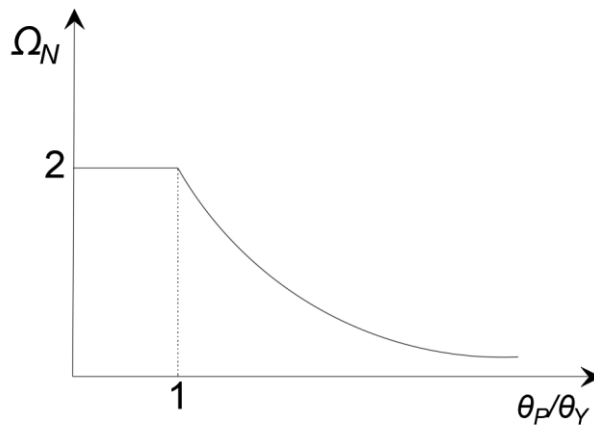


Figure 2.8: Trend of dynamic amplification factor

As the position of the column removed varies either notionally or as a result of a given location and intensity of the exceptional action, floor areas subjected to load amplification due to their direct involvement in vertical oscillations vary, as illustrated in Figure 2.9.

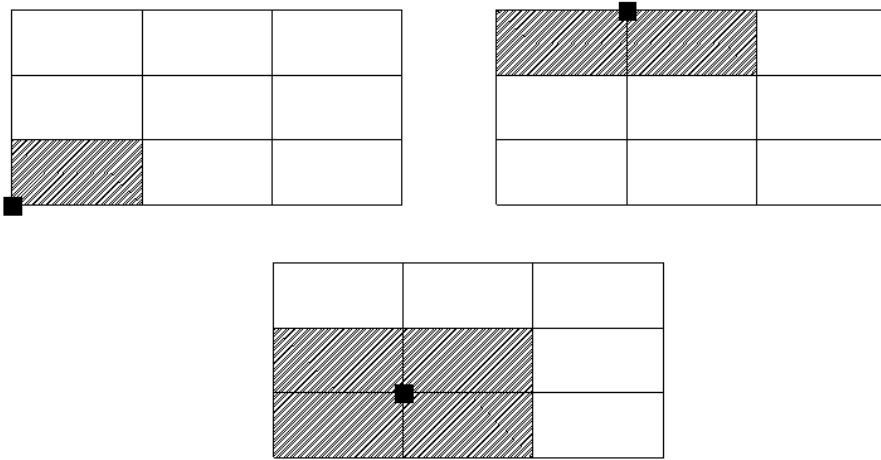


Figure 2.9: Load amplification under varying position of removed column

In addition, the Unified Facilities Criteria (UFC) [30] provided an exceptional load combination, according to Equation 5:

$$G_N = \Omega_N(1.2D + 0.5L) \quad (7)$$

where D and L stand for dead and live loads, respectively. This represents the combination of gravity loads on floor areas over failed columns, when an abnormal load condition is applied. Equation 7 is more conservative than that provided by Eurocode 0 [1], where partial safety factors of D and L are set to 1 and 0.3, respectively.

2.5.3 Structural modelling

As a result of exceptional actions, a large number of variables involved and the degree of uncertainty associated with them must be considered; for this reason, the study of the behaviour of a structure is a very complex operation. The aim of the latter is to assess the risk of disproportionate collapse, but the accuracy of results is closely related to the analysis typology, the type of modelling and behaviour of the structural materials.

The ability to absorb and dissipate energy after a localized damage is directly linked to the constitutive laws used for materials of structural elements and their connections. In this respect, particularly in case of structural members directly subjected to impulsive

loading, material behaviour can be influenced by strain rate (so-called strain rate sensitivity). For example, strain rate sensitivity of materials is usually observed in the case of explosion or impact of high-speed vehicles. This aspect leads to an increase in the strength and/or stiffness of materials, which can be taken into account in the evaluation of robustness. Strain rate varies in the range $\dot{\epsilon} = 10^2 \div 10^4 \text{ s}^{-1}$.

For this reason, a dynamic increase factor (DIF) should be considered, in order to increase material strength in dynamic conditions. This factor is given by the ratio between dynamic strength, f_{dyn} , and static strength, f_{stat} as follows:

$$DIF = \frac{f_{dyn}}{f_{stat}} \quad (8)$$

As illustrated in Table 2.1, the factor value changes according to the material considered.

Material	DIF _{max}
Steel reinforcement	1.5
Compression concrete	2
Tensile concrete	7

Table 2.1: Typical maximum values of dynamic increase factor for concrete and reinforcing steel

Finite element software packages allow the simulation of material behaviour through different formulations from the linear elastic to the non-linear hysteretic type. Some parameters of these laws can be modified by the designer, so his/her experience plays a key role in the choice and calibration of constitutive laws. The following constitutive and structural models can be taken into account:

- Linear elastic constitutive model: This model is the easiest to use and to interpret, especially in the preliminary phases of the study in which the material nonlinearities are generally neglected. Its use can help the designer to highlight any critical points in the structural model. This model is not suitable for the study of complex phenomena such as disproportionate collapse, because the behaviour of materials is markedly nonlinear due to large deformations.

- Nonlinear constitutive models dependent / independent of the load application speed: The study of disproportionate collapse generally involves inelastic deformations, and hence strongly nonlinear behaviour of materials. Material plasticity represents an essential contribution to energy dissipation and load redistribution, so inelastic behaviour cannot be overlooked during the analysis. In rate-dependent constitutive models, stress-strain relationships change during analysis according to current levels of strain rate in materials. In rate-independent constitutive models, conservative values of DIF are assigned to material properties before nonlinear analysis.
- Local versus global models: Local models are required to study the behaviour in particular points (discontinuity zones, load application points, stress concentration zones, nodes, connections, etc.). Global models are used to obtain general information, such as the trends of stresses and displacements throughout the structure. In addition, local models are useful in the study of constructive details of which experimental tests are not available. Such example, the study of a beam-column connection can be related to a simple non-linear link to be used in the global model whose moment-rotation law is derived from the local model.

2.5.4 Structural response analysis methods

Either local damage or collapse of an element may result in the transition from the original configuration to a damaged configuration; this generates dynamic effects which can be taken into account in different ways depending on the type of analysis chosen. The analyses that can be performed are:

- Linear static analysis: in some cases it is possible to evaluate the structural behaviour with this type of analysis, increasing the effects through an appropriate dynamic amplification coefficient. This analysis is characterized by:
 - Linear elastic modelling.
 - Maximum dynamic amplification of gravity loads.
 - Strain rate effect eventually considered.

- Strength-based safety verifications of structural components in shear and flexure.

The advantage of this analysis is that it can be carried out with simple software and be managed even by less experienced designers. On the other hand, however, its use for the structural robustness assessment generally leads to an approximate solution. For this reason this analysis should be limited to very simple structures.

- Nonlinear static analysis (local/uniform/global push-down): it takes into account the geometrical non-linearity due to the large deformations that the structure undergoes after a damage and/or local collapses. So that, this kind of analysis allows to adequately capture the catenary effect and/or the members effect of the horizontal elements. It is characterized by:

- Inelastic modelling.
- Estimate of dynamic amplification of gravity loads.
- Consideration of the strain rate effect.
- Safety verifications in terms of ultimate load capacity and deformations.

It is important the choice of the materials constitutive law and the simulation of the nonlinear behaviour of the connections. In addition, particular attention should be paid to the dependence of the results on the discretization used.

- Linear dynamic analysis: This type of analysis allows one to take into account the dynamic effects related to local damage/collapse, but not the effects related to the non-linearity of the problem. It is characterized by:

- Linear elastic modelling.
- Maximum dynamic amplification of gravity loads
- Consideration of the strain rate effect
- Strength-based safety verifications of structural components in shear and flexure.

- Nonlinear dynamic analysis (single-run/incremental time-history): more complete and suitable analysis for the problem simulation. It is characterized by:

- Inelastic modelling,

- Exact evaluation of gravity-load dynamic amplification
- Exact integration of strain rate effect
- Safety verifications in terms of ultimate load capacity and deformations.

Due to the complexity and the large number of parameters involved, this type of analysis can only be carried out by experienced designers. In addition, it should also be taken into account the computational burden that such modelling involves, especially in the case of large structures.

2.5.5 Robustness measures

The quantification of structural robustness through appropriate measures is a key point for an effective assessment and mitigation of disproportionate collapse risk. A robustness measure should meet at least some of these requirements:

- Expressivity, interpreted as the ability to quantify all features of robustness, in order to distinguish between a robust and non-robust structure.
- Objectivity, related to the insensitivity of the robustness measure to user decisions.
- Simplicity, as an attribute of the measure's definition.
- Calculability, understood as the possibility of the measure to be evaluated with relatively low computational cost.
- Generality, related to the ability of the measure to be appropriate for any kind of structure.

Many robustness measures are available in the literature that differ from each other depending on the approach used. These are classified as follows:

- Reliability/risk-based, in which robustness is considered as a threat-dependent characteristic, able to considered the effects of abnormal loading or initial damage of the structure.
- Deterministic measures, where robustness is considered as a threat-independent characteristic, independent from the events that may trigger a disproportionate collapse.

A careful review of the scientific literature allows one to distinguish between robustness measures due to their dependence or independence on the potentially damaging event and the semi-probabilistic or probabilistic approach used.

Baker et al. [38] considered robustness as a system property associated with the relative risk due to indirect consequences. They proposed a robustness index, I_{rob} , given by the ratio between the direct risk level associated with localised damage to single structural components and the sum of direct consequences associated with the loss of each component of the system.

The level of robustness was quantified by Frangopol et al. [39] through a function, β_r , of the reliability indices related to the intact and damaged conditions. It was defined according to Equation (9):

$$\beta_r = \beta_{intact} / (\beta_{intact} - \beta_{damaged}) \quad (9)$$

in which $\beta_{damaged}$ and β_{intact} are the reliability index of damaged structure and the reliability index of intact structure, respectively.

Parisi and Augenti [40] proposed the pushdown-based robustness measure, λ , expressed as follows:

$$\lambda = C_v / D_v \quad (10)$$

where C_v and D_v represent the vertical load-bearing capacity of damaged structure after single or multiple member loss and vertical design load corresponding to exceptional load combination, respectively.

Starossek and Haberland [41] proposed a robustness measure R_s , function of determinants of the stiffness matrix in damaged and intact conditions

2.6 From robustness to disaster resilience

The damage or even the collapse of a critical structure may have important effects on society, because they strongly influence the resilience of the built environment. The resilience is the ability of a structural system to advance and absorb potential disruptions, accommodate changes within or around the system and recover its features as soon as

possible after an impact. On the other hand, a non-resilient structure can be classified as a structural system with insufficient level of robustness and/or repairability. The resilience is influenced by (i) the functionality, *i.e.* the level of "performance" of a system or of one or more components, and (ii) the control period, that is the period of time during which the performance of the functionality is estimated in order to calculate the resilience. The functionality can be estimated qualitatively and/or quantitatively, depending on the object of the study and the data and models available.

2.6.1 Resilience of urban systems

Urban resilience is understood as the ability of an urban system and its subsystems to adapt to changing conditions, withstand and rapidly recover from disruptions caused by emergencies. The evolution of urban resilience is a process comprising three main aspects: resistance, recovery and adaptation. A city contains numerous types of physical elements, nonphysical elements and various complex relations among different subsystems. The studies available in literature, focused on resilience quantification, are typically performed from a macroscopic perspective or focused on a limited number of subsystems subject to single disaster. The assessment of urban resilience is quantified through two main methods:

1. Physical resilience approach.
2. Social–economic resilience approach.

The first one focuses on the performance evaluation of physical elements in cities, including individual buildings, urban lifeline facilities and transportation systems. So that it evaluates the recovery of system functions by quantifying the resistance of physical systems [42]-[46].

The other one focuses on nonphysical elements, such as social and economic systems. This method assesses the resilience by quantifying the ability of a community to resume normalcy after disasters [47]-[51].

A resilience triangle was proposed by Bruneau et al. [43] in order to quantify system resilience; the last one was considered influenced by three factors: failure probability, failure consequence and repair time. An Equation was formulated as follows:

$$R = \int_{t_0}^{t_1} [100 - Q(t)] dt \quad (11)$$

in which $Q(t)$ represents the degradation of the system's performance over time, while t_0 and t_1 are the endpoints of the time interval considered. $Q(t)$ can be calculated according to Equation 12:

$$Q(t) = Q_\infty - (Q_\infty - Q_0)e^{-bt} \quad (12)$$

where:

- Q_∞ represents the capacity of the structural system when it is fully functioning.
- Q_0 represents the post-event capacity.
- b is an empirically derived parameter that represents the rapidity of the recovery process.
- t is the post-event time (in days).

The seismic resilience of urban buildings from the perspective of economic loss and recovery time was evaluated by Zeng et al. [52]. The earthquake loss prediction method proposed by FEMA P-58 [53]-[54] was extended from an individual building to a community, in order to provide the economic loss and downtime for quantifying the resilience of the region.

A city-scale time history analysis driven framework for the quantitative evaluation of building seismic resilience and repair scheduling with repair resource constraints was proposed by Xiong et al. [55]. A calculation method for the post-earthquake residual functionality of buildings was included in the framework, based on engineering demand parameters (EDPs) and on a repair scheduling method that considers the recovery process with insufficient repair resources. The framework was investigated in a case study of 68,930 residential buildings in Beijing city.

A resilience index was formulated by Cimellaro et al. [56], according to Equation 13:

$$R_{com} = \int_A \int_{t_{0E}}^{t_{0E}+T_{LC}} Q_{TOT}(\vec{r}, t) / (A_c T_{LC}) dt dr \quad (13)$$

where:

- A_c is the area of the selected region.
- t_{0E} is the time instant when the event occurs.
- T_{LC} is the control time for the period of interest.
- $Q_{TOT}(\vec{r}, t)$ is the global functionality-performance function of the area considered.
- \vec{r} is the spatial vector defining the position.

Different methods were developed for urban resilience quantification, focused on the development of multidisciplinary frameworks, integrating civil engineering and graph theory. Bozza et al. [57] provided a summary of literature review on resilience quantification, as shown in Table 2.2.

Authors	System Model	Resilience Metric
Bruneau et al., 2003 Bruneau & Reinhorn, 2006 Cimellaro et al., 2010a Bocchini & Frangopol, 2011 Dorbritz, 2011	None—the performance curve of the system is studied	Performance-based conceptual framework to quantify resilience as the degradation suffered by the system studied. $R = R$ (robustness, redundancy, resourcefulness, rapidity).
Davis, 2014	None—the performance curve of the system is studied	Theoretical approach to resilience as related to communities through the identification of the water system service categories.
Reed et al., 2009	Power delivery and telecommunication systems modeled as interdependent networked systems	Resilience is quantified as the quality of the system studied
Chang & Shinozuka, 2004	Water system modeled as a networked system	Resilience is quantified as the joint probability of meeting robustness and rapidity standards.
Ouyang & Dueñas-Osorio, 2014	Electric power grids modeled through topological, betweenness,	Technical resilience is computed as the time-dependent annual resilience metric through a probability-based

Ouyang & Dueñas-Osorio, 2012	and direct current power flow models	framework accounting for multiple non-correlated events.
Paredes & Dueñas-Osorio, 2015	Electric power grids and water system modeled as coupled networked lifelines	Resilience is computed according to Ouyang & Dueñas-Osorio (2012)
Mensah & Dueñas-Osorio, 2015	Electric power grids and distributed wind generation modeled as a Bayesian network	Resilience is computed according to Ouyang & Dueñas-Osorio (2012) using Minimum Spanning Trees (MSTs) for distribution networks to reduce computational complexity.
Todini, 2000	Water distribution networks modeled as closed loops	A heuristic approach to compute resilience as the water supply through a vector optimization problem.
Leu et al., 2010 Berche et al., 2009	Transportation networks modeled as complex networks	Resilience is computed as a function of the network connectivity metrics (betweenness, clustering, etc.).
Murray-Tuite, 2006	Transportation networks modeled as graphs	Diverse metrics are used to compute each dimension contributing to resilience (adaptability, safety, mobility, and recovery).
Omer et al., 2009	Telecommunication cable system modeled through a network topology model	Resilience is assessed as a function of the system's power flows.
Miller-Hooks et al., 2012	Freight transportation network modeled as a graph	Resilience is computed as the expected system throughput through a two-stage stochastic program.
Heaslip et al., 2010 Freckleton et al., 2012	None	A methodology is proposed to assess resilience through fuzzy inference systems using a hierarchy of the variables involved: the individual, the community, the economy, and the recovery metrics.
Renschler et al., 2010	Social-physical systems modeled as interacting layers	A holistic framework to quantify resilience as the system quality
Cavallaro et al., 2014 Bozza et al., 2015b Asprone et al., 2013 Franchin & Cavalieri, 2013 Franchin & Cavalieri, 2015	Hybrid social-physical networks modeled as complex networks	Resilience is quantified as the variation in the global efficiency of the network, from the pre-event phase to the final recovery.

Table 2.2: Summary of literature review on resilience quantification [57]

2.6.2 Resilience of infrastructures and structural systems

An infrastructure guarantees the normal operation of a city with significant social functions and economic values. As discussed by Burby et al. [58] the losses due to disasters can be mitigated by avoiding areas with high disaster risks through rational land-use planning. Nevertheless, people settled in high-risk areas of one or more disasters due to the limited land resources available and the widely distributed high risk areas; so that, the most effective way is to improve the resilience of urban infrastructure. According to Bruneau et al. [43] the resilience of community infrastructures to earthquakes can be defined as the ability to absorb a shock if it occurs (with an abrupt reduction of performance) and to recover rapidly after the shock (re-establish normal performance).

A wider definition on disaster infrastructure resilience was provided by Bozza et al. [57], who defined resilience as the ability to anticipate, respond to, adapt to, and recover from a disaster, ensuring a minimum level of service while undergoing changes. In addition, a resilient infrastructure overcomes negative consequences of a disaster and return to normal operations (original state or an adjusted state) as quickly as possible.

Different models were proposed to describe the resilience of urban infrastructures:

- A multicriteria decision-making model for the analysis of planning strategies to reduce future social and economic costs in an area subjected to natural hazards was developed by Opricovic and Tzeng [59].
- An agent-based model of recovery, focusing on the effect of the agents' environments, such as buildings and transportation networks, on their recovery processes was provided by Chang and Miles [60].
- A preliminary agent-based model accounting for homeowners' dynamic interactions with neighbors' activities, such as reconstruction and relocation, was proposed by Nejat and Damnjanovic [61].

The resilience of a structure refers to a building's ability to absorb disturbance from external hazards and its ability to recover the functionality. Several authors addressed this issue, quantifying resilience through indexes or indicators.

As discussed by Marjanishvili and Katz [62], unlike robustness, understood as an absolute property of the system, resilience is a variable property that varies with design decisions; the latter one coincides with the ability of the structure to resist, adapt and recover after an extreme event. The authors identified resilience as inversely proportional to the consequences resulting from the intensity of the given threat.

The assessment of the global and local seismic resilience of the structure was given by Ning and Zheng [63]; the global seismic resilience index of structure was expressed as function of residual seismic capacity ratio, given by the ratio of the residual seismic capacity of the structure under specific damage state to its initial state. In addition, the local structural seismic resilience was expressed as the mean value of the ratio of the seismic capacity of the structure in a certain damage region.

A conventional potential for resilience, dealing with natural hazards (tsunamis), was assessed by Mebarki et al. [64], function of conventional quantitative structural resilience, $F_R(t)$. The last one was given by the ratio between the residual bearing capacity (*i.e.* the maximal tsunami pressure) and the elastic pressure for which the extreme fibre of the structure reaches the yielding stress.

As mentioned above, a non-resilient structure can be classified as a structural system with insufficient level of robustness and/or repairability. The repairability can be expressed as the ability of the structure to be repaired after a damaging event with limited amount of time/costs. This concept is related not only to structural components, but generally to the whole building systems. A damaged structure should be repaired in order to restore it to an original or an acceptable condition and several variables determine the repairability of the structure, such as structural typologies, age of construction, construction technologies, non-structural components. It is possible to relate the repairability measures to the extension of the repair interventions, repair time and repair cost; these are the variables that most influence this parameter. The reparability of buildings damaged after an earthquake/malicious event depends on the assessment of the

safety variation associated with the residual capacity; an estimate of the repair costs to bring the building to its original state and, if necessary, of any retrofit costs to be incurred is also essential.

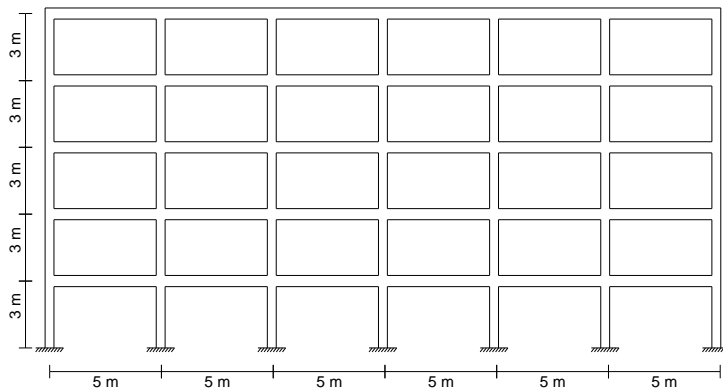
A repairability index for reinforced concrete structural members was proposed by Alarcon et al. [65]; it was based on the fracture and continuum damage mechanics. This index was used to obtain an estimation of the repair limit and the value of damage corresponding to this limit. The repair limit proposed by these authors was an extension of that proposed by Park and Ang [66], Chancellor et al. [67]; in their study they addressed the topic of new class of seismic lateral force resisting systems that sustains little or no damage under severe earthquakes developed, in order to reduce or prevent structural damage to structural elements.

A new method of analysis was proposed by Grigorian [68], in order to prevent the collapse and guarantee self-alignment and repairability to the structure. This method was studied for the structural design of pin-supported rocking wall-moment frames with supplementary devices and post-tensioned stabilizers. This method extended one previously analysed by the same authors [69,70], who proposed a class of free-standing rocking moment frames without wall with the same technical characteristics as those analysed later.

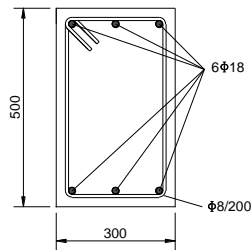
CHAPTER 3 – INFLUENCE OF MATERIAL PROPERTIES ON PROGRESSIVE COLLAPSE RESISTANCE OF RC BUILDINGS UNDER DIFFERENT COLUMN LOSS SCENARIOS

3.1 Characteristics, modelling and analysis of case-study structure

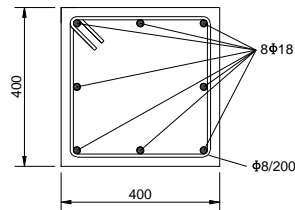
The structure analysed in the first phase of this work is a RC frame building designed only to gravity loads, according to Eurocode 2 [71]. This choice was motivated by the fact that, on one hand, the structure was assumed to be located in a non-seismic region, and on the other, it was selected between those used in previous studies [33,34]. The case-study structure is characterized by a rectangular plan and consists of five floor levels, five primary frames with six bays in the x-direction and seven secondary frames with four bays in the y-direction. Primary frames provide the main support to one-way slabs, according to typical features of European constructions [72]. For this reason, one of those 2D framed systems was extracted from the entire capacity model (Figure 3.1a). Centre to-centre plan dimensions are constant along the building height, with inter-storey height $h_i = 3$ m and the same span length in both directions, *i.e.* $L_x = L_y = 5$ m. Beams are characterized by rectangular cross section (Figure 3.1b), 300×500 mm² in size, and uniform longitudinal reinforcement consisting of 6Ø18 steel bars. Columns have a squared cross section (Figure 3.1c), 400×400 mm² in size, and uniform longitudinal reinforcement consisting of 8Ø18 steel bars. All RC members have the same transverse steel reinforcement made of Ø18 stirrups with 200 mm spacing, as well as a concrete cover set to 40 mm.



(a)



(b)



(c)

Figure 3.1: (a) Reference frame model of the case-study structure; cross sections and reinforcement arrangements of (b) beams and (c) columns

3.2 Capacity and load modelling

In this study, the structural elements were discretized in a number of 3D, inelastic, beam-column fibre elements, able to capture the inelastic behaviour, explicitly including material and geometric nonlinearities, through the finite element code Seismostruct [73]. The use of the fibre approach is due to its capacity to simulate the flexural, arching, and catenary behavioural modes of RC beams, as described by Kunnath et al. [74]. The optimal number of fibre elements for a realistic structural response analysis depends on the shape and materials of the member cross section, as well as the amount of inelasticity

that the member is expected to develop under a given load condition. In this study, each cross section was discretized in 200 fibres and each beam-column fibre element had five integration points. Geometric nonlinearities in the form of both large displacements/rotations and P-Delta effects were considered by means of a total co-rotational transformation [75]. The shear failure mechanism was not assessed for the structure under consideration due to the fact that previous studies [33,34] demonstrated that it was not susceptible to shear.

The mechanical behaviour of materials is described through uniaxial constitutive models: (i) a bilinear hysteretic model with isotropic strain hardening was adopted for reinforcing steel, assuming a hardening ratio $k = 0.01$ and Young's modulus $E_s = 200$ GPa and (ii) an uniform confinement model by Mander et al. [76] was used to simulate the stress-strain behaviour of concrete. Material properties were set as follows:

- Characteristic cylinder compressive strength of concrete $f_{ck} = 20$ MPa.
- Characteristic yield strength of reinforcing steel $f_{yk} = 450$ MPa.
- Design strength of concrete $f_{cd} = 0.85f_{ck}/1.5$.
- Design strength of reinforcing steel $f_{yd} = f_{yk}/1.15$.

The coefficient 0.85 related to design strength of concrete was selected in the interval [0.8,1] allowed by EC2 [71], which accounts for long-term effects of gravity loads on compressive strength.

Gravity loads were uniformly distributed on the structure, according to exceptional combination formulated by UFC Guidelines [30], described by Equation (7) section 2.5.2, with dead and live loads equal to 3 kN/m² and 2 kN/m², respectively. This assumption is motivated by the fact that Eurocode 1 [77] identifies a notional accidental load (clause 3.1) and some design criteria for horizontal ties (annex A, clause A.5), with a view to limit the extent of localized failure. As a result, a load combination (for design of buildings against accidental loads) can be derived only based upon Equation 6.11b of Eurocode 0 (EC0) [78] and the partial safety factors given in table A1.1 of that European code, implying the design load be taken as $D + 0.3L$. Besides this, EC0 allows the safety factors to vary from a country to another according to each specific National Annex, thus

providing a further motivation to the choice of the UFC-compliant design. The latter standard provides specific indications for the analysis of framed buildings under a column-removal scenario and the latest release of the UFC guidelines prescribes a more demanding load combination compared to the current European rules.

3.3 Computational procedure for single-column removal scenarios

In order to obtain the progressive collapse resistance, in this phase of the study, a threat-independent approach was considered. To this aim different column removal scenarios were selected among those shown in Figure 3.2. Corner and central column lines were labelled as 1 and 2, respectively, whereas floor levels from 1 to 4 were denoted as A–D. A selected column was instantaneously removed from the structural model through a special-purpose death element routine that assigned a deactivation time to one or more selected members. The residual (*i.e.*, pre-damaged) structural model dynamically responded to uniformly-distributed downward loads on beams, which were assumed to be the intensity measure (IM) for such an extreme loading condition. The progressive collapse assessment consisted of a single nonlinear time history analysis (NLTHA) performed with a given intensity of gravity loads or an incremental dynamic analysis (IDA), that is characterized by a series of NLTHAs performed with an incremental intensity of gravity loads. A set of 24 IDAs was carried out in order to assess three measures of progressive collapse capacity:

- Maximum multiplier of design load that the residual structure can sustain after column removal, α_{max} , given by the ratio between the maximum load capacity, $Q_{b,max}$, and the design load, Q_{bd} .
- Corresponding vertical drift, $\theta_{Q_{b,max}}$, which turns out to be the chord rotation of beams reached in the transient phase of structural response to the maximum load capacity, $Q_{b,max}$.

- Residual vertical drift, θ_r , which is the vertical drift of beams corresponding to the attainment of the steady-state response to gravity loads.

The vertical drift of beams located directly above the removed column was derived as $\theta = \tan^{-1}(D_v/L_b)$, where D_v is the downward displacement of the residual structure after column removal monitored at the upper joint (control point) of the removed column until system failure is reached, and L_b is the beam length. The vertical drift is an important kinematic variable that allows the characterization of the Vierendeel action that develops in the framed structure subjected to column removal [79,80].

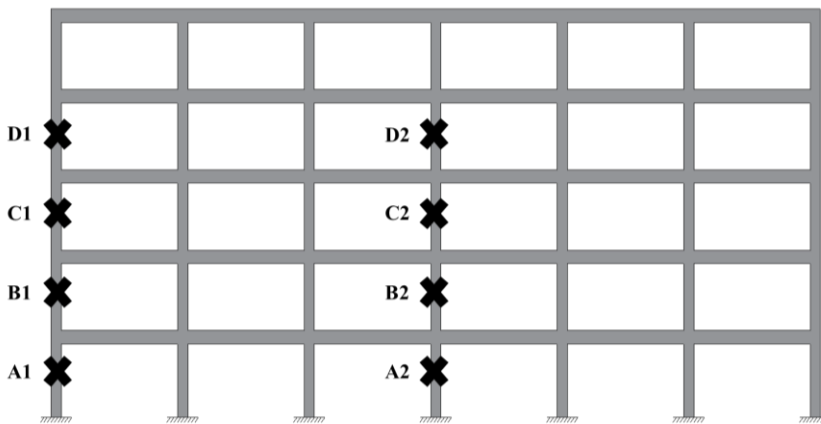


Figure 3.2: Column designation involved in single removal scenarios

3.3.1 Sensitivity of progressive collapse measures to capacity modelling properties

In the first step of the work, the sensitivity of progressive collapse measures to capacity modelling properties, both mechanical and geometric, was investigated. Progressive collapse analysis was performed for three different values of ultimate steel strain, ε_{st} ; the last one was set equal to 4%, 10% and 20%. This choice was due to the fact that the actual ultimate elongation of modern steel bars is never equal to 4%, but this conventional strain limit for the EC2-conforming building class is taken into account for

potential comparisons with other studies in which the actual elongation capacity of reinforcing steel was not fully exploited in progressive collapse simulations [33,34]. By contrast, the highest value assigned to ε_{su} provides a more realistic quantification of the fracture steel strain, in line with several studies available in the literature [81,82]. Subsequently, based on previous analysis results, the ultimate steel strain was set to 20% and the sensitivity of maximum drift demand, $\theta_{max,Qbd}$, to capacity model properties was assessed. The variation of five key model properties was considered: (i) the compressive strength of concrete, f_c , (ii) the yield strength of steel reinforcement, f_y , (iii) the span length of primary beams, L_x , (iv) the span length of secondary beams, L_y , and (v) the longitudinal reinforcement ratio of primary beams, ρ . Their statistics were defined according to a modern RC building class of interest; three statistical values, $\mu - \sigma$, μ and $\mu + \sigma$ were assigned to those properties. The mean, μ , and coefficient of variation (CoV) of the capacity model properties are shown in Table 3.1. Those statistics were extracted or derived from other studies available in the literature, except for the mean compressive strength of concrete that was assumed to be $f_{cm} = f_{ck} + 8$ according to EC2 [71]. It is noted that the selection of less than 10 model variables in progressive collapse sensitivity/fragility analysis is consistent with past investigations by other researchers, for example a study by Yu et al. [86].

Category	Item	Property	μ	CoV	Sources
Material	Concrete	f_c	28 MPa	10%	[71,83]
	Steel	f_y	500 MPa	10%	[83,84]
Geometry	Beam	L_x	5 m	20%	[85]
		L_y	5 m	20%	[85]
	Reinforcement	ρ	1%	5%	[34,35]

Table 3.1: Mean and coefficient of variation of capacity model properties

3.3.1.1 Influence of ultimate steel strain

As discussed above, the first group of analysis was carried out to evaluate the influence of ultimate steel strain on the progressive collapse capacity measures. The analysis

results are collected in Table 3.1, that outlines the selected capacity measures and corresponding failure conditions under varying ε_{su} and column-removal scenario. The maximum load capacity, $Q_{b,max}$, is expressed in percentage of design load and its sensitivity to ultimate steel deformation appears to be significant. Indeed, an increase of ε_{su} from 4 to 10% produced an increase in load capacity ranging from 38% (scenario B2) to 51% (scenario D1) of design load, and hence a percentage increase ranging from 44 to 71%. An increase of ε_{su} from 4 to 20% produced an increase in load capacity ranging from 53% (scenario B2) to 78% (scenario D1) of design load, and hence a percentage increase ranging from 61% to 108%. The highest increase factors were associated with corner column-removal scenarios, regardless of the floor level. The mean of $Q_{b,max}$ for ε_{su} set to 4%, 10%, and 20% was respectively equal to 78, 124, and 141%, with small dispersion levels reflected by CoV equal to 10% and 5%. This highlights the importance of assuming appropriate strain limits for steel reinforcement when progressive collapse resistance of RC framed buildings is assessed.

As regards the drift capacity at maximum resistance, $\theta_{Q_{b,max}}$, an important sensitivity to ε_{su} was found, with mean equal to 1, 3, and 9%, and CoV equal to 11, 30, and 29%, for the same values of ultimate steel strain. In that respect, assuming $\varepsilon_{su} = 20\%$ induced a significant increase in drift capacity when either the corner or central column at floor level 4 was removed, as shown by numerical results related to scenarios D1 and D2 in Table 3.2.

When ε_{su} was assumed to be 4% and a column was removed, the vertical drift corresponding to $Q_{b,max}$ first reached a peak and then reduced to a residual level. For instance, if scenario B2 is considered, the peak vertical displacement of the control point of the reference frame model was $D_{v,Q_{b,max}} = 47.27$ mm. Given that the span length of primary beams was $L_b = L_x = 5$ m, the peak vertical drift turned out to be $\theta_{Q_{b,max}} = \tan^{-1}(D_{v,max}/L_b) = 0.95\%$, which matches with the value in Table 3.2. On average, the residual drift was 89% of the maximum drift. Conversely, when ε_{su} was set to 10% or 20%, the vertical drift corresponding to $Q_{b,max}$ gradually increased over time until collapse, resulting in residual drifts equal to maximum drifts (irrespective of the scenario

under consideration). When ε_{su} was set to 4%, $Q_{b,max}$ was found to be 72% and 84% in the case of scenarios A1 and A2, respectively. Approximately the same capacity estimates were found when considering the corresponding scenarios at upper floor levels. Indeed, the mean load capacity over all corner column-removal scenarios was equal to 71% ($CoV = 2\%$), while that related to all central scenarios is equal to 86% ($CoV = 2\%$). Nonetheless, when the ultimate steel strain was increased up to 20%, a slightly higher influence of floor location was observed, evidencing the highest load capacity in the case of column removal at floor 4. As expected, such an outcome is motivated by a cumulative effect of gravity loads on nonlinear dynamic response of the residual structure, which increased as the location of the removed column moves from the upper floors to the ground floor. Similar considerations could be made in terms of maximum drift capacity, which however reduced from corner to central column-loss scenarios. The results of the column removal scenarios showed a greater influence of capacity measures to the location of the removed column rather than in elevation. To this aim the drift time histories of Figures 3.3 and 3.4. are associated with scenario A1, related to a corner column, and scenario A2, related to a central column. The images show that if the ultimate steel strain was set to 4% the dynamic response was characterized by a transient phase in which the vertical drift increased up to a peak level and then gradually reduced, oscillating around an ideal “damping” curve until a steady-state (residual) drift was attained. If ε_{su} was set to 10% or 20%, the drift time history degenerated in a monotonically increasing curve as Q_b approaches $Q_{b,max}$.

An overall view on the sensitivity of progressive collapse capacity to ultimate steel strain and location of the removed column was provided by IDA curves shown in Figure 3.5. The last one shows that the curves appear to be rather linear if $\varepsilon_{su} = 4\%$; this indicates that the ductile response of individual fibres does not necessarily produce a significantly nonlinear response of the entire structure. When ε_{su} increased to 10%, the global nonlinearity effects became more significant, leading to a strong amplification of both load and drift capacities. As ε_{su} was further increased to 20%, the catenary action of beams above the removed column played a key role in the progressive

collapse capacity of the RC structure. In those conditions, the vertical drift capacity drastically increased, resulting in ultimate drift levels that were consistent with experimental tests [87].

ε_{su}	Scenario	α_{max} (%)	θ_{Qbmax} (%)	θ_r (%)
4%	A1	72	1.1	0.97
	A2	84	0.9	0.86
	B1	70	1.08	0.94
	B2	87	0.95	0.94
	C1	70	1.11	0.96
	C2	84	0.88	0.75
	D1	72	1.15	0.98
	D2	88	0.89	0.76
10%	A1	118	4.32	4.32
	A2	123	2.11	2.11
	B1	115	3.57	3.57
	B2	125	2.24	2.24
	C1	120	4.29	4.29
	C2	130	2.86	2.86
	D1	123	4.34	4.34
	D2	134	2.38	2.38
20%	A1	134	9.26	9.26
	A2	140	6.87	6.87
	B1	135	8.67	8.67
	B2	140	8.22	8.22
	C1	135	8.94	8.94
	C2	140	5.89	5.89
	D1	150	14.74	14.74
	D2	150	10.63	10.63

Table 3.2: Progressive collapse measures of the case study structure under varying ultimate steel strain and column-removal scenario

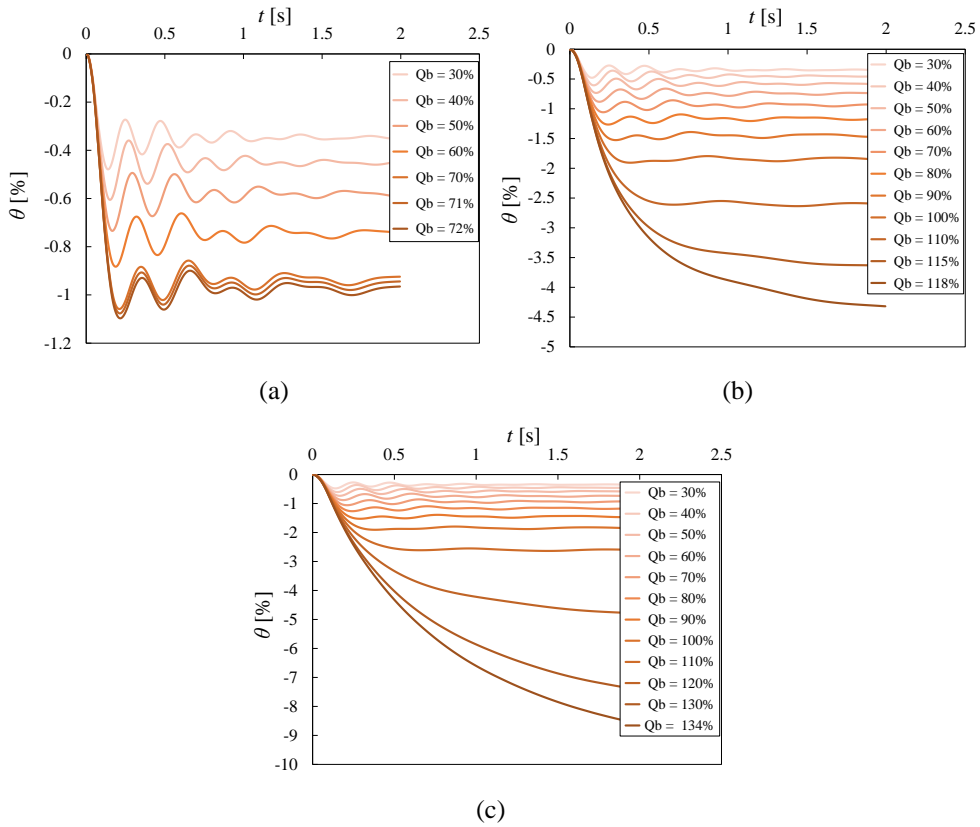


Figure 3.3: Drift time histories under column-removal scenario A1: (a) $\epsilon_{su} = 4\%$, (b) $\epsilon_{su} = 10\%$, (c) $\epsilon_{su} = 20\%$

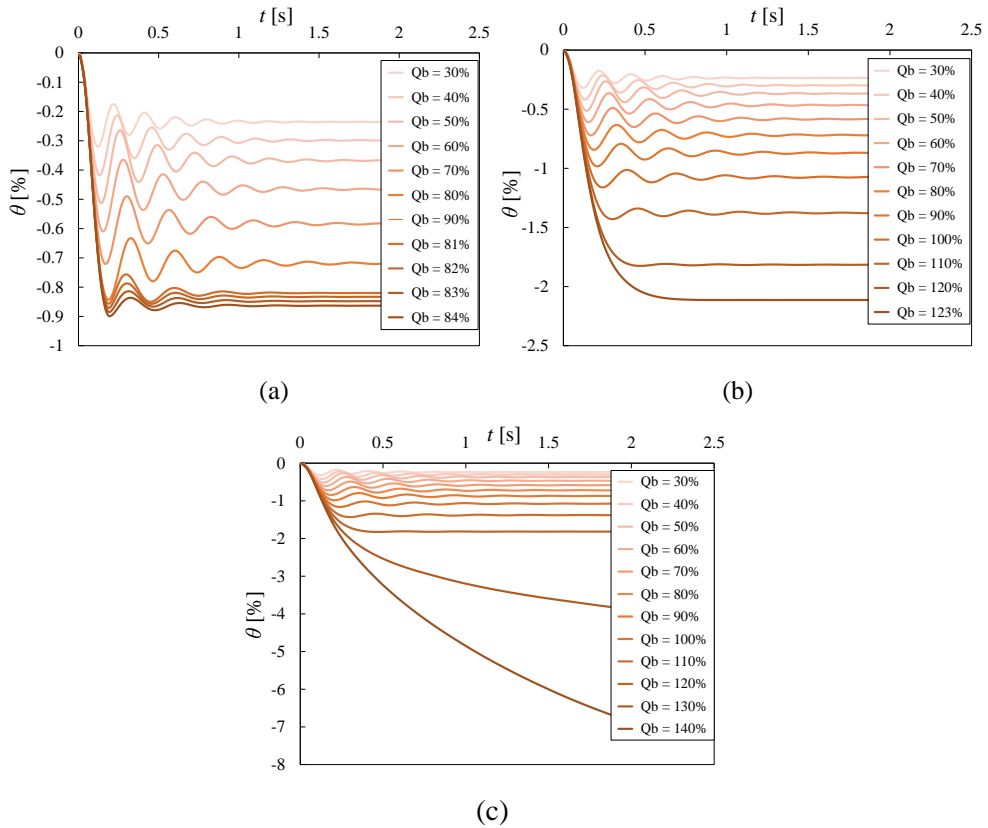


Figure 3.4: Drift time histories under column-removal scenario A2: (a) $\epsilon_{su} = 4\%$, (b) $\epsilon_{su} = 10\%$, (c) $\epsilon_{su} = 20\%$

Chapter 3- Influence of material properties on progressive collapse resistance of RC buildings
under different column loss scenarios

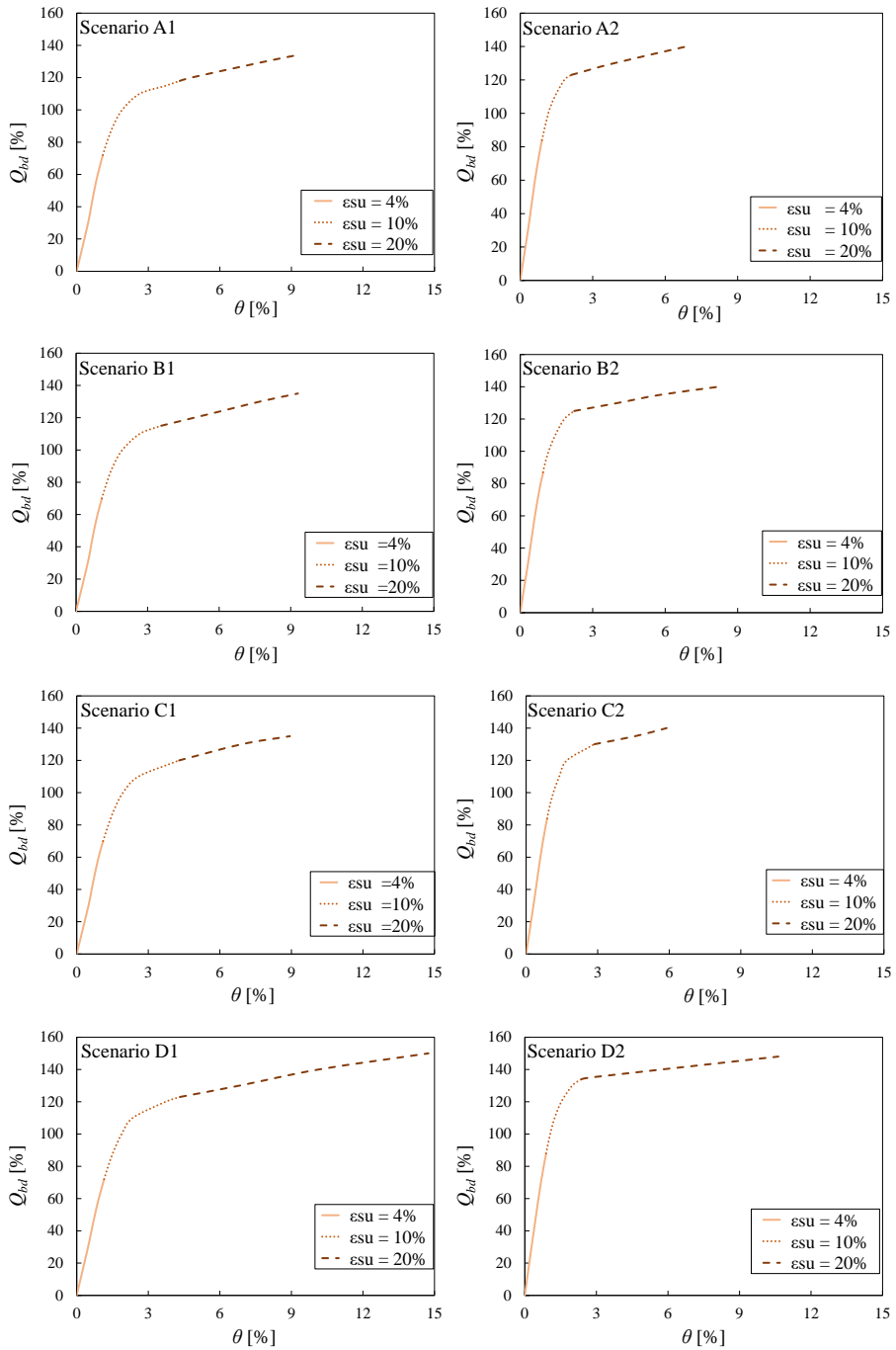


Figure 3.5: IDA curves under varying column-removal scenario

3.3.1.2 Influence of material strengths and geometric properties

Based on previous analysis results, the ultimate steel strain in the reference capacity model was set to 20% for the following phase. As discussed above, five key model properties were selected and the influence of their variation on progressive collapse capacity measures was assessed. The sensitivity of maximum drift demand $\theta_{max,Qbd}$ to the capacity model properties was investigated; this is due to the fact that vertical drifts of beams are key measures for damage analysis of framed structures subjected to a column-loss. Structural demand was assessed through a single-run NLTHA, assuming a design load Q_{bd} and by varying the value of a capacity model property at a time. The five properties and their statistics are shown in Table 3.3.

This outlines the maximum drift demands on the reference capacity model and their values as the capacity model properties and column-removal scenario varies. Except for scenarios C2 and D2 (*i.e.*, central column removed at floor level 3 or 4), drift demand was not significantly influenced by concrete strength. This is due to the fact that in these two scenarios the reduction of this parameter led to a decrease of the vertical equal to or greater than 10% compared to the case where the structure is considered with the average value of f_c . In the other scenarios, in fact, reductions of less than 10% were observed, thus negligible. By contrast, the other model properties had a strong impact for all column-removal scenarios, with the exception of scenario D1. The reduction of f_y and ρ had a fatal effect, resulting in the loss of system balance under design load, and hence progressive collapse of the framed structure (symbol C in Table 3.3). The same outcome was found when either L_x or L_y increased from 5 to 6 m. In the former case, both gravity loads and vertical flexibility of primary beams drastically increased. The increase in f_y induced a significant drop in drift demand on beams, ranging in the interval [32%, 61%] with mean equal to 45% and $CoV = 24\%$ over all scenarios. Mean and CoV of drift demand reduction were found to be lower than above, that is, 13 and 23%, when ρ was set to its upper bound. Nonetheless, the maximum beam drift drastically decreased

especially when either L_x or L_y were reduced. Indeed, the highest sensitivity level was found in relation to the span length of primary beams, the reduction of which induced a demand drop ranging from 89% to 92%, with mean equal to 91% and $CoV = 1\%$. The reduction of L_y from 5 to 4 m caused a demand drop between 72% and 85%, with mean equal to 77% and $CoV = 7\%$.

Scenario			A1	A2	B1	B2	C1	C2	D1	D2
Property	Value		$\theta_{max,Qbd} [\%]$							
μ			-8.60%	-6.87%	-8.67%	-6.84%	-8.27%	-6.15%	-12.75%	-8.25%
f_c [MPa]	$\mu-\sigma$	25.2	-8.30% [-3%]	-6.76% [-2%]	-8.36% [-4%]	-6.26% [-8%]	-7.97% [-4%]	-5.56% [-10%]	C C	-7.14% [-13%]
f_y [MPa]	$\mu-\sigma$	450	C	C	C	C	C	C	C	C
L_x [m]	$\mu-\sigma$	4	-0.85% [-90%]	-0.62% [-90%]	-0.89% [-90%]	-0.62% [-91%]	-0.92% [-89%]	-0.61% [-90%]	-1.10% [-91%]	-0.63% [-92%]
L_y [m]	$\mu-\sigma$	4	-1.27% [-85%]	-1.50% [-78%]	-2.43% [-72%]	-1.45% [-79%]	-2.34% [-72%]	-1.43% [-77%]	-3.59% [-72%]	-1.48% [-82%]
ρ [%]	$\mu-\sigma$	0.96	C	C	C	C	C	C	C	C
Scenario			A1	A2	B1	B2	C1	C2	D1	D2
Property	Value		$\theta_{max,Qbd} [\%]$							
μ			-8.60%	-6.87%	-8.67%	-6.84%	-8.27%	-6.15%	-12.75%	-8.25%
f_c [MPa]	$\mu+\sigma$	30.8	-8.34% [-3%]	-6.63% [-3%]	-8.45% [-3%]	-6.53% [-5%]	-8.07% [-2%]	-5.77% [-6%]	-12.28% [-4%]	C C
f_y [MPa]	$\mu+\sigma$	550	-5.44% [-37%]	-3.42% [-50%]	-5.51% [-36%]	-3.33% [-51%]	-5.10% [-38%]	-2.37% [-61%]	-8.65% [-32%]	-3.62% [-56%]
L_x [m]	$\mu+\sigma$	6	C	C	C	C	C	C	C	C
L_y [m]	$\mu+\sigma$	6	C	C	C	C	C	C	C	C
ρ [%]	$\mu+\sigma$	1.04	-7.63% [-11%]	-5.83% [-15%]	-7.76% [-10%]	-5.73% [-16%]	-7.38% [-11%]	C	-11.60% [-9%]	-6.97% [-16%]

Table 3.3: Sensitivity analysis results

3.4 Proposal of performance limit states for progressive collapse analysis

The safety assessment of a structure that may suffer progressive damage or even collapse after a column failure should rely upon a clear and mechanics-based definition of

performance limit states. In this respect, there are studies available in literature that proposed some sets of two/three limit states and developed fragility curves for progressive collapse risk analysis [33, 34,86]. Nonetheless, the definition of conditional limit states for such a load situation, and particularly for European structures, is still far from being generally shared by the scientific community in view of codification. In the light of this, the next step of this work focused on the definition of performance limit states for progressive collapse analysis.

3.4.1 Definition of performance limit states

Five progressive collapse limit states were considered in this study; their relevant damage levels, items checked during structural analysis, damage measure (DM) variables and thresholds are shown in Table 3.4. A vector-valued DM was used to capture the attainment of Limit state (LS1), Limit State 3 (LS3) and Limit State 5 (LS5), whereas a scalar DM allowed the achievement of LS2 and LS4 to be identified. Axial strains and vertical drifts of beams were monitored. The description and achievement of the limit states are shown in Figure 3.6. In detail, LS1 was assumed to be reached when either the maximum steel strain $\varepsilon_{s,max}$ attained the yield steel strain ε_{sy} or the maximum strain in the concrete cover $\varepsilon_{c,max}$ reached the unconfined concrete strain at peak strength ε_{cp} . The yield strain of reinforcing steel was set to $\varepsilon_{sy} = f_y/E_s$, whereas ε_{cp} was defined according to Mander et al. [76]. Limit State 2 (LS2) was assumed to occur when θ reached a threshold value θ_m , which was set to 0.50% according to past experimental and numerical studies [33, 34, 88, 89, 90]. A vector-valued DM composed of $\varepsilon_{c,max}$ and $\varepsilon_{cc,max}$, the latter being the maximum strain in the concrete core (*i.e.*, in confined concrete), was also used to capture the attainment of LS3. That damage level was assumed to be reached when either $\varepsilon_{c,max}$ attained the ultimate strain ε_{cu} in the concrete cover (*i.e.*, in unconfined concrete) or $\varepsilon_{cc,max}$ achieved the confined concrete strain at peak strength ε_{ccp} . This last mechanical property was basically assumed to be the same for both confined and unconfined concrete, hence $\varepsilon_{cp} = \varepsilon_{ccp}$. Limit State 4 (LS4) was associated with concrete

core crushing, which was tagged when $\varepsilon_{cc,max}$ attained the ultimate strain of confined concrete ε_{ccu} . The latter property was defined in line with Mander et al. [76]. LS5 was introduced in this study to identify the occurrence of a damage level realistically associated with a progressive collapse phenomenon. It was assumed to be caused by (a) tensile fracture of longitudinal steel bar (*i.e.*, $\varepsilon_{s,max} = \varepsilon_{su}$), (b) ultimate vertical drift of a beam in floor areas above the removed column (*i.e.*, $\theta = \theta_u$), (c) loss of system equilibrium or (d) loss of numerical convergence. Therefore, a vector-valued DM composed of $\varepsilon_{s,max}$ and θ was used in combination with some measures of system stiffness and numerical solution. It is noted that $Q_{b,LS}$ turned out to be $Q_{b,max}$ when LS5 was considered. It is also emphasized that, in conventional structural safety assessments under ordinary (rather than abnormal) loads, the ultimate limit state can be associated with either LS4 or LS5. By contrast, in progressive collapse analysis, LS5 occurs distinctly after LS4. This is motivated by the fact that LS4 is related to a compressive arch stage of beams, whereas LS5 is associated with a catenary resisting mechanism of beams.

Limit state	Item	DM variable	DM threshold	Treshold value [%]
LS1	Reinforcement	$\varepsilon_{s,max}$	$\varepsilon_{s,y}$	0.25
	Concrete cover	$\varepsilon_{c,max}$	ε_{cp}	0.23
LS2	Beam	θ	θ_m	0.50
LS3	Concrete cover	$\varepsilon_{c,max}$	ε_{cu}	0.35
	Concrete core	$\varepsilon_{cc,max}$	ε_{cep}	0.23
LS4	Concrete core	$\varepsilon_{cc,max}$	ε_{ccu}	0.87
LS5	Reinforcement	$\varepsilon_{s,max}$	ε_{su}	20
	Beam	θ	θ_u	15

Table 3.4: Items, variables and thresholds of performance limit states

Limit State 1 (Slight damage)	Minor concrete cracking or steel yielding in critical portions of beams located in floor areas above the removed column, allowing immediate occupancy of the building after slight structural repair
Limit State 2 (Moderate damage)	Moderate cracking of concrete cover in the abovementioned beams, resulting in the need for moderate repair of critical portions of beams
Limit State 3 (Significant damage)	Concrete spalling and concrete core's cracking onset in critical portions of the abovementioned beams, resulting in low safety for building occupants and need for major structural repair
Limit State 4 (Extensive damage)	Crushing of concrete core in critical portions of beams located in floor areas above the removed column and slight-to-moderate repair of remaining beams, calling for extensive repair in both structural and non-structural components (e.g., infill walls)
Limit State 5 (Collapse)	Performance level that identifies the partial or total collapse of the building structure

Figure 3.6: Definition of performance limit states

3.4.2 Sensitivity analysis of limit state capacity

Nonlinear time histories analyses were performed to evaluate the residual capacity of the case-study framed structure after column removal, for each limit state of interest. The first group of analysis was carried out on the reference capacity model with the mean properties, *i.e.* their values were set equal to μ . The results were collected in terms of limit state load multiplier, α_{LS} , and they are shown in Table 3.5 for each column removal scenario. The limit state load multiplier corresponds to the percentage of the design load of reaching each limit state. As sake of example, when a corner column was removed (scenario A1) the load capacity withstands by the structure was equal to 40% of design load for limit state 1; on the other hand, this limit state was reached with 50% of the design load when a central column was removed (scenario A2). So that the corner column-loss scenarios (A1, B1, C1 and D1) are more critical than their central counterparts, resulting in lower levels of load capacity.

From LS2 and LS3 the capacity increased by 20%, with the exception of scenario D2 that caused a 30% increase in α_{LS} . A load capacity irrelevance to the column-removal

scenarios at floor levels 1 and 2 was found for scenario LS4. By contrast, corner scenarios were again more critical than central scenarios when a column was removed at floor levels 3 and 4 (scenarios C and D), reflecting a 12–15% difference between their load capacities. Similar results with higher capacity levels were found in the case of LS5.

Limit state	Scenario							
	A1	A2	B1	B2	C1	C2	D1	D2
	α_{LS} (%)							
LS1	40	50	40	50	40	50	40	50
LS2	60	70	60	70	60	70	60	70
LS3	60	70	60	70	60	70	60	80
LS4	120	120	120	120	125	137	125	140
LS5	134	140	135	140	135	140	150	150

Table 3.5: Limit state load multiplier under varying column-removal scenario

Whereas the results show an higher sensitivity to the in-plan location of column-removal scenarios rather than the floor level where this initial damage may occur, a subset of NLTHAs corresponding to scenarios A1 and A2 was selected. The second group of analysis was carried out in order to identify the influence of the five key model properties, already discussed before, on load capacity corresponding to each limit state. For a faster understanding, the results were collected in terms of tornado diagrams, that show the sensitivity of an output variable (here generally denoted as R) to a set of input variables (here generally denoted as v) by ordering the latter from the top to the base as their bar length (*i.e.*, swing) reduces. Such diagrams are common and effective tools in decision analysis, as evidenced by Porter et al. [91] who assessed the sensitivity of seismic loss estimates for buildings. Tornado diagrams are also used in previous sensitivity analyses by, among others, Kim et al. [92] and Yu et al.[86]. For this study the tornado diagrams were developed in terms of percentage variations of load capacity, $\Delta_{Qb,LS}$, with respect to their values associated with mean model properties. In this way it was possible to identify the possible asymmetric variations in load capacity that may arise from the same positive and negative variations in capacity model properties.

Tornado diagrams are shown in Figure 3.7 and Figure 3.8; these underline that three properties mostly influence the limit state load capacity, *i.e.* f_y , L_y and L_x . Specifically, as L_x and L_y were reduced, the load capacity of the residual structure increased and such a beneficial effect is higher in central column-loss scenarios. The reduction of f_y had a negative impact on load capacity, particularly for limit states associated with slight/moderate and extensive/collapse damage levels. Therefore, concrete crushing in the cover or core of beam cross sections (*i.e.*, LS3) appeared to be insensitive to variations in yield steel strength. Also f_c had no influence on load capacity at LS1 and LS2, because those limit states were associated with flexural behaviour of beams. A relative influence of this property increased when a significant or extensive damage level (*i.e.*, LS3 or LS4, respectively) was considered, being they roughly associated with the activation of compressive arch action in beams above the removed column. Finally, the catenary action of beams, which was exploited when an extensive damage level or collapse was reached, depends on both ρ and f_y .

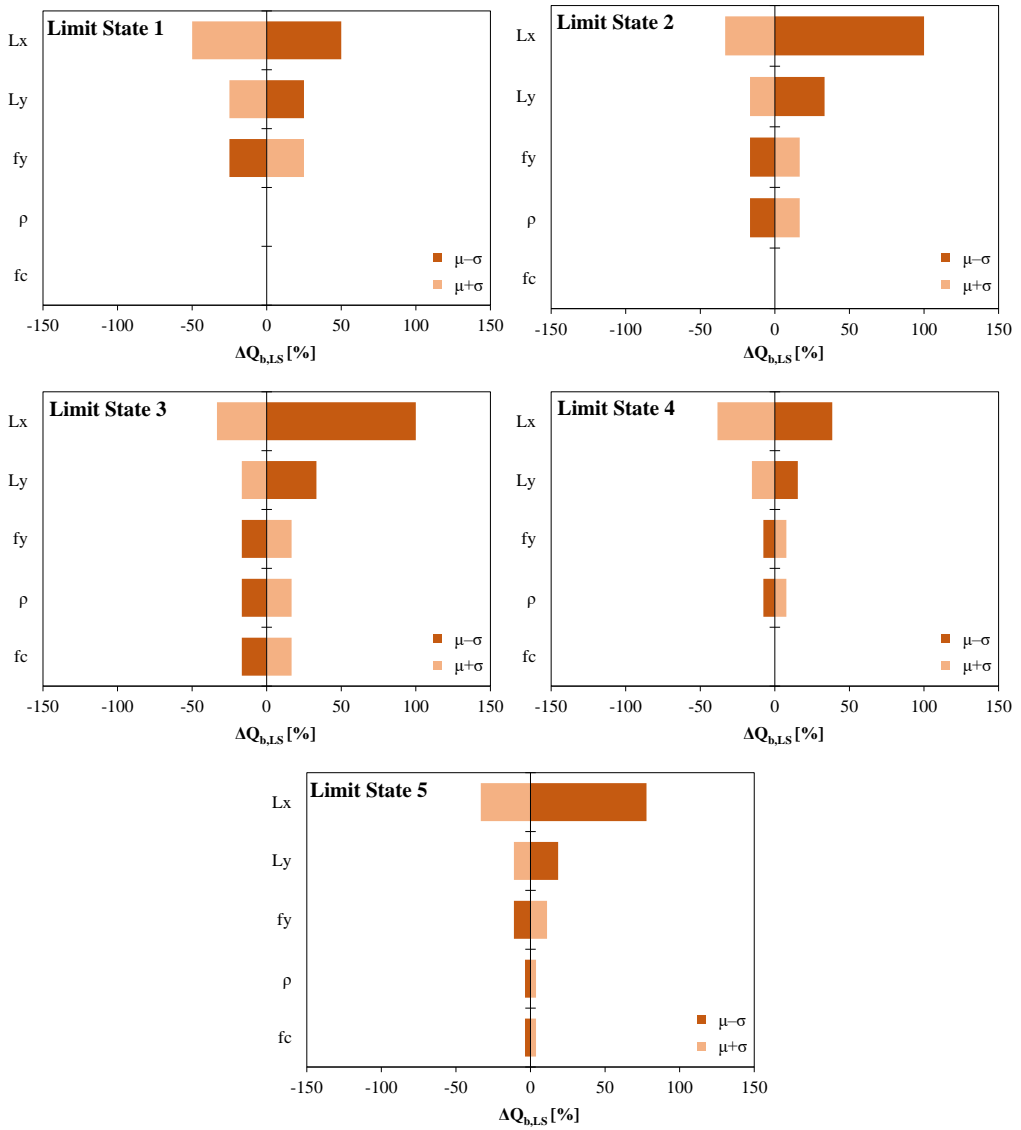


Figure 3.7: Tornado diagrams for scenario A1

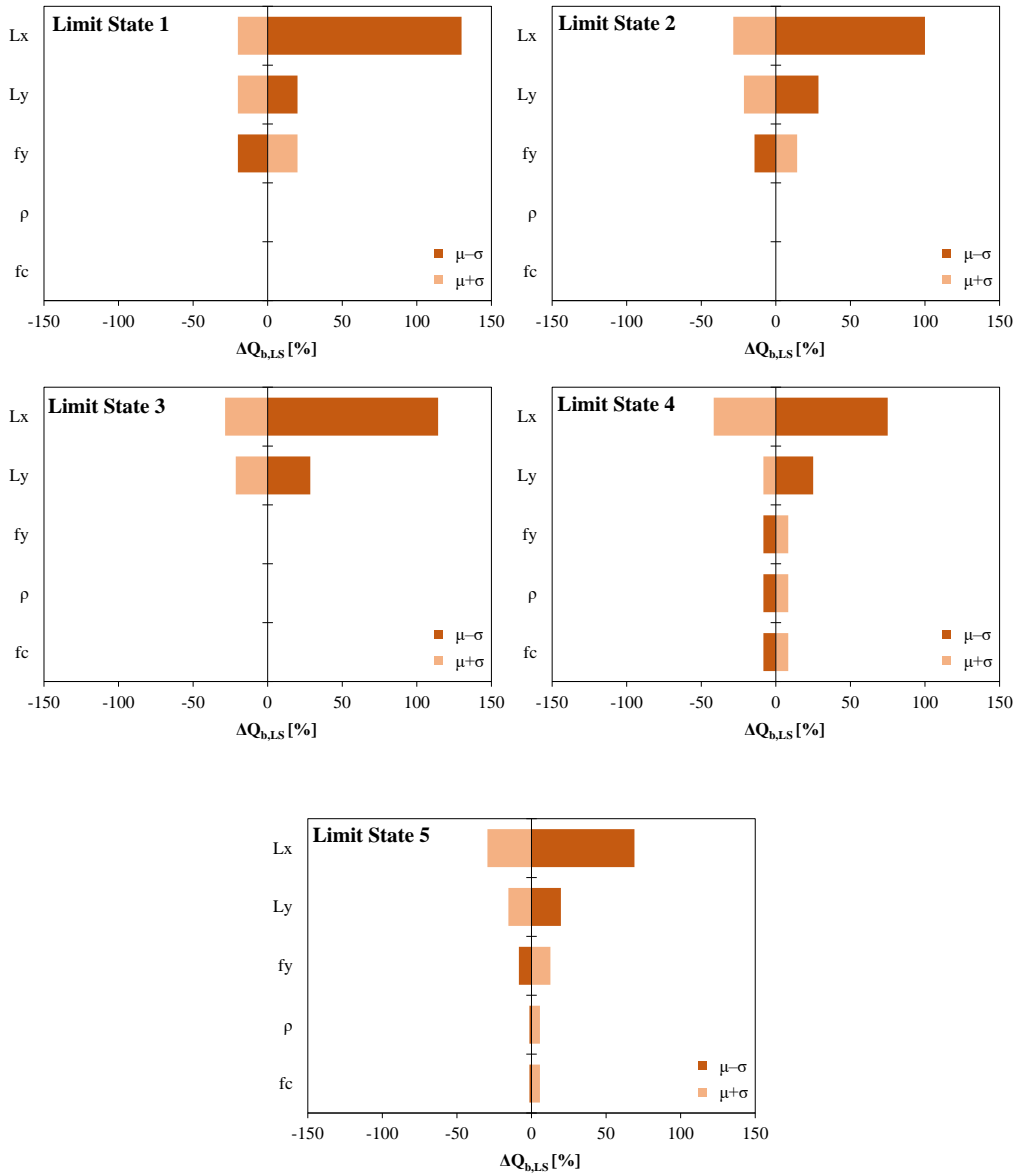


Figure 3.8: Tornado diagrams for scenario A2

3.5 Computational procedure for multiple-column removal scenarios

Once evaluated the structure behaviour after a single column removal, the next step was addressed towards a multiple columns removal, in order to assess the influence of the location of the removed columns and their deactivation time on progressive collapse capacity of the structure. To this end nonlinear time histories analysis were performed for the case study structure. Previous analyses showed greater variability in results for removal of columns in plan rather than in elevation, so this next step was performed only for ground floor columns. This is also consistent with what might actually happen, considering for example an extreme action such as impact. Figure 3.9 shows the denomination of the columns, different from the previous case. The columns were progressively numbered from the left- to the right-hand side of the frame from A1 to A7. The assessment of progressive collapse resistance for multi-column loss scenarios is represented in Figure 3.10. First of all different scenarios, involving couples of columns, A_i and A_j , were selected; two different column removal types were chosen:

- Simultaneous loss of columns, with $t_{di} = t_{dj} = 10^{-2}$ s.
- Sequential loss, with different values of deactivation times.

The last one was implemented by removing the column A_i (or A_j) at $t_d = 10^{-2}$ s and column A_j (or A_i) at either 10^{-1} s or 1 s. This produced sequential losses in which the second column was removed after a time lag $\Delta t_d = |t_{di} - t_{dj}| = 9 \cdot 10^{-2}$ s or $\Delta t_d = 9.9 \cdot 10^{-1}$ s. The control point of the analysis was variable according to the scenario considered, as it was coincident with the one of the beam-column joints located on top of the removed columns. The results of NLTHA analysis were collected in terms of: (i) maximum vertical displacement $D_{v,max}(\alpha_i)$ associated with the given load multiplier α_i on the displacement time history and (ii) maximum vertical drift of beam(s) having one end joint adopted as control point. The vertical drift was expressed according to the following Equation:

$$\theta = \tan^{-1}(D_v(t) / L_b) \quad (14)$$

where L_b is the beam span length, as in the previous analysis, and it turns to be the chord rotation of the beam(s). The failure occurred when one of this conditions was reached: (1) achievement of $\varepsilon_{su}=20\%$ in a beam or (2) $\theta_u = 15\%$, which was approximately a mean collapse drift of RC sub-assemblages tested in past experimental studies [87], (3) loss of system equilibrium, which produced divergence of drift time history and (4) loss of numerical convergence. In correspondence of such step, two alternatives were possible: if none of the failure conditions was attained, inertia masses were increased by a multiplier $\alpha_{i+1} = \alpha_i + \Delta_\alpha$ where Δ_α indicates the mass increment and some stages were repeated, according to the flowchart (Figure 3.10); on the other hand, if a failure condition was reached, the IDA curves were plotted. These represent the relation between Q_b (or α) and $D_{v,max}$ (or $\theta = \max \theta (t)$). The assessment of progressive collapse capacity was, then, repeated over the total number of prescribed column-loss scenarios, column-removal types and control points. In the next sections the analysis are described; each scenario was labelled according to the couple of columns A_i-A_j (with $j > i$), while the control point was tagged through a frame node N_k or N_m , (with $k = i + 7$ and $m = j + 7$, where 7 indicates the number of column lines). The variation of the column deactivation time produced 24 column removal scenarios as discussed subsequently.

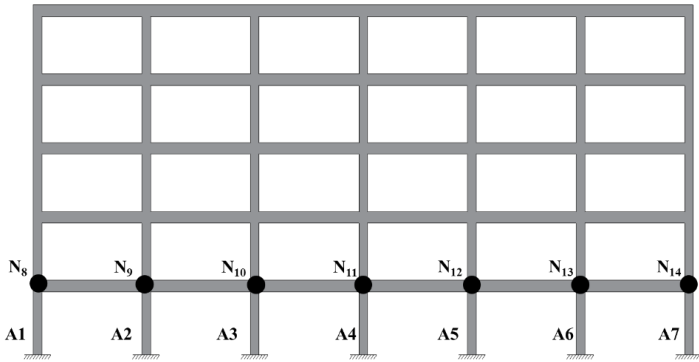


Figure 3.9: Designation of columns and frame nodes (control points) involved multiple column removal scenarios

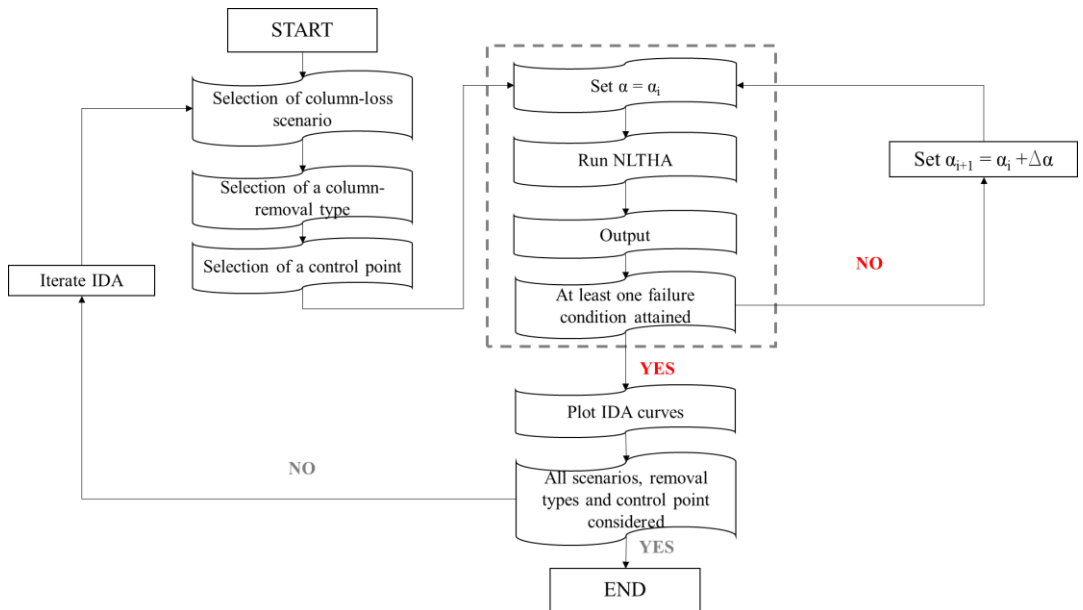


Figure 3.10: Flowchart of progressive collapse evaluation under multi-column loss scenarios

3.5.1 Structural response to simultaneous removal scenarios

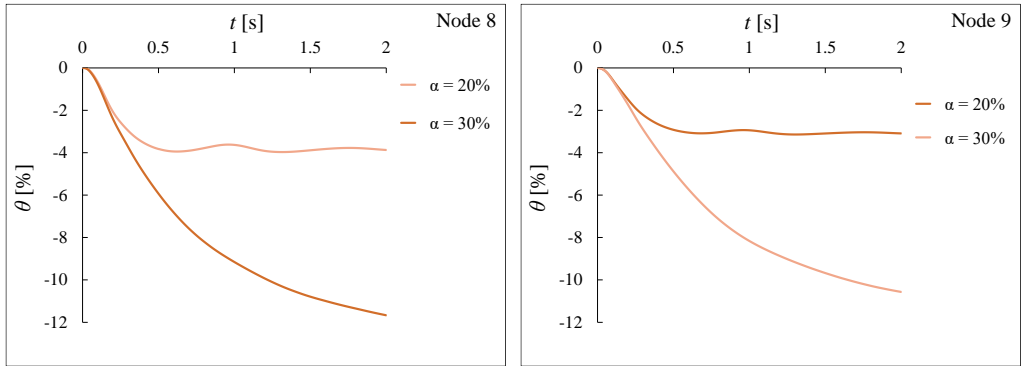
As discussed above, the influence of simultaneous removal scenarios on progressive collapse capacity of the structure was assessed. Nonlinear time history analysis were carried out for 12 scenarios, due to the symmetry of the structure. Each scenario involved two columns, A_i and A_j , and these were removed with $t_{di} = t_{dj} = 10^{-2} s$ and the results were collected in terms of α_{max} and θ_{max} . Table 3.6 shows that the scenario involving a couple of columns, one located in the corner of the structure and the adjacent one (*i.e.* scenario A1-A2) came out to be the worst one, in terms of maximum multiplier of design load. In that case, the structure was able to withstand only 30% of design gravity load on beams; it increased to 61% and 63% when the removal scenarios involved columns A2-A3 and A3-A4. On the other hand, the scenario A1-A2 was characterized by the largest vertical drifts. The highest level of progressive collapse resistance was found when the opposite columns were removed, *i.e.* scenario A1-A7, and it was 1.4 times the design loads. The same result was obtained for scenario A2-A6, that involved the sudden removal of opposite inner columns located close to corner columns. On the other hand, the maximum drift reached by the structure at the location of removed columns reduced from 11.37% to 8.31%, with a percentage drop of 27%. A mean load capacity, equal to 134% of design loads, was found for the scenarios involving a corner column and an internal one or a couple of internal columns; in that case the vertical drift capacity was found to have a mean value of 7.01%. The lowest values of vertical drifts was found for scenario A2-A4, as shown in Table 3.6. The results also underlined that the simultaneous removal of a corner column (A1) and any internal column produced the highest sensitivity of the vertical drift to the control point. Figure 3.11 shows the drift time histories of three scenarios, as the control point changes. These one identify three different situations: the removal of (i) a corner column and the following column (Figure 3.11a), (ii) a corner column and a central one (Figure 3.11b) and (iii) two opposite corner columns (Figure 3.11c). In addition, these scenarios are related with the minimum load capacity, the highest sensitivity of drift capacity to the control point and

the maximum load capacity, respectively. Figure 3.12 and Figure 3.13 show the IDA curves related to simultaneous removal scenarios: the first one is related to those involving a corner column and an internal column or opposite corner columns, while the other one to the removal of two internal columns. For scenarios A1-A2, A1-A7 and for any scenario involving two internal columns, the two curves are overlapping; this implies that these combinations of removed columns had a negligible sensitivity of the incremental dynamic response to the control point.

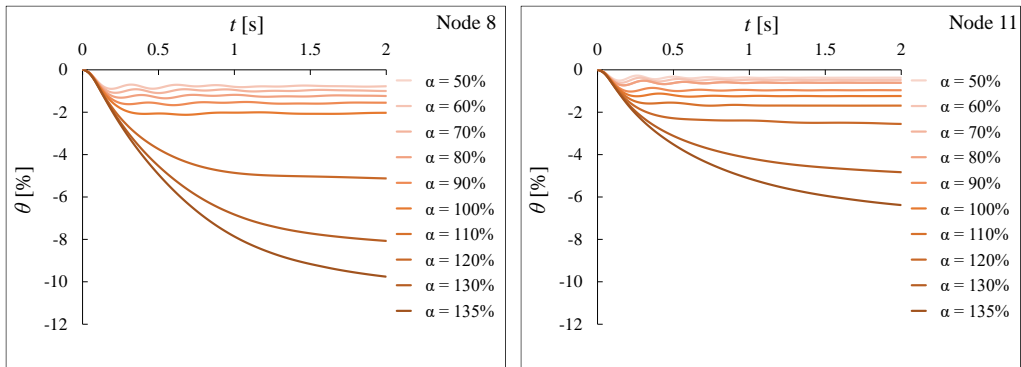
Scenario	α_{max} [%]	θ_{max} [%]		Scenario	α_{max} [%]	θ_{max} [%]	
		N_k	N_m			N_k	N_m
A1-A2	30	11.67	10.57	A2-A3	61	9.82	9.84
A1-A3	136	10.18	6.88	A2-A4	127	4.25	3.71
A1-A4	135	9.76	6.38	A2-A5	132	5.65	5.08
A1-A5	136	10.06	6.54	A2-A6	140	8.31	8.31
A1-A6	134	9.30	6.30	A3-A4	63	11.07	11.07
A1-A7	140	11.37	11.37	A3-A5	138	7.03	7.05

Table 3.6: Progressive collapse capacity measures for simultaneous column-loss scenarios

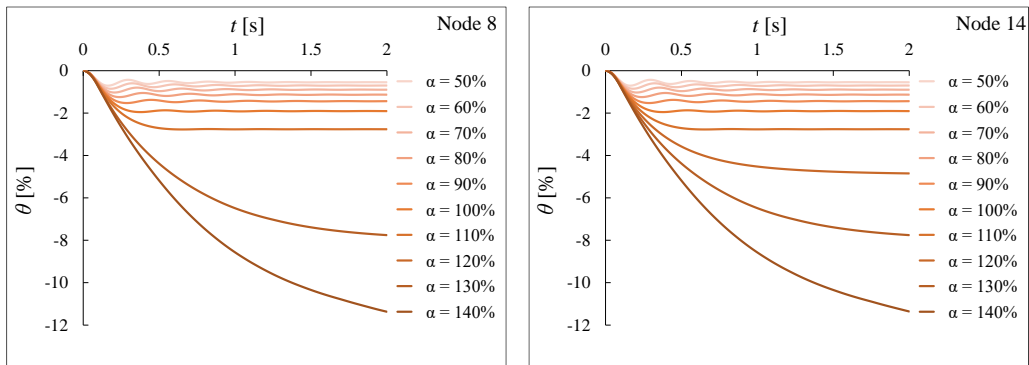
Chapter 3- Influence of material properties on progressive collapse resistance of RC buildings under different column loss scenarios



(a)



(b)



(c)

Figure 3.11: Drift time histories corresponding to: (a) scenario A1-A2, (b) scenario A1-A4, (c) scenario A1-A7

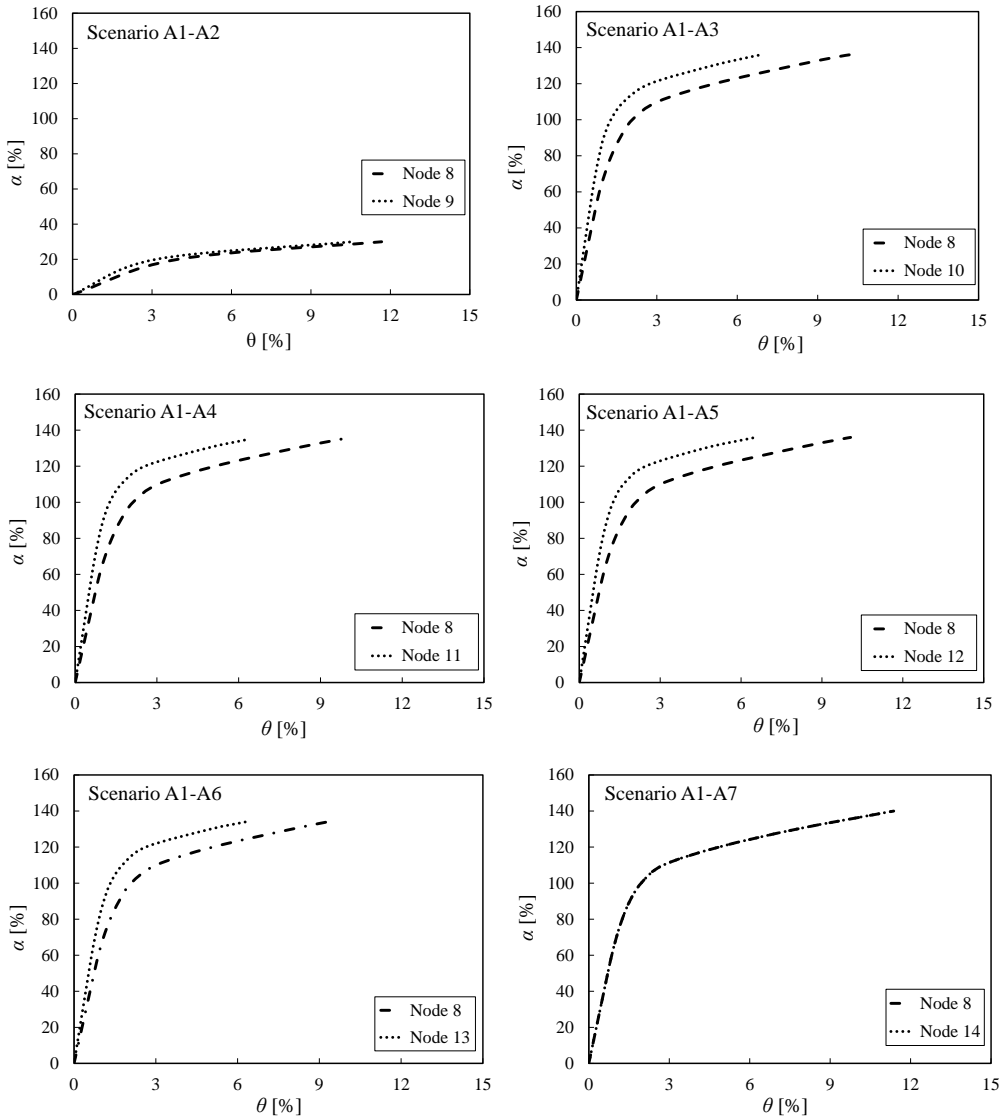


Figure 3.12: IDA curves corresponding to the simultaneous loss of either a corner column and an internal column or opposite corner columns

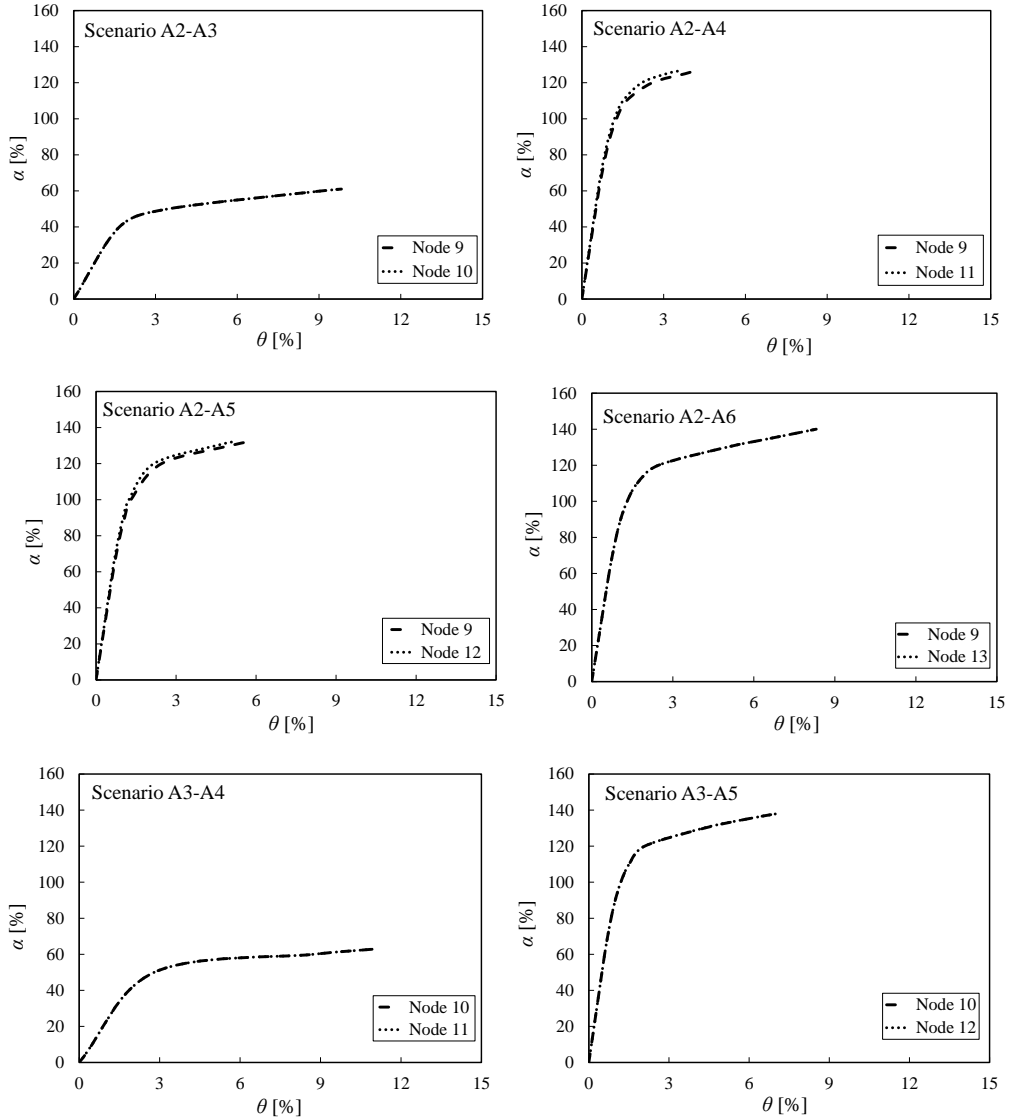


Figure 3.13: IDA curves corresponding to the simultaneous loss of two internal columns

3.5.2 Structural response to sequential removal scenarios

An important impact of scenarios involving the corner column A1 was found by previous analysis. These produced a significant variability in the progressive collapse resistance

of the structure, particularly in terms of load capacity. For this reason the following analysis were carried out only for scenarios involving the corner column, assigning a different deactivation time to each column. Two different deactivation times t_{di} and t_{dj} to each couple of columns A_i and A_j , with $t_{di} < t_{dj}$ and vice versa were considered. According to Figure 3.14 six scenarios were considered, each of them with four combinations of deactivation times, resulting in 24 scenarios. Table 3.7 shows the analysis results in terms of capacity measures and their percentage variation with respect to the output of simultaneous loss scenarios. These results highlighted that scenarios A1-A2 and A1-A3 had the maximum impact among the sequential column removal scenarios. Scenario involving the corner column and the consecutive one showed the maximum increase (*i.e.* 13%) of α_{max} when t_{di} and t_{dj} were 1s and 0.01s, respectively. By contrast, the maximum reduction of this parameter was found for scenario A1-A3, when the column A1 was removed at 0.01 s and the other one at 0.1 s. Moreover this scenario was also marked by the greater sensitivity of the vertical drift of control point, being characterized by the greater increase (+11%) and decrease (-63%) of this last one. A negligible impact of the sequential removal scenarios was found in some cases: when the column A1 was removed at 0.1 s the maximum load capacity of the structure was not changed if columns A3 and A4 were removed at 0.01 s. In addition, also the vertical drift suffered by the control node of these two columns, *i.e.* nodes 10 and 11, didn't vary. No change in α_{max} was also found for scenarios with $t_{d1}=1$ s and $t_{d5}=t_{d7}=0.01$ s, $t_{d1}=0.01$ s and $t_{d6}=t_{d7}=1$ s. IDA curves related to the column removal scenarios are shown from Figure 3.15 to Figure 3.20, varying the control node of the analysis and the different combination of the deactivation times of the two columns. These curves are characterized by different colours and different markers, so as to be able to easily understand the variations of θ and α to the variation of the considered scenario. In addition, Figure 3.23 shows the maximum tensile strain/stress and the minimum compressive strain/stress in steel and in concrete fibres, respectively, for scenario A1-A2. The steel strain in the model elements B9-10a and B9-10b (see Figure 3.21 for the denomination) progressively increased over time, reaching the $\varepsilon_{su,max}$ in the element B9-10b at $\theta_{max} = 11.67\%$. In that stage stress time

histories, plotted in Figure 3.23, show that large strain levels were reached by concrete fibres, without carrying stresses, according to the strain softening of the material model. For this reason, it is useful to plot compressive axial strains in concrete fibres up to -5% . A similar strain evolution was obtained in the scenario A1-A4 (Figure 3.24 and Figure 3.25), especially in the model elements B8-9a and B8-9b located in the outer beams that reached $\theta_{max} = 9.76\%$. The evolution of strains and stresses in end model elements of the beams located above column A1 in the scenario A1-A7 is shown in Figure 3.26.

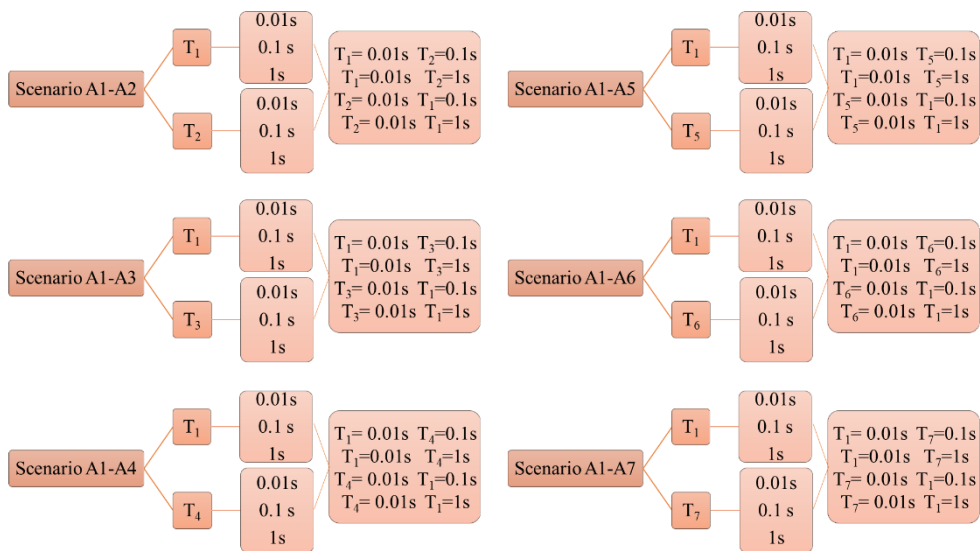


Figure 3.14: Scenarios corresponding to different column deactivation times

Chapter 3- Influence of material properties on progressive collapse resistance of RC buildings
under different column loss scenarios

Scenario	Deactivation times		α_{max} [%]	θ_{max} [%]	
	t_{di}	t_{dj}		N_k	N_m
A1-A2	0.01	0.1	29 (-3%)	10.43 (-11%)	9.37 (-11%)
	0.01	1	31 (+3%)	9.64 (-17%)	8.59 (-19%)
	0.1	0.01	27 (-10%)	8.53 (-27%)	7.55 (-29%)
	1	0.01	34 (+13%)	11.40 (-2%)	10.28 (-3%)
A1-A3	0.01	0.1	119 (-13%)	4.91 (-52%)	2.54 (-63%)
	0.01	1	138 (+1%)	10.88 (+7%)	6.01 (-13%)
	0.1	0.01	136 (0)	10.88 (-1%)	6.85 (0)
	1	0.01	139 (+2%)	8.96 (-12%)	7.61 (+11%)
A1-A4	0.01	0.1	129 (-4%)	7.77 (-20%)	4.59 (-28%)
	0.01	1	139 (+3%)	10.49 (+7%)	5.57 (-13%)
	0.1	0.01	135 (0)	9.68 (-1%)	6.37 (0)
	1	0.01	134 (-1%)	7.84 (-20%)	5.89 (-8%)
A1-A5	0.01	0.1	134 (-1%)	9.31 (-4%)	5.81 (-6%)
	0.01	1	135 (-1%)	9.63 (-1%)	5.03 (-19%)
	0.1	0.01	129 (-5%)	7.67 (-21%)	4.34 (-30%)
	1	0.01	136 (0)	8.11 (-16%)	6.43 (+4%)
A1-A6	0.01	0.1	131 (-2%)	8.30 (-12%)	5.25 (-11%)
	0.01	1	134 (0)	9.31 (0)	5.81 (-8%)
	0.1	0.01	132 (-1%)	8.61 (-7%)	5.61 (-11%)
	1	0.01	129 (-4%)	6.59 (-29%)	4.76 (-24%)
A1-A7	0.01	0.1	135 (-4%)	9.44 (-17%)	9.31 (-18%)
	0.01	1	140 (0)	11.44 (+1%)	8.49 (-25%)
	0.1	0.01	135 (-4%)	9.31 (-18%)	9.44 (-17%)
	1	0.01	140 (0)	8.49 (-25%)	11.44 (+1%)

Table 3.7: Progressive collapse capacity measures for sequential column-loss scenarios ***

* Black bold values: maximum increase and decrease of maximum load capacity;

** Red bold values: maximum increase and decrease of maximum vertical drift.

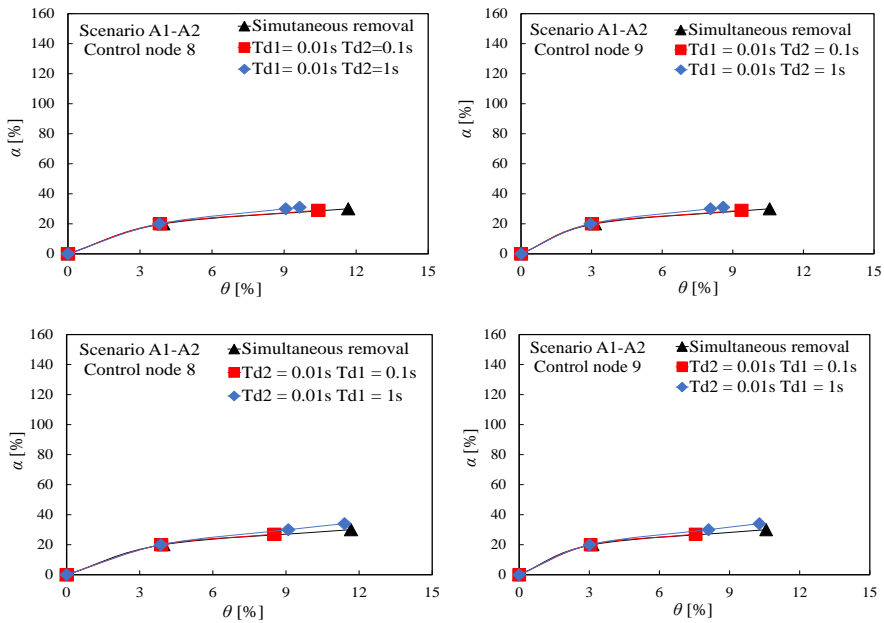


Figure 3.15: IDA curves corresponding to the sequential removal scenario A1-A2, by varying control point and deactivation time

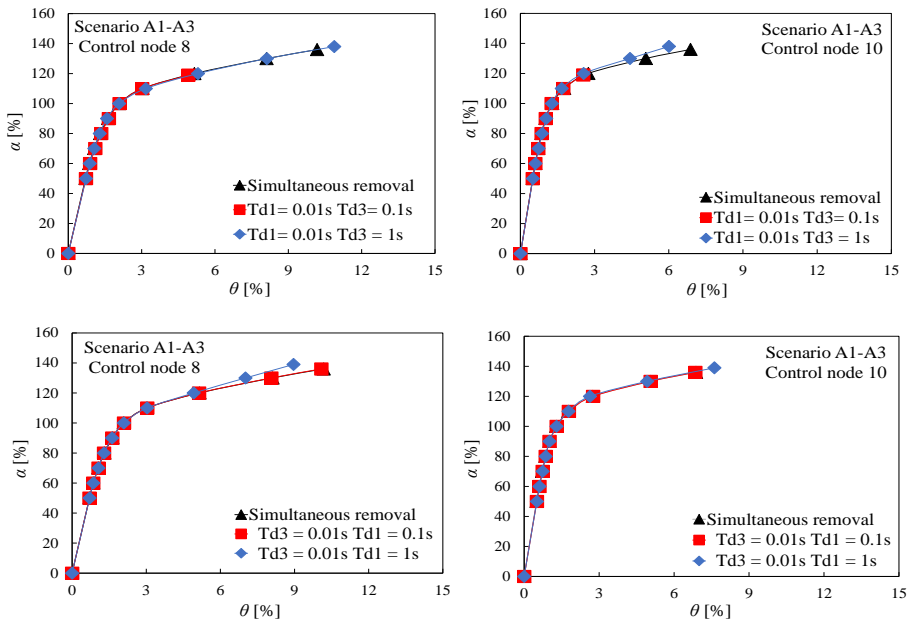


Figure 3.16: IDA curves corresponding to the sequential removal scenario A1-A3, by varying control point and deactivation times

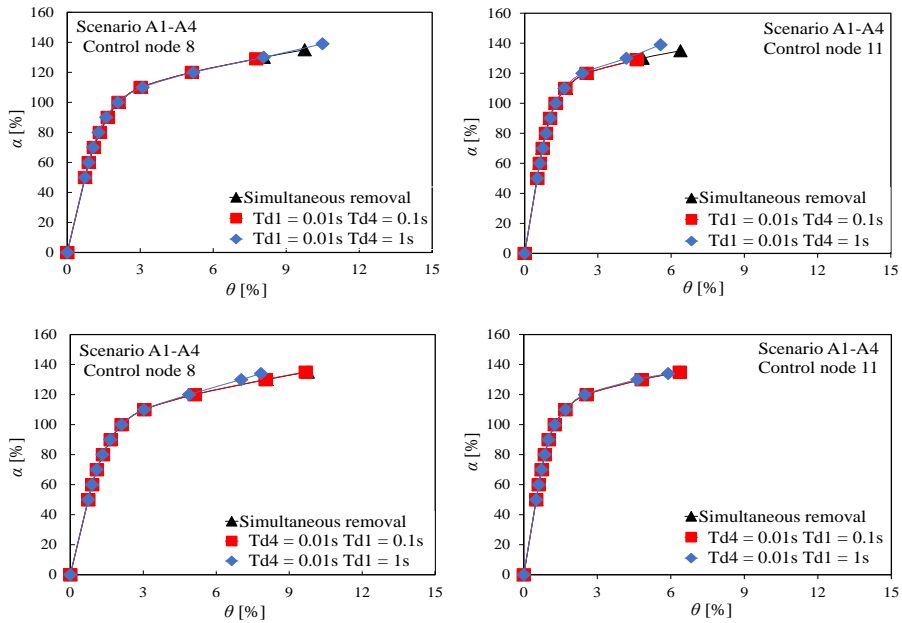


Figure 3. 17: IDA curves corresponding to the sequential removal scenario A1-A4, by varying control point and deactivation times

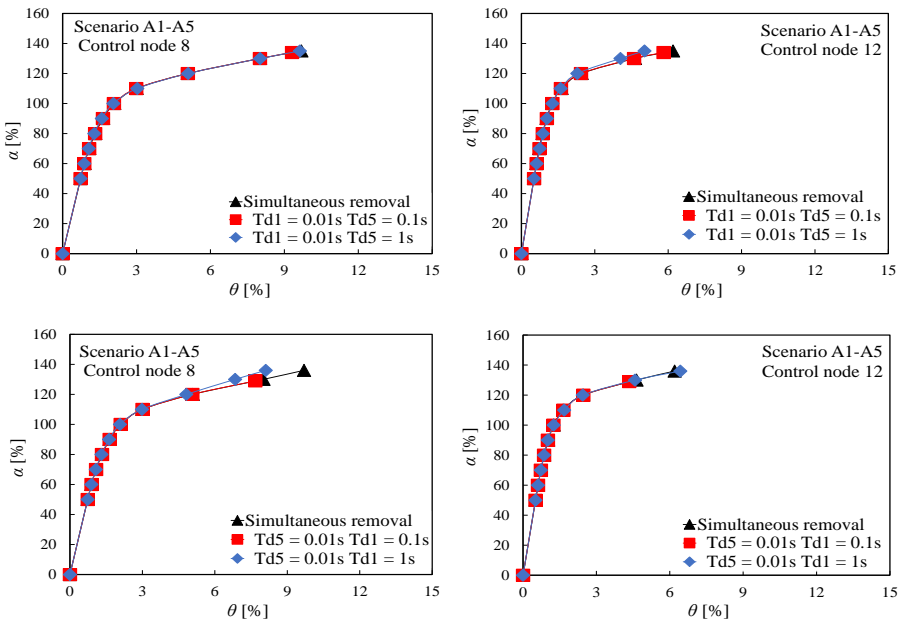


Figure 3. 18: IDA curves corresponding to the sequential removal scenario A1-A5, by varying control point and deactivation times

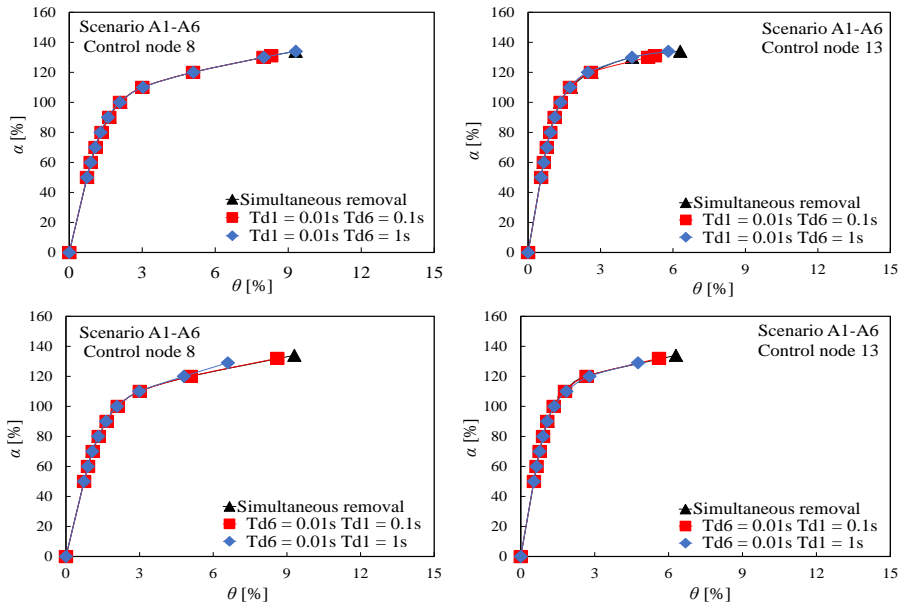


Figure 3. 19: IDA curves corresponding to the sequential removal scenario A1-A6, by varying control point and deactivation times

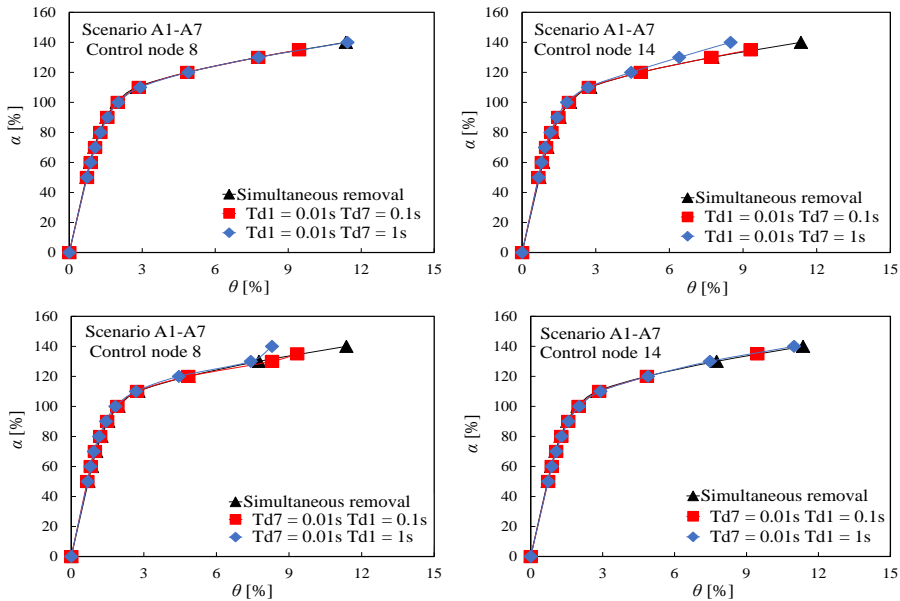


Figure 3. 20: IDA curves corresponding to the sequential removal scenario A1-A7, by varying control point and deactivation times

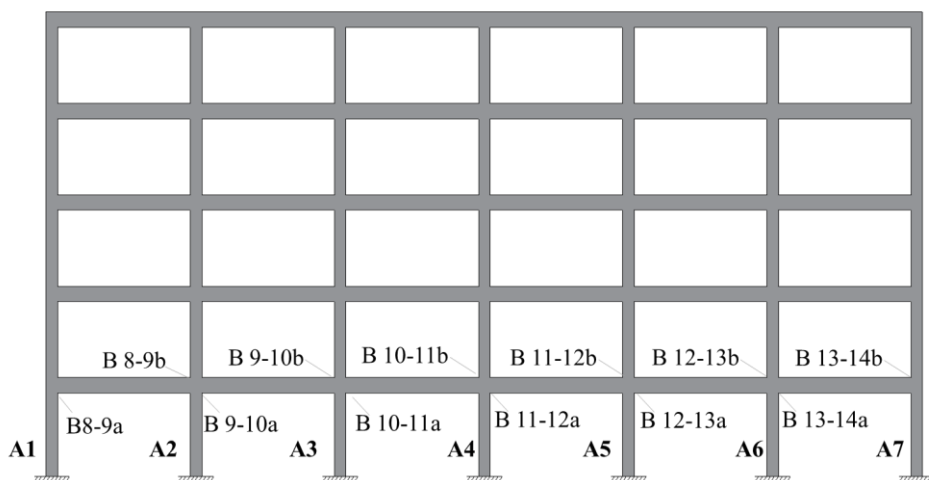
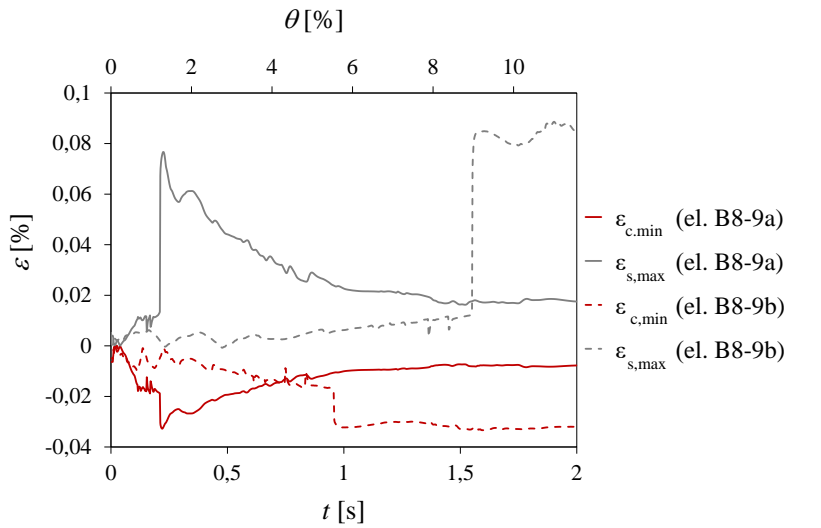
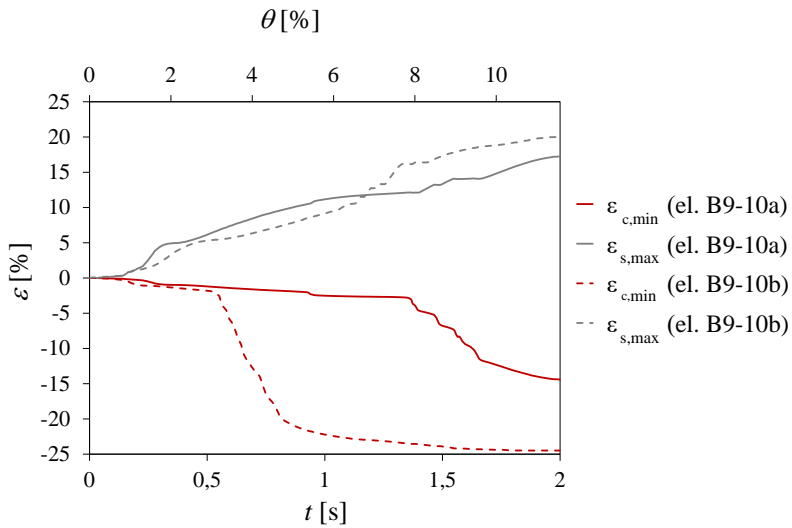


Figure 3.21: Labelling of model elements

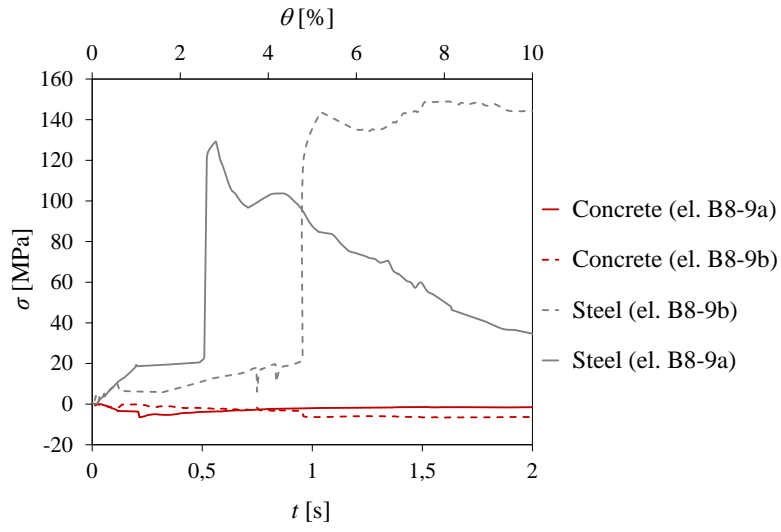


(a)

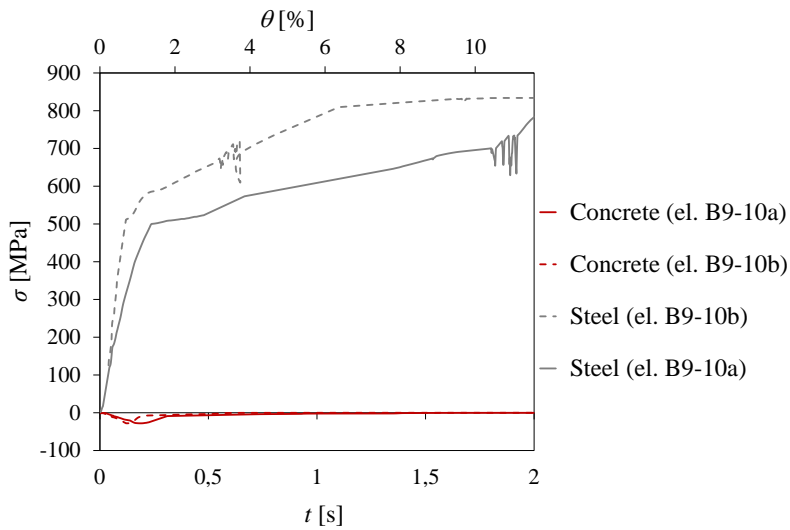


(b)

Figure 3.22: Maximum tensile strain/stress in steel fibres and minimum compressive strain/stress in concrete fibres under varying time and drift corresponding to the scenario A1-A2: strains in model elements: (a) B8-9a and B8-9b, (b) B9-10a and B9-10b

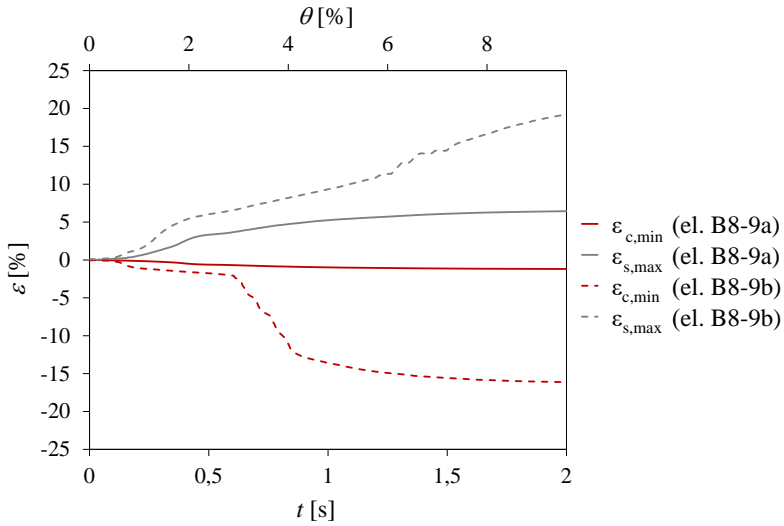


(a)

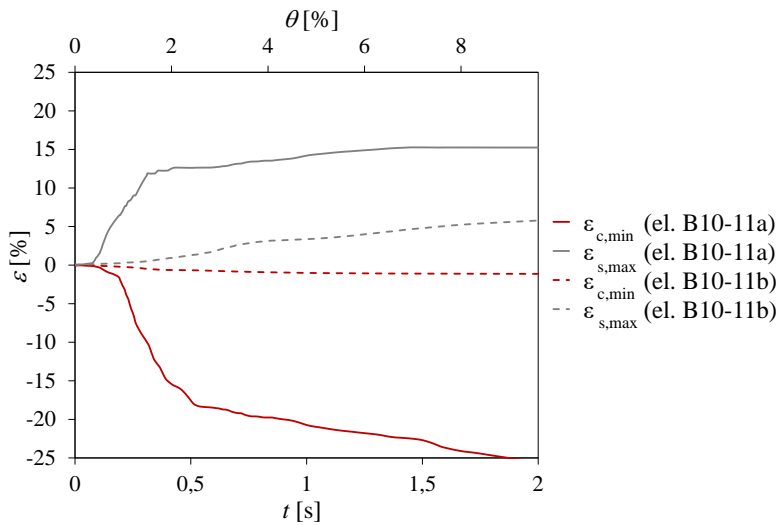


(b)

Figure 3.23: Maximum tensile strain/stress in steel fibres and minimum compressive strain/stress in concrete fibres under varying time and drift corresponding to the scenario A1-A2: stresses in model elements: (a) B8-9a and B8-9b, (b) B9-10a and B9-10b.

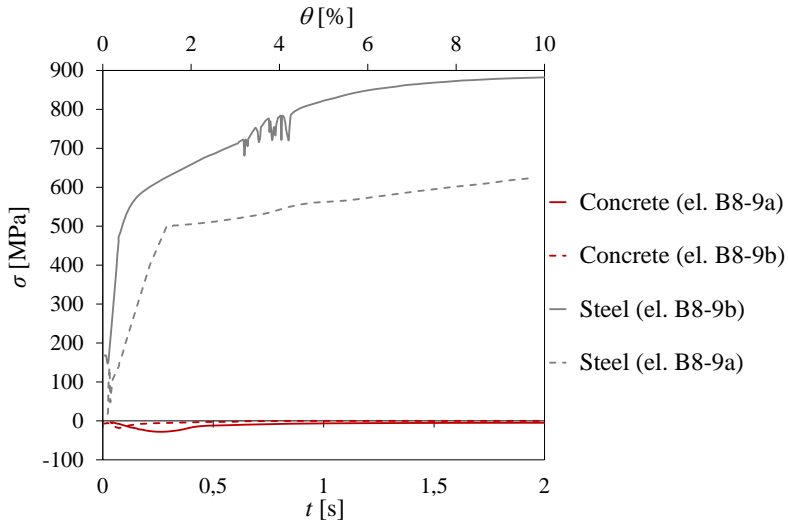


(a)

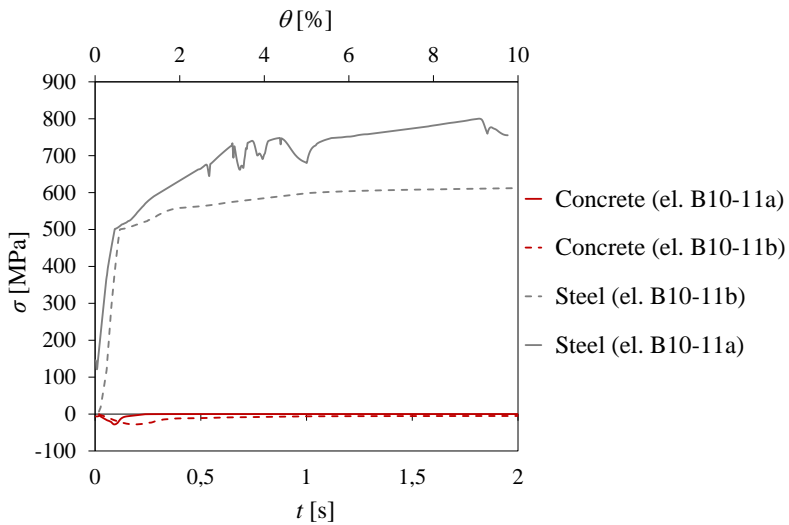


(b)

Figure 3.24: Maximum tensile strain/stress in steel fibres and minimum compressive strain/stress in concrete fibres under varying time and drift corresponding to the scenario A1-A4: (a) strains in model elements: (a) B8-9a and B8-9b, (b) B9-10a and B9-10b



(a)



(b)

Figure 3.25: Maximum tensile strain/stress in steel fibres and minimum compressive strain/stress in concrete fibres under varying time and drift corresponding to the scenario A1-A4: stresses in model elements: (a) B8-9a and B8-9b, (b) B9-10a and B9-10b.

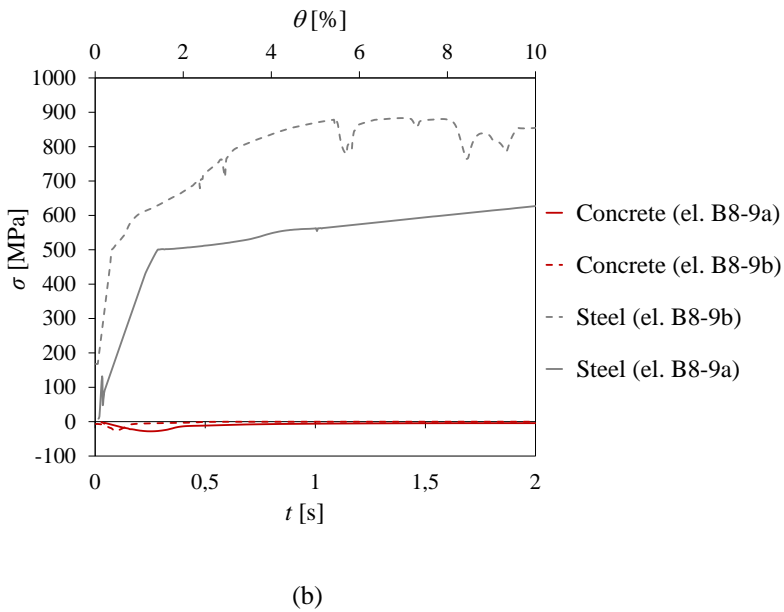
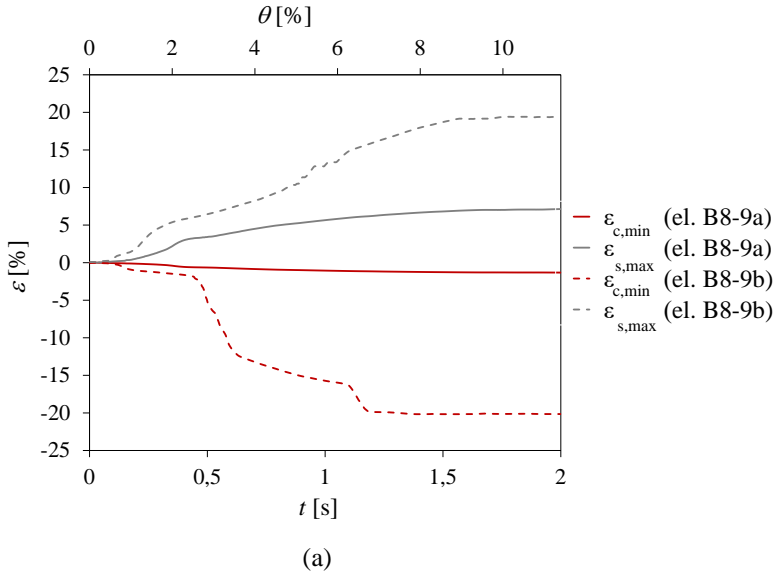


Figure 3.26: Maximum tensile strain/stress in steel fibres and minimum compressive strain/stress in concrete fibres under varying time and drift corresponding to the scenario A1-A7 (model elements B8-9a and B8-9b): (a) strains; (b) stresses

CHAPTER 4 – PROGRESSIVE COLLAPSE RESISTANCE OF A REAL RC BUILDING COLLAPSED DURING STRUCTURAL RETROFITTING OPERATIONS

4.1 Problem statement

Last decades have been characterized by a growing frequency of occurrence of progressive collapses due to poor maintenance and management of existing structures and infrastructure. There are other stages of the building lifetime such as construction and retrofitting that can threaten structural safety, frequently resulting in either the need for evacuation/demolition or even progressive collapse with huge impact on economy and people [93-9599]. As far as existing structures are concerned, the literature includes a small number of investigations on progressive collapse risk mitigation through various retrofitting measures [96,97]. Very few studies evaluated the gravity load-bearing capacity of existing buildings during retrofitting operations, particularly in transient stages during which the structure may be temporarily weakened or subjected to loads different from those assumed at the time of its structural design. This phase of work wants to investigate the ability of existing reinforced concrete structures to prevent a progressive collapse when they are subject to retrofitting. In this context, the work has assessed the effects of the removal of concrete cover in columns on the resistance to the progressive collapse of a real structure typical of the heritage built in the fifties of the last century, which collapsed in 2001. The removal of concrete cover is a routine operation in the context of retrofitting interventions, both traditional and innovative, and therefore its dangerousness is very often underestimated.

4.2 Description of case-study building

The case-study structure is a RC framed structure that was situated in Naples, Italy. It was designed only to gravity loads, according to Royal Decree n. 2229/39 [98] and to past practice rules [99, 100]. In 2001, the building suffered the collapse of a corner, as shown in Figure 4.1a, due to wrong retrofit interventions. The structure was subsequently reconstructed and today it is found as shown in Figure 4.1b. The reconstructed corner of the building reflected the original architectural characteristics, while meeting current safety levels according to the current Italian building code. In addition, Figure 4.2 shows the typical layout of steel reinforcement in a ground-floor column, as taken out from the residual structure during the forensic investigations. The latter one indicated that the progressive collapse of the corner building was consequent to two different retrofitting interventions: the simultaneous removal of concrete cover from ten columns at the ground floor and soil excavation around column bases. The forensic investigation was committed to Prof. N. Augenti, in order to establish the causes and responsibilities of the collapse. Evidence of the building corner after collapse is shown in Figure 4.3a and b, that show floor slabs overlapped to each other, columns ejected as rigid bodies, and soil excavation around column bases.

The floor plan is illustrated in Figure 4.4 and it is characterized by an irregular shape with size of $43.82 \times 19.40 \text{ m}^2$. The building is characterized by an 8-storey RC framed structure with cast-in-place shallow foundations, beams, columns, one-way joist floors and two staircase systems and by an inter-storey height of 3 m at any floor level.

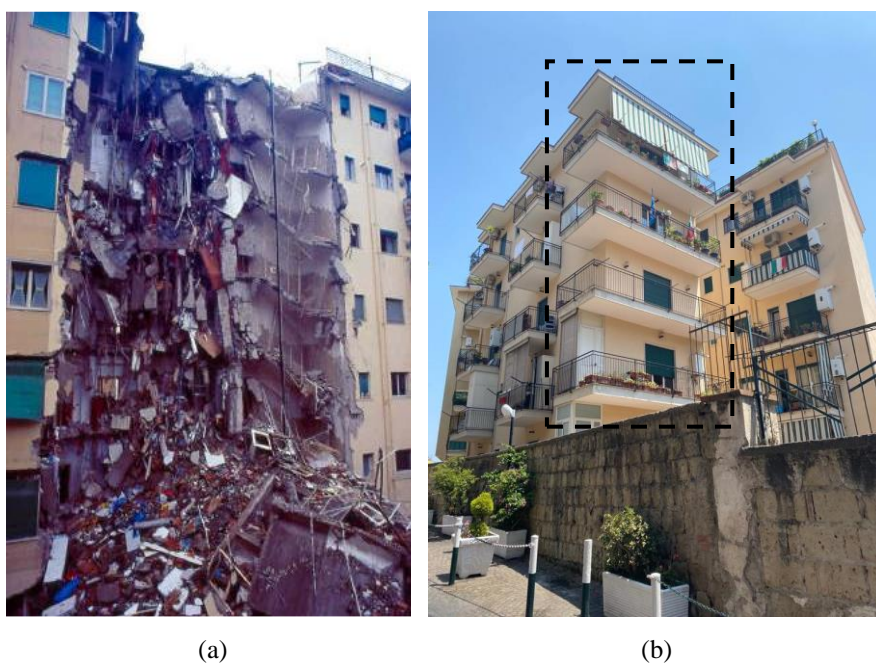


Figure 4.1: Building corner (a) after collapse and (b) after reconstruction (black hatching indicates the portion built after the collapse)



Figure 4.2: Steel rebar details in a ground-floor column specimen extracted from the residual structure.



(a)



(b)

Figure 4.3: Corner building after debris removal: (a) overlapped floor slabs, ejected columns and staircase; (b) detail of ground-floor columns subjected to concrete cover removal and soil excavation at the base

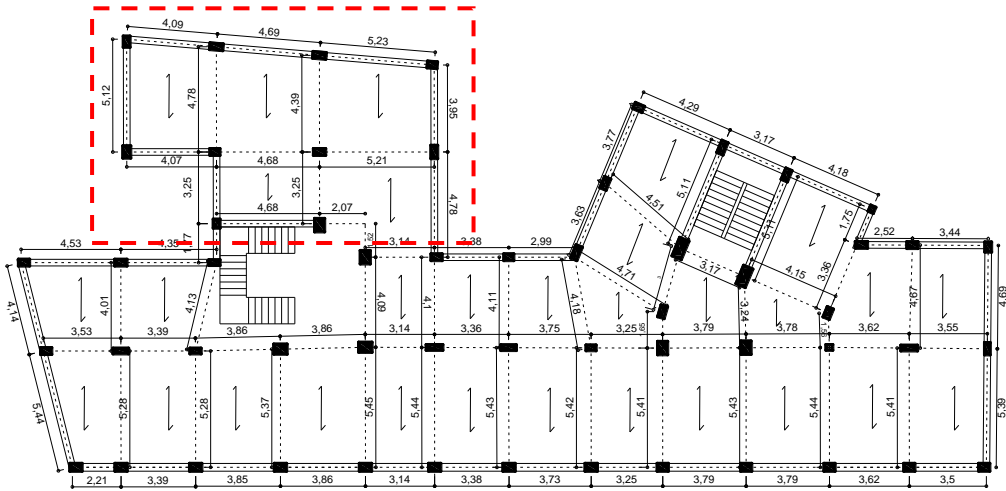


Figure 4.4: Typical floor plan of case-study structure with identification of span length of beams, spanning direction of floor joist slabs and staircases (dimensions in m). [In red the building corner that collapsed during retrofitting interventions].

4.3 Methodology of the study

The majority of the structure was modelled through an integration of available data, personally provided by Augenti [105], with a simulated design procedure. The latter one allowed to define the quantity and the arrangement of the steel reinforcement in the structural elements, due to the lack of original design. The sensitivity of progressive collapse resistance of the structure subjected to retrofit measures was assessed through nonlinear pushdown analysis on two different models of the structure. In the next section, the retrofitting measures are described in detail.

4.3.1 Definition of structural retrofitting scenarios

As illustrated in Figure 4.5, nine structural retrofitting scenarios were considered, related to concrete cover removal (CCR) from a different number of columns at ground floor and soil excavation (SE) around column bases. This choice was due to reproduce the real conditions which the structure was subjected to at the time of collapse [105]. The

concrete cover was first removed from one column and different locations of this were considered, in order to investigate the worst scenario. Indeed, the concrete cover was removed from a corner, side and an internal column. Then, the number of columns subjected to retrofitting operations was gradually increased from one to three, six and ten. In these scenarios the concrete cover was removed at the same time from the structural elements, in order to reproduce the real situation at the time of the collapse. The reason is to traced back to the fact that the real operations of structural consolidation, that then caused a progressive collapse of the structure, were carried out contemporarily on more columns at ground floor. The soil excavation scenarios involved either a single column or three columns at the same time. Two different locations, i.e. internal and corner, were considered for the SE scenarios involving a single column. Then, the number of columns involved in the SE scenarios increased from one to three. In the specific the columns involved in this last scenario were two of corner and a central one. In the following sections the scenarios with the relative results are treated in detail.

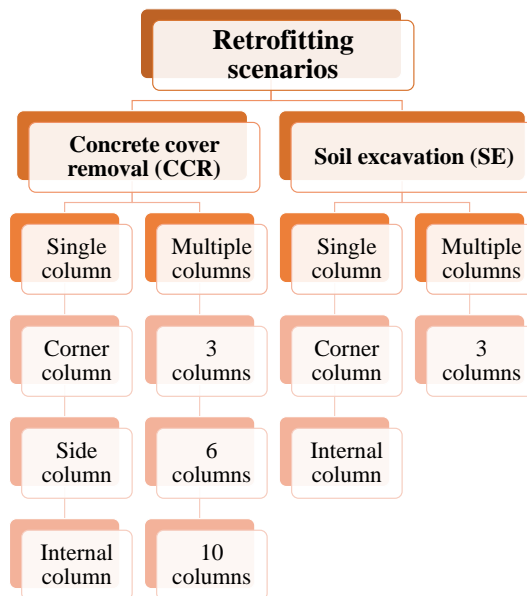


Figure 4.5: Definition of CCR and SE scenarios for progressive collapse analysis.

4.3.2 Simulated design procedure

As discussed above, the existing information from past forensic investigations were integrated with a simulated design procedure, in order to develop the capacity model of the structure, according to design codes and practice rules used at the time of construction [98-100]. According to Royal Decree 2229/1939 [98] the simulated design of the case-study structure was based on the permissible stress method (PSM) that required meeting the following inequality in the most stressed cross sections:

$$\sigma_{\max} \leq \sigma_{adm} \quad (15)$$

where:

- σ_{\max} represents the maximum axial stress induced by loads.
- σ_{adm} is the permissible stress of the material.

The gravity loads were defined in terms of nominal values, performing a linear structural response analysis according to the principle of effects superposition because of a linear elastic behaviour assumed for all structural materials [99]. This involved that permissible stresses were far below the actual peak strength of concrete and reinforcing steel (as specified in the following section), allowing a homogenisation of RC cross sections and computation of sectional stresses with no consideration of elastic-plastic redistribution. Structural design of typical residential RC buildings in Italy was usually carried out in accordance with tributary floor areas for columns, possibly considering continuity of floor systems and their transverse load distribution on secondary beams through floor strips with 0.5–1.0 m width. In addition, gravity loads were basically summed up with no combination driven by partial safety factors, as assumed by semi-probabilistic design procedures provided by current building codes. According to Royal Decree n. 2229/1939 [98], in force at the time of construction [99,100] the concrete unit weight, γ_c , was set to 2500 kg/m³ and concrete strength class was defined by the peak compressive strength after 28 days of curing ($\sigma_{r,28}$). The reinforcing steel was classified by the Italian Code in soft, semi-hard or hard steel. The concrete of the case study structure was characterized

by a strength class Rck160 (according to the value of $\sigma_{r,28}$ in kg/cm²), whereas the steel reinforcement consisted of smooth reinforcing bars, which were made of AQ42 steel type as typically detected in similar buildings of the same period, as shown in Figure 4.6. The material characteristic are illustrated in Table 4.1; two different values of permissible stress of concrete were considered, as prescribed for the building design of that years [98]. In detail, the lower and upper bounds of the concrete permissible stress were assigned to cross sections that were respectively designed under compressive loading and bending combined with compressive loading. A single value of permissible stress was assigned to reinforcing steel. The design gravity loads were defined by summing up nominal values of dead and live loads, in line with the permissible stress method; these were set to $D= 4.7$ kN/m² and $L=2$ kN/m². A detailed analysis was performed to evaluate the dead load of the floor slabs, considering the geometric characteristics of cross section and the unit weights of materials assumed in the period of the building construction. The infill walls were characterized by two wythes of hollow brick masonry, separated one from each other by a 100-mm-wide central cavity. The total thickness of infill walls was $t_w = 300$ mm, resulting in a self-weight per unit length equal to 8.00 kN/m. The dead load due to self-weight of beams and columns was automatically computed after the structural modelling of the building.

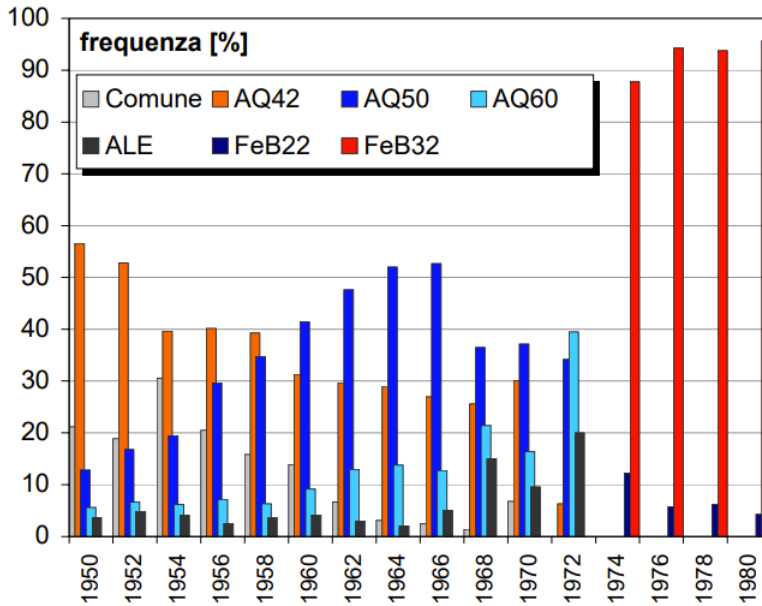


Figure 4.6: Steel use percentages for different categories as the year of construction [99]

Material	Property	Value [MPa]
Concrete	Peak compressive strength after 28 days of curing, $\sigma_{r,28}$	16
	Permissible compressive stress, $\sigma_{c,adm}$	4.5-5
Reinforcing steel	Permissible stress, $\sigma_{s,adm}$	140

Table 4.1: Material properties

After this first step of analysis, related to loads and material properties definition, it was necessary to evaluate the amount and the arrangement of steel rebar in structural elements. To this aim the structural joints were labelled (Figure 4.7), in plan, in order to identify beams and columns. Each node was labelled as $i-j$ where i and j stand for the grid lines in the x - and y -directions of the building plan. Then, the structural elements were labelled as follows:

- Each beam was marked as B_{a-b_k} , in which a and b indicate the left- and right-hand side nodes (with $b > a$) and k the floor level where the beam was located.
- Each column was indicated with C_{i-j_lm} , in which x and y indicate the positions of the nodes with reference, respectively, to the x - and y -axis, while l and m define the floor levels where the lower and upper nodes of the column were respectively located.

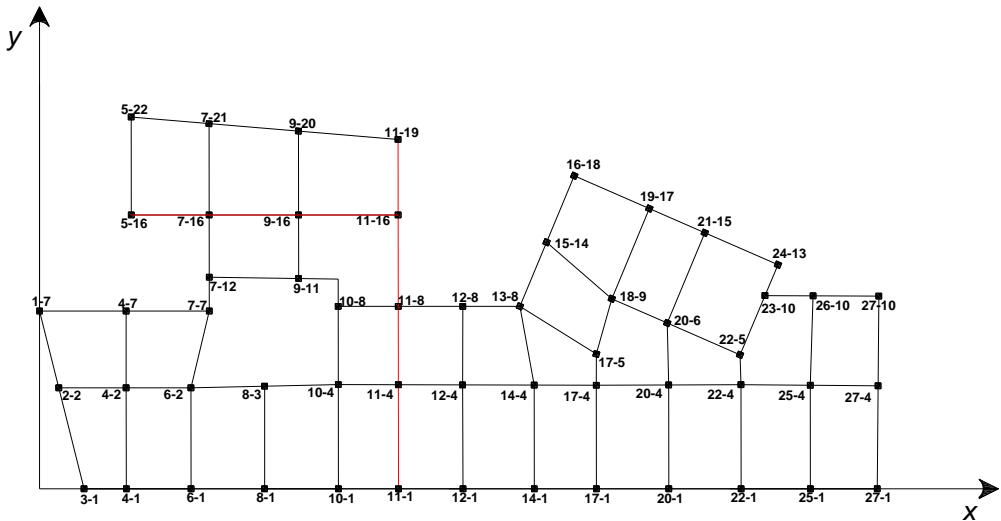


Figure 4.7: Labelling of beam-column joints

In order to obtain the amount and arrangement of steel rebar in beams two alignments of consecutive beams, one for each main direction of the plan highlighted by the red colour in Figure 4.7, were considered. Some considerations were made, in accordance with the reference Italian code [98], as follows: the shear force was resisted by (i) bent bars with transition points between their longitudinal and diagonal segments arranged as a function of the bending moment distribution, and (ii) stirrups that were sized to provide at least 50% of shear resistance. The diameter of stirrups was set to 6 mm with spacing equal to 200 mm, according to age of construction. The minimum quantity of reinforcement was

obtained by taking into account the beam depth, h , given a width equal to the thickness of infill masonry walls (*i.e.* $b = t_w = 300$ mm), the maximum internal forces under gravity loads only and permissible stresses outlined in the previous section.

After calculating the stresses acting on the beams, through the areas of influence, the reinforcements were designed following the procedures present in the manuals and in the construction technique texts most widely used at the design time [98,100].

Once the maximum stresses, beam dimensions and allowable material stresses were known, the minimum amount of reinforcement required was calculated using the coefficients r and t given in the tables of the manual [100], for rectangular reinforced concrete sections with simple reinforcement, as a function of the stresses in the steel and concrete and for values of the homogenisation coefficient $n = 10$. The value of r needed to find the corresponding value of t taken to calculate A_f was derived using the following expressions:

$$r = \frac{h}{\sqrt{\frac{M}{b}}} \quad (16)$$

$$A_f = t \cdot b \cdot \sqrt{\frac{M}{b}} \quad (17)$$

The strictly necessary reinforcement values thus obtained were transformed into steel bars in number and diameter, as illustrated in Table 4.2.

Figures 4.8a and b show the longitudinal sections of the two continuous beams in both directions of the building plan. In addition, Figure 4.9 shows the details of cross sections close to the mid-span and beam-column joints.

As regards the vertical elements, at that time, they were usually sized considering a concentric compressive loading, resulting in small and poorly reinforced sections. The stirrups were arranged with a spacing of not more than 10 times the diameter of the bars longitudinal or one-half the size of the side, without the bending of 135° . After the

collapse of the corner building some columns didn't survey, so their size and their reinforcement were unknown. Therefore, it was necessary the identification of these sections and to this aim it was assumed the average axial load demand-to-capacity ratio (DCR) of the other columns. At the end of this process sixteen different column sections were found, labelled as A through to P, depending on the size and the reinforcement, according to Table 4.3 and Figure 4.10. The longitudinal reinforcement consisted of 4Ø16 bars for all the sections corners, while on section sides it consisted of 4 or 8Ø12 bars. Two-leg Ø6 stirrups with 200 mm spacing were considered as transverse reinforcement. The past Italian code [98] also provided for stability verification at peak load in the event that the ratio between the effective column length and the least sectional dimension, i.e. the slenderness ratio, was $\lambda > 15$. All simulated columns met that safety verification.

Beam direction	Section	b [cm]	h [cm]	r	t	$A_{f,min}$ [cm ²]	A_f	σ_c [MPa]	σ_f [MPa]
x	Mid-span	50	30	0.41	0.00188	6.87	6Ø16	4.34	86.57
	Beam-column joint	50	30	0.38	0.00232	9.26	6Ø16	4.94	98.48
y	Mid-span	50	30	0.61	0.00123	3.01	6Ø16	1.94	38.67
	Beam-column joint	50	30	0.51	0.00149	4.36	6Ø16	2.65	52.90

Table 4.2: Design of beam reinforcement and evaluation of material stresses

Chapter 4- Progressive collapse resistance of a real RC building collapsed during structural retrofitting operations

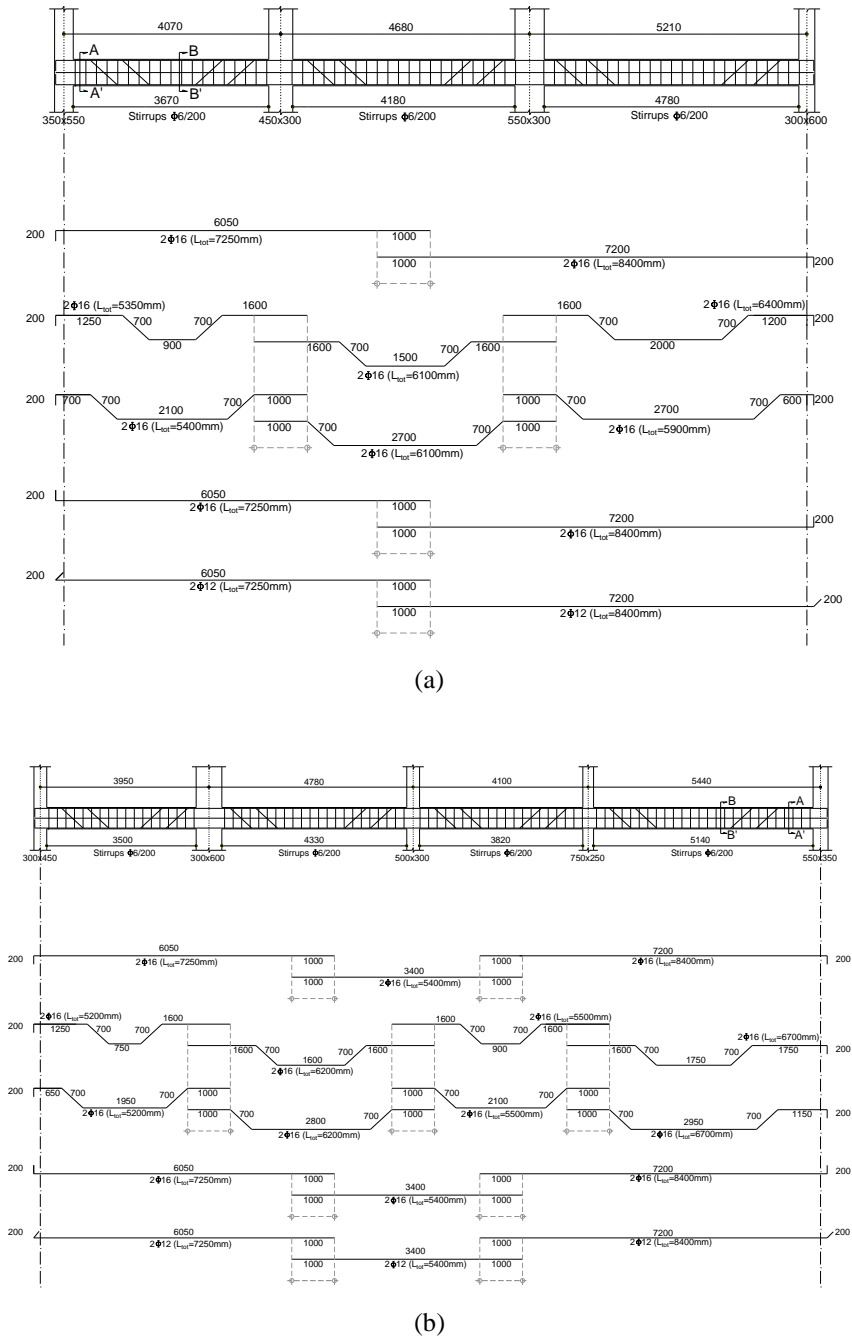


Figure 4.8: Longitudinal sections of beams with longitudinal and transverse reinforcement: (a) x-direction and (b) y-direction (dimensions in mm).

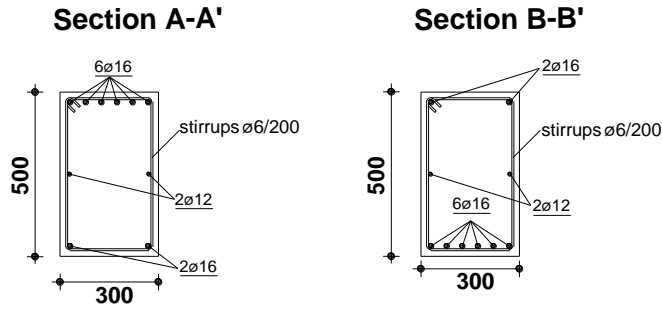


Figure 4.9: Beam cross sections (dimensions in mm)

Section group	Depth [mm]	Width [mm]	Longitudinal reinforcement	Transverse reinforcement
A	450	300	4Ø16 + 4Ø12	Ø6/200 mm
B	600	450	4Ø16 + 4Ø12	
C	900	450	4Ø16 + 4Ø12	
D	450	250	4Ø16 + 4Ø12	
E	600	300	4Ø16 + 4Ø12	
F	500	300	4Ø16 + 4Ø12	
G	550	300	4Ø16 + 4Ø12	
H	400	300	4Ø16 + 4Ø12	
I	300	250	4Ø16 + 4Ø12	
J	650	300	4Ø16 + 8Ø12	
K	500	250	4Ø16 + 4Ø12	
L	500	350	4Ø16 + 4Ø12	
M	550	350	4Ø16 + 4Ø12	
N	550	250	4Ø16 + 4Ø12	
O	750	250	4Ø16 + 8Ø12	
P	700	250	4Ø16 + 8Ø12	

Table 4.3: Size and steel reinforcement of columns sections

Chapter 4- Progressive collapse resistance of a real RC building collapsed during structural retrofitting operations

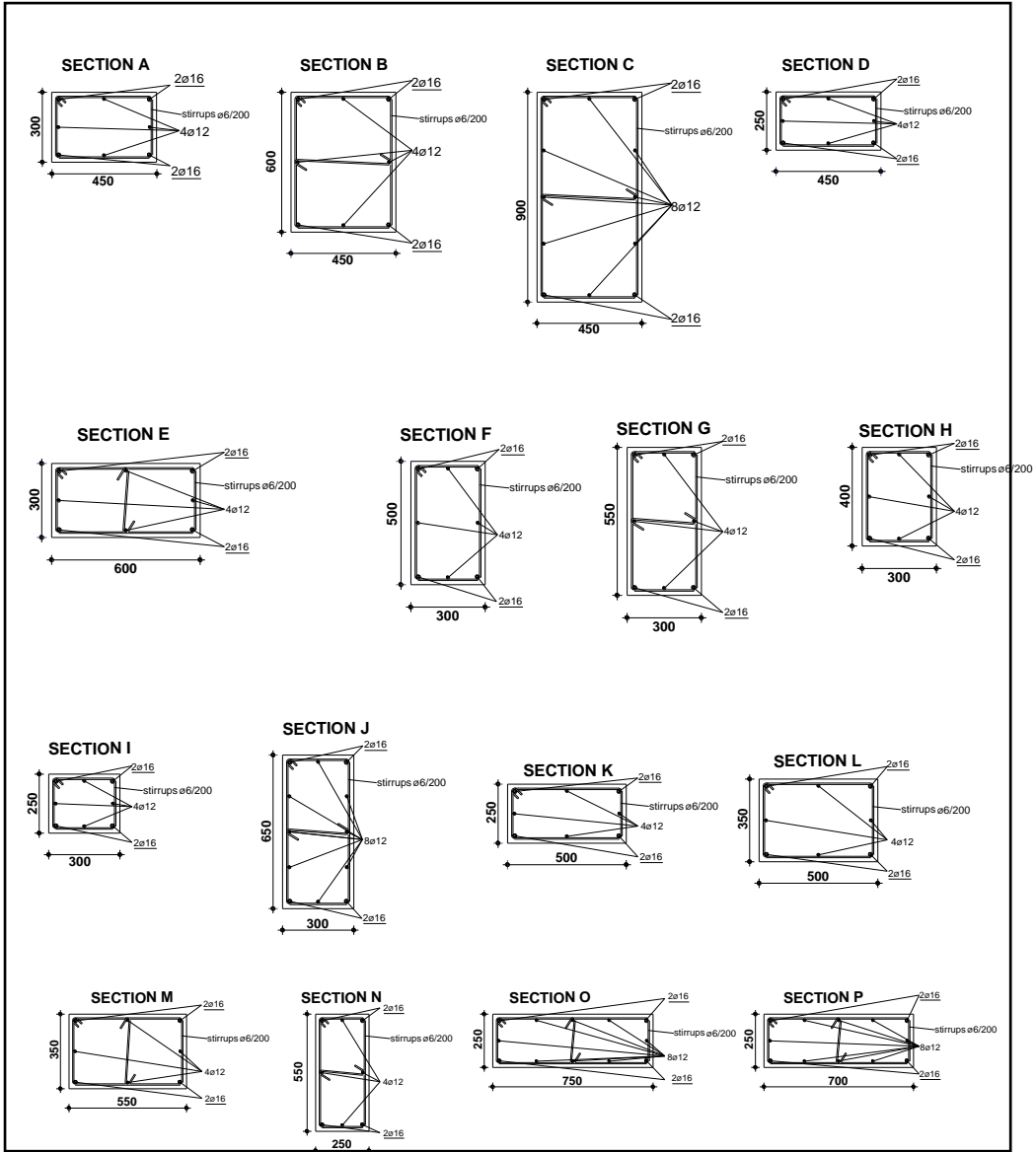


Figure 4.10: Columns sections (dimensions in mm)

4.4 Progressive collapse assessment through pushdown analysis

4.4.1 Capacity and load modelling conditions

After the definition of structural characteristics, obtained through the integration of the forensic investigations data with the simulated design procedure, the next step was related to the modeling of the structure through the Finite Element (FE) code Seismostruct [73]. Large displacements/rotations and large deformations associated with P-Delta effects were taken into account through a total co-rotational formulation [75]. This formulation was based on an exact description of the kinematic transformations associated with large displacements and three-dimensional rotations of the beam-column member. In this way, the element's independent deformations and forces were accurately computed. A spread plasticity approach with force-based fibre formulation was used to describe the nonlinear capacity of the structure [101-104]. The sectional stress-strain state of the structural elements was obtained through the integration of the nonlinear uniaxial stress-strain response of the individual fibres in which the section was subdivided. In this study, each cross section was subdivided in 200 fibres according to previous studies on progressive collapse capacity of RC framed structures [106,107]. The concrete behaviour was described by a uniaxial nonlinear constant confinement model by Mander et al. [76]; this model incorporates the confinement effect due to transverse reinforcement. The Monti-Nuti model [108] was used for reinforcing steel, due to its ability to describe the post-elastic buckling behaviour of reinforcing bars under compression [108]. According to statistics of structures built before 1960 [99,109], the mean values of cylinder concrete strength and yield steel strength were set to $f_{cm} = 16.23$ MPa and $f_{yd} = 250$ MPa, respectively. In order to assess the progressive collapse resistance of the structure two different models of the structure were considered:

- A complete capacity model (CM) (Figure 4.11) of the structure, representative of the whole structure.

- A partial capacity model (PM), which indicates only the building corner subjected to retrofitting measures and collapsed.

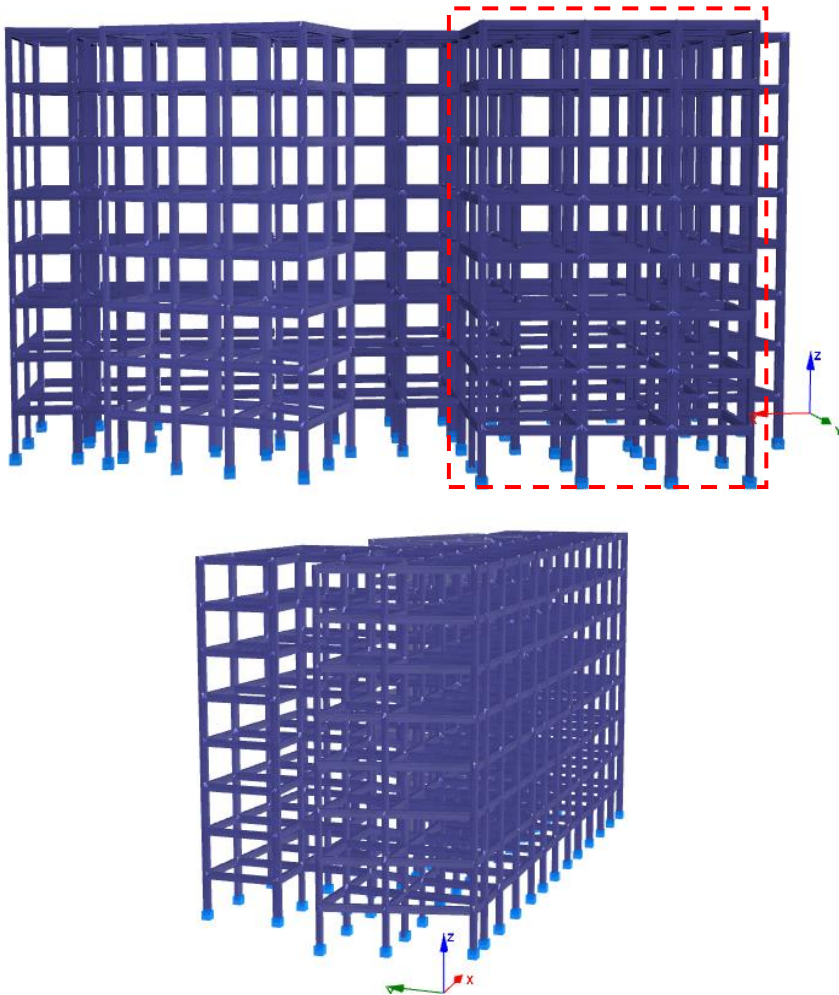


Figure 4.11: Complete capacity model (CM) of the structure: (a) frontal view, (b) lateral view. (In red the building corner that suffered collapse).

Floor systems were not included in the capacity model because of the lack of data, particularly on their geometrical properties and steel rebar that play a key role in membrane action of slabs at large deformations. Therefore, gravity loads were directly assigned to the beams according to the following combination rule recommended by

UFC guidelines [30] for progressive collapse assessment via nonlinear static (pushdown) analysis, as described by Equation (7) in section 2.5.2.

As discussed in this section, the amplification factor is applied for progressive collapse scenarios, *i.e.* the notional removal of one or more columns, hence representing a sudden element deletion and its inertia effects in nonlinear time history analysis (see *e.g.* [33]). In this case it was set equal to unity because the retrofitting operations that produced the collapse of the building corner did not cause damage conditions similar to those conventionally considered in progressive collapse analysis. More specifically, it would be unrealistic to assume that either concrete cover removal or soil excavation around ground-floor column bases was made instantaneously as in the case of the sudden loss of columns due to, for instance, impact or blast damage.

Different types of analysis were performed for the two models of the structure, considering or not the self-weight of the infill masonry walls, which are not always considered in this kind of problem.

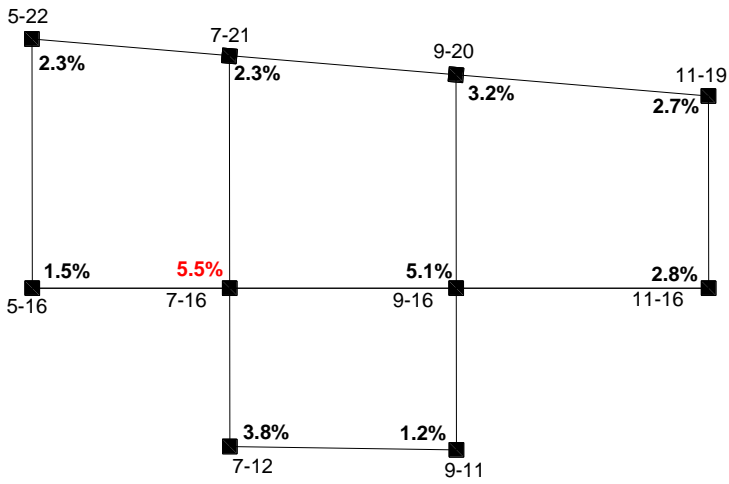
4.4.2 Simulation of retrofitting operations

Nonlinear pushdown analyses were carried out for four different models of the structure: complete model with/out infill masonry walls and partial model with/out infill masonry walls. A load multiplier, α , was used and it was defined as the ratio between the gravity load resisted by the structure at each displacement step, Q_b , and design gravity load, Q_{bd} , defined according to Equation (7), section 2.5.2. The maximum multiplier value greater than unity identifies a robust structure, able to withstand gravity loads with magnitude equal to or greater than Q_{bd} . Nonlinear pushdown analysis with displacement control were carried out by changing the intensity of gravity loads on beams under a monotonically increasing downward displacement D_v imposed to a control node of the structure. The latter one was coincident with the beam-column joint on top of the most stressed column. The last one was chosen through the computation of demand capacity ratios (DCRs) associated with column base sections at the ground floor level. In detail,

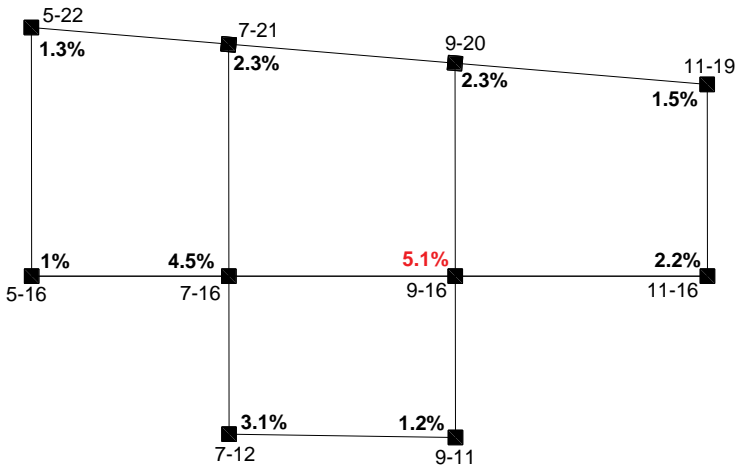
DCRs were calculated for the columns of the building corner subjected to retrofitting operations. As illustrated in Figure 4.12, columns C7-16 and C9-16 were the most stressed for the model with and without consideration of the self-weight of the infill walls, respectively. For this reason the beam-column joints on top of that columns were selected as control point for pushdown analysis.

As illustrated in Figure 4.5, nine scenarios of structural retrofitting were considered. The total loss of core confinement in concrete cover removal scenarios was simulated through replacement of the intact sections by reduced-size sections without concrete cover, setting the confinement factor to unity. In that way, the cover removal was explicitly reproduced, thus assuming the loss of internal confinement accordingly.

The scenarios considered are many, since they contemplate the variability in the number and position of the columns affected by the removal of the concrete cover or the loss of constraint at the base, which corresponds, for example, to the excavation around the surface foundation of each column (typically a plinth) with a consequent loss of load-bearing capacity of the foundation-train system. The loss of constraint is entirely equivalent to the elimination of the column and as such has been implemented in SeismoStruct [73]. Therefore, the soil excavation was simulated by deleting the restraint at the base of each involved column and assigning an incremental downward displacement to the beam-column joint located on top of the most stressed column among those involved in the SE scenario.



(a)



(b)

Figure 4.12: Demand-to-capacity ratios of columns in terms of axial loading produced by gravity loads: (a) model without infill walls, (b) model with infill walls

4.5 Effect of structural retrofitting operations

4.5.1 Implications of concrete cover removal from ground-floor columns

As discussed above, nonlinear pushdown analyses were carried out for different retrofitting operations. In the first phase, the influence of CCR scenarios on progressive collapse resistance was investigated. These analyses were performed on four different models, considering the complete and partial model and the presence or not of the infill walls. The results were collected in terms of maximum load multiplier, α_{max} , and its variation, $\Delta\alpha_{max}$, with respect to the maximum load multiplier of the intact structure and they are shown in Table 4.4 and Table 4.5, for complete and partial capacity model, respectively. The first one shows the values of α_{max} and $\Delta\alpha_{max}$ for the complete capacity model, with and without the consideration of the infill walls. The red values indicate the maximum reductions of maximum load multiplier. These results outline that the intact structure was able to withstand 2.57 times the design gravity loads. A slight load-bearing capacity loss was found for CCR scenarios that involved one column, except for those involving an internal column *i.e.* C9-16 and C7-16. A further decrease of maximum load multiplier was shown when the concrete cover was removed by three columns at same time, reaching a -21%. This happened when concrete cover removal was simultaneously removed by two internal columns (*i.e.* C9-16, C7-16) and by a corner column (*i.e.* C11-19). The maximum reduction of α_{max} was found for the scenario involving all the columns belonging to the building corner, reaching a value of 2 times the design gravity loads with a decrease of approximately 22%.

Table 4.5 shows the results obtained on the partial model, that were very similar. Indeed, for CCR scenarios involving a single column the maximum reduction of α_{max} was found when the concrete cover was removed from a central column (C7-16, C9-16). As the number of columns involved in the retrofitting measures simultaneously increased, also $\Delta\alpha_{max}$ increased. Dealing with CCR scenarios involving three columns, the worst case turned out to be again the scenario involving two internal columns and one corner

column, with α_{max} decreasing by 19.4% and 20.2% with and w/o infill walls, respectively. Also in this case when the concrete cover was removed simultaneously from ten column, a α_{max} value of 2.2 times the design gravity loads was reached, *i.e.* the minimum load-bearing capacity of the structure. The analyses carried out on the partial capacity model confirmed once again the numerical outcomes and trends.

The pushdown analysis results were also illustrated in terms of pushdown curves (Figure 4.13 and 4.14) related to the intact structure and the most significant CCR scenarios applied to the complete capacity model, in which the self-weight of the infill walls was considered and neglected, respectively. These curves outline the reduction of the maximum load multiplier as the number of columns subjected to concrete cover removal increases.

In addition, it is possible to underline the significantly different values of computation time, T , for the pushdown analysis of complete and partial capacity models. Figure 4.15 illustrates that the use of a partial capacity model allowed a huge reduction of T by up to 20 times. In this case, for CCR scenarios, as reflected in the similar results, the use of the partial capacity model produced a negligible error in the prediction of progressive collapse capacity, which ranged between -2% (maximum underestimation) and 1% (maximum overestimation) with mean value equal to -1%.

Chapter 4- Progressive collapse resistance of a real RC building collapsed during structural retrofitting operations

Scenario	Column(s)	Model with infill walls		Model w/o infill walls	
		α_{\max}	$\Delta\alpha_{\max}$	α_{\max}	$\Delta\alpha_{\max}$
Intact structure		2.57	–	2.78	–
CCR from single column	C11-19	2.57	-0.01%	2.77	-0.25%
	C9-16	2.18	-15.35%	2.26	-18.66%
	C7-16	2.07	-19.39%	2.48	-10.89%
	C5-22	2.57	-0.06%	2.78	-0.02%
	C7-21	2.54	-1.14%	2.77	-0.28%
	C11-16	2.57	-0.17%	2.77	-0.47%
	C5-16	2.54	-1.14%	2.77	-0.23%
	C9-20	2.57	-0.21%	2.77	-0.31%
	C7-12	2.57	0.02%	2.77	-0.34%
	C9-11	2.56	-0.48%	2.77	-0.42%
CCR from 3 columns	C11-19, C5-22, C7-16	2.08	-19.21%	2.51	-9.59%
	C11-19, C5-22, C9-16	2.24	-12.81%	2.26	-18.63%
	C11-19, C7-16, C9-16	2.04	-20.57%	2.24	-19.39%
CCR from 6 columns	C9-16, C5-22, C11-19, C7-16, C9-20, C7-21	2.03	-21.07%	2.23	-19.75%
CCR from 10 columns	C9-16, C5-22, C11-19, C7-16, C9-20, C7-21, C5-16, C11-16, C7-12, C9-11	2.02	-21.62%	2.21	-20.47%

Table 4.4: Maximum load multiplier and its variations related to CCR scenarios on complete capacity model, with and without consideration of infill walls.

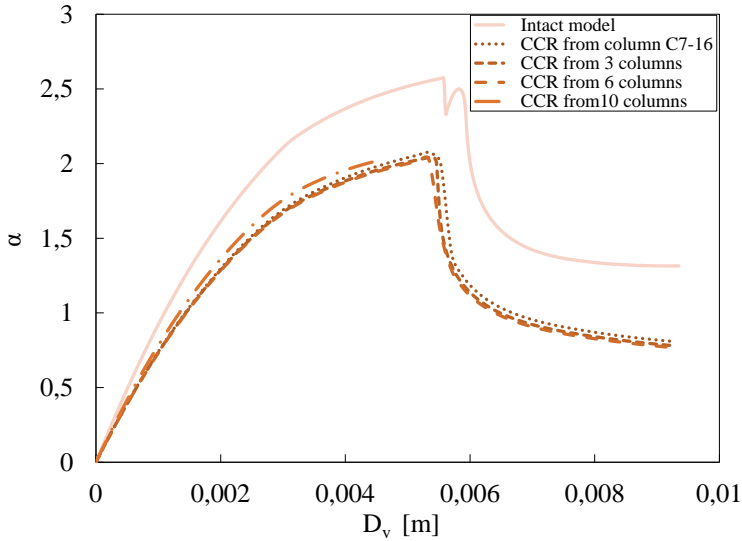
* Red values: Higher reductions of maximum load multiplier

Chapter 4- Progressive collapse resistance of a real RC building collapsed during structural retrofitting operations

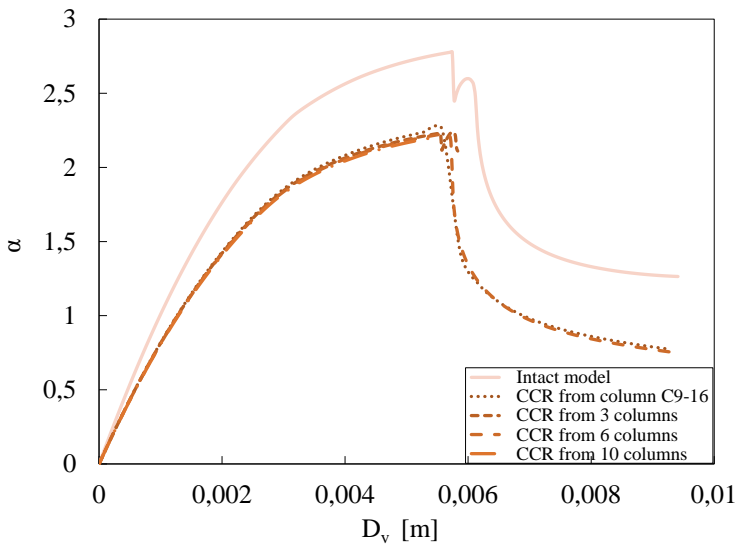
Scenario	Column(s)	Model with infill walls		Model w/o infill walls	
		α_{\max}	$\Delta\alpha_{\max}$	α_{\max}	$\Delta\alpha_{\max}$
Intact structure		2.55	–	2.78	–
CCR from single column	C11-19	2.54	-0.24%	2.78	-0.05%
	C9-16	2.20	-13.70%	2.27	-18.45%
	C7-16	2.07	-18.87%	2.57	-7.54%
	C5-22	2.55	-0.05%	2.78	0.00%
	C7-21	2.54	-0.20%	2.78	-0.08%
	C11-16	2.56	0.38%	2.78	-0.24%
	C5-16	2.54	-0.23%	2.79	0.29%
	C9-20	2.54	-0.05%	2.78	-0.28%
	C7-12	2.51	-1.50%	2.78	-0.14%
	C9-11	2.55	0.06%	2.78	-0.20%
CCR from 3 columns	C11-19, C5-22, C7-16	2.06	-18.90%	2.49	-10.64%
	C11-19, C5-22, C9-16	2.20	-13.48%	2.27	-18.49%
	C11-19, C7-16, C9-16	2.03	-20.21%	2.24	-19.48%
CCR from 6 columns	C9-16, C5-22, C11-19, C7-16, C9-20, C7-21	2.02	-20.59%	2.25	-19.32%
CCR from 10 columns	C9-16, C5-22, C11-19, C7-16, C9-20, C7-21, C5-16, C11-16, C7-12, C9-11	1.99	-21.79%	2.22	-20.21%

Table 4.5: Maximum load multiplier and its variations related to CCR scenarios on partial capacity model, with and without consideration of infill walls.

* Red values: Higher reductions of maximum load multiplier

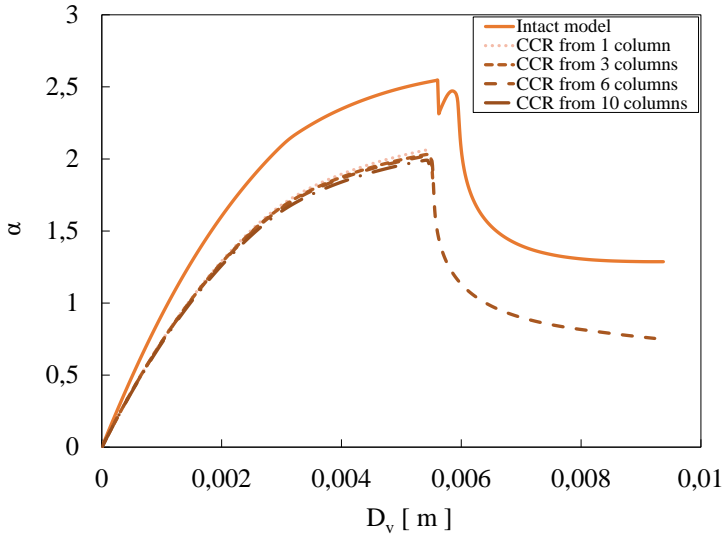


(a)

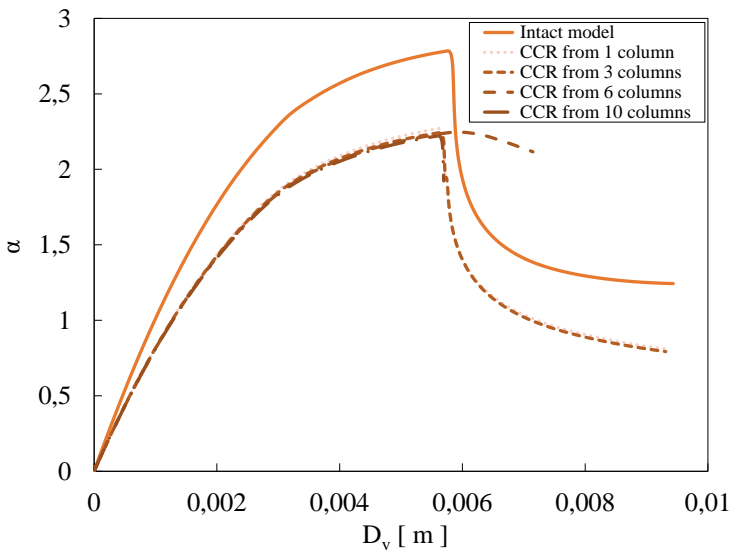


(b)

Figure 4.13: Pushdown capacity curves of complete capacity model under CCR scenarios: (a) with infill walls; (b) without infill walls.



(a)



(b)

Figure 4.14: Pushdown capacity curves of partial capacity model under CCR scenarios: (a) with infill walls; (b) without infill walls.

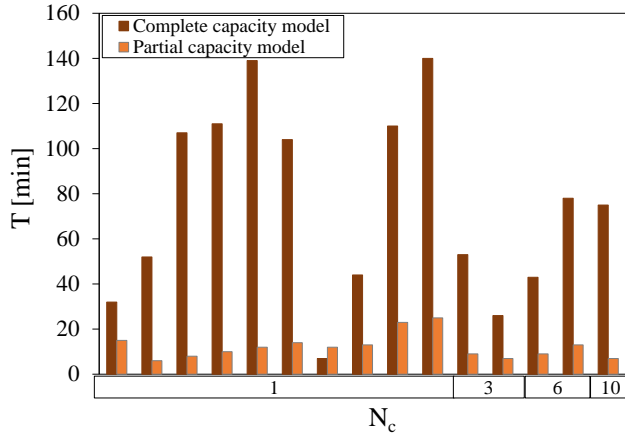


Figure 4.15: Computational time of complete and partial capacity models with infill walls

4.5.2 Impact of soil excavation around column bases

In a retrofitting operation involving the removal or reinstatement of the concrete cover from the column, the removal of soil at the base of the columns is necessary. To this aim in this study the impact of soil excavation around column bases on progressive collapse resistance was investigated. As outlined in Figure 4.5, three SE scenarios were considered in the study, by varying the location and number of columns involved. Two positions of the columns were defined for the scenarios involving a single column, *i.e.* internal and corner. Also in this case, the analysis were carried out for four different models of the structure, according to the complete or partial model and to the presence or not of the infill walls. Table 4.6 and Table 4.7 show the analysis results for the complete and partial capacity model, respectively. An important reduction of α_{max} was found for the SE scenario involving an internal column, C9-16, with a decrease of 95%, considering the model without infill walls. For the same scenario, taking into account the contribution of the infill walls, the reduction is lower, *i.e.* 53%. Again, single column scenarios involving a central column were found to be more burdensome than those involving a perimeter one. A decrease of 96% was obtained with the simultaneous

removal of supports at the base of three columns; this led to almost the total loss of load-bearing capacity. While for previous analyses the partial capacity model led to similar results, some differences were found in this case. Indeed, the use of partial capacity models produced an error in collapse capacity prediction equal to 7%, 1% and -27%, if compared to data of the complete models under soil excavation around column C9-16, column C11-19 and columns C9-16, C5-22, C11-19, respectively.

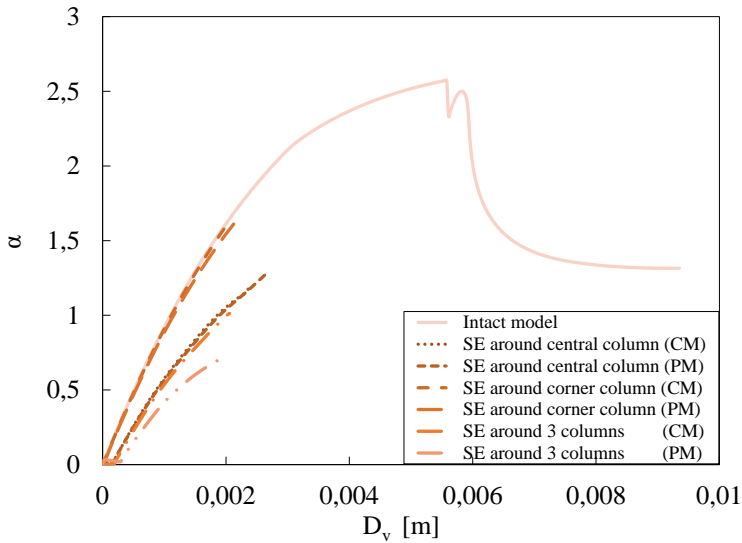
Figure 4.16 shows the pushdown capacity curves of complete and partial capacity models under SE scenarios, with or without the presence of the infill walls. For SE scenario involving three columns is easy to understand, from a graphical point of view, the complete loss of gravity-load capacity. More conservative results are shown by the pushdown curves of partial capacity model, particularly in models without consideration of infill walls as also outlined by Table 4.7.

Scenario	Column(s)	Model with infill walls		Model w/o infill walls	
		α_{\max}	$\Delta\alpha_{\max}$	α_{\max}	$\Delta\alpha_{\max}$
Intact structure		2.57	-	2.78	-
SE around 1 column	C9-16	1.20	-53.4%	0.12	-95.5%
	C11-19	1.60	-37.8%	2.71	-2.5%
SE around 3 columns	C9-16, C5-22, C11-19	1.01	-60.6%	0.11	-96.2%

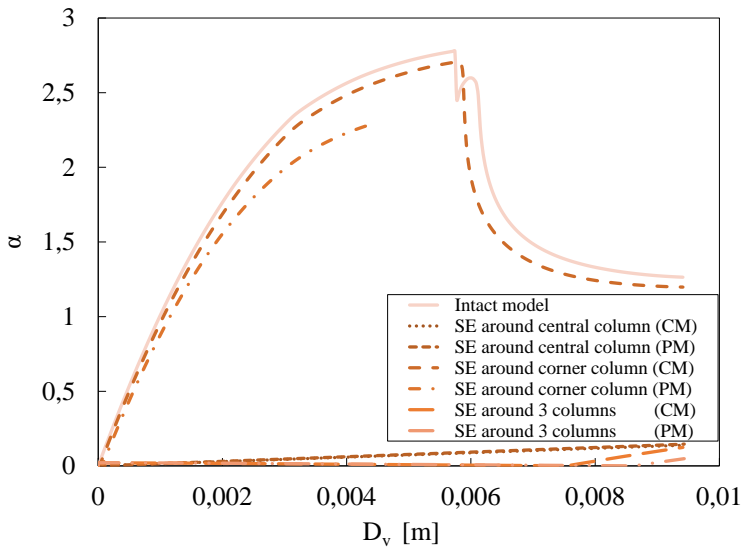
Table 4.6: Maximum load multiplier and its variations related to SE scenarios on complete capacity model, with and without consideration of infill walls.

Scenario	Column(s)	Model with infill walls		Model w/o infill walls	
		α_{\max}	$\Delta\alpha_{\max}$	α_{\max}	$\Delta\alpha_{\max}$
Intact structure		2.55	-	2.78	-
SE around 1 column	C9-16	1.28	-49.7%	0.13	-95.29%
	C11-19	1.61	-36.7%	2.30	-17.4%
SE around 3 columns	C9-16, C5-22, C11-19	0.74	-71.0%	0.03	-98.9%

Table 4.7: Maximum load multiplier and its variations related to SE scenarios on partial capacity model, with and without consideration of infill walls.



(a)



(b)

Figure 4.16: Pushdown capacity curves of complete and partial capacity models under SE scenarios: (a) with infill walls; (b) without infill walls.

CHAPTER 5 – INFLUENCE OF SEISMIC RETROFITTING WITH FRP SYSTEMS ON STRUCTURAL ROBUSTNESS: MULTI-HAZARD ANALYSIS

5.1 Case-study structure and modelling

The majority of the existing buildings in seismic prone regions were built before the publication of modern codes against earthquakes, and this leads to the need for structural retrofitting. In addition, structures may be subject to multiple hazards that may be either triggered by earthquakes (*e.g.*, landslides, soil liquefaction, tsunamis) or associated with other natural or anthropogenic events, such as floods, vehicle collision, blast, and fire. From here it follows that a multi-hazard performance assessment of building structures is important to implement integrated retrofit strategies. To date, many retrofit methods have been studied and used to improve or adapt structural safety against earthquakes, but the same cannot be said for structural robustness. The choice of this study stems from this lack, in order to investigate the influence of seismic retrofitting on structural robustness. A numerical study on the impact of Carbon Fibre Reinforced Polymers (CFRP) retrofitting on the structural robustness of low-rise RC frame buildings designed only to gravity loads was performed. Seismic performance and structural robustness were assessed in OpenSees [110] software through pushover and pushdown analyses of a fibre-based finite element model.

5.1.1 Characteristics and modelling of the structure

The structure under study is a multi-story Reinforced Concrete (RC) frame building that was designed only to gravity loads in accordance with recommendations of Eurocode 2 [71]. The structure was analyzed in previous studies [34, 106, 107] because it is representative of low rise, modern European RC buildings not designed for earthquake

resistance; it was also presented in chapter 3, specifically in section 3.1. It is characterized by a rectangular shape in plan and consists of five storeys, five primary frames with six bays in the x -direction, and seven secondary frames with four bays in the y -direction. A 2D framed system in the x -direction was extracted from the 3D structural model, as illustrated in Figure 5.1. The frame was characterized by the same span length along x -direction and y -direction, for a total of 30 m and 15 m, respectively. Beams and columns were characterized by a rectangular and square cross section, respectively; in detail they were $300 \times 500 \text{ mm}^2$ and $400 \times 400 \text{ mm}^2$ in size. The longitudinal reinforcement was uniform and consisted of $6\text{Ø}18$ and $8\text{Ø}18$ steel bars, for beams and columns respectively. The steel reinforcement was made of ribbed bars. For both beams and columns, the transverse steel reinforcement is made of $\text{Ø}8$ stirrups with 200 mm spacing, whereas the concrete cover is set to 40 mm.

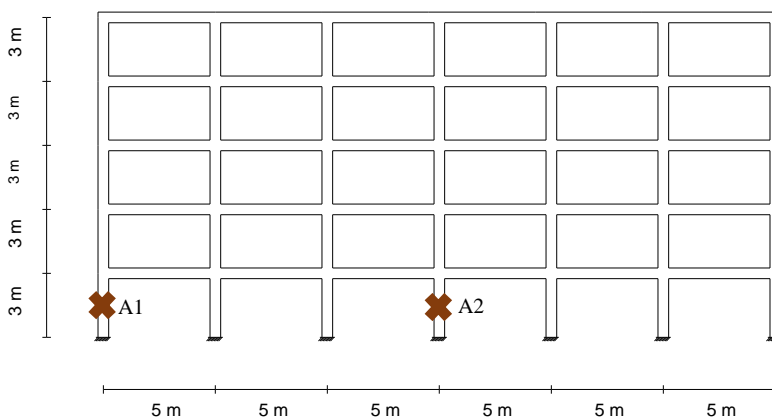


Figure 5.1: Elevation view of case-study structure

The structure was modelled through the finite element code OpenSees [110], that was experimentally validated for progressive collapse analysis in previous studies [*e.g.* 34]. A spread plasticity FE approach with displacement-based [111,112] fibre formulation was used to simulate the nonlinear capacity modelling of the structure. The cross sections of structural elements were discretized in 120; in detail, 100 fibres relating to the

confined concrete and 20 fibres for the remaining part. A direct integration of individual fibres' uniaxial material response was used to simulate the diffusion of inelasticity over cross-sections and member length, allowing the assessment of sectional stresses and strains during the incremental loading process. A mesh sensitivity analysis was carried out by assuming both smaller and larger numbers of fibres. The analysis results outlined that the selected discretization of cross-sections into 120 fibres was able to provide reliable results, ensuring a very good trade-off between computational accuracy and cost. The structure was characterized by C20/25 concrete and B450C steel reinforcement bars. The mechanical properties are listed in Table 5.1. The stress-strain behaviour of confined concrete within core of RC cross-sections was simulated through the uniaxial Kent-Scott-Park constitutive model [113], illustrated in Figure 5.2a. It is characterized by three branches: (i) a nonlinear rising branch up to peak compressive strength f'_{cc} and axial strain ϵ_{cc0} , (ii) a linear descending branch up to residual compressive strength f'_{ccu} and axial strain ϵ_{ccu} and (iii) a residual strength plateau with unlimited strain. The characteristic compressive strength of unconfined concrete, f_{ck} , and the mean compressive strength, f_{cm} , were assumed equal to 20 MPa and 28 MPa, respectively, according to Eurocode 2 [71]. In case of concrete cover, the lack of concrete confinement was assumed, and this led to assume the peak compressive strength as $f'_c = f_{cm} < f'_{cc}$, with $\epsilon_{cu} < \epsilon_{ccu}$ and zero residual strength. A uniaxial bilinear model, Figure 5.2b with kinematic hardening, defined through Young's modulus E_0 , yield strength f_y , and hardening ratio k , was used to describe the reinforcing steel behaviour. Geometric nonlinearities in the form of both large displacements/rotations and P-Delta effects were considered by means of a total corotational transformation. Beam-column joints were modelled as rigid elements as done in several previous research studies (e.g., [33, 72, 106]).

Material	Structural member	f_y [MPa]	E_0 [GPa]	k	f'_{cc} [MPa]	f'_{ccu} [MPa]	E_c [GPa]	ϵ_{cc}	ϵ_{ccu}	ϵ_{cu}
Concrete	Beam (core)	–	–	–	29.41	5.88	24.87	$2.36 \cdot 10^{-3}$	$8.01 \cdot 10^{-3}$	–
	Column (core)	–	–	–	29.14	5.82	24.87	$2.34 \cdot 10^{-3}$	$6.90 \cdot 10^{-3}$	–
	Any (cover)	–	–	–	28.00	5.60	23.50	$2.38 \cdot 10^{-3}$	–	$3.50 \cdot 10^{-3}$
Steel	Any	450	200	0.01	–	–	–	–	–	–

Table 5.1: Steel and concrete mechanical properties

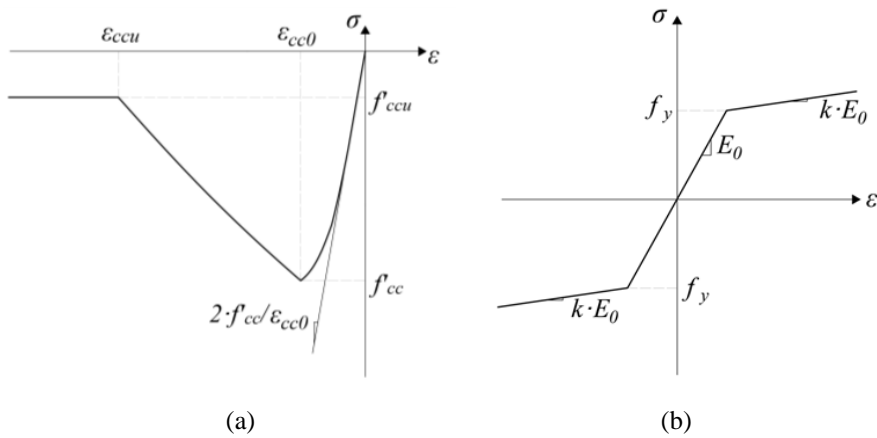


Figure 5.2 : Constitutive model: (a) Kent-Scott-Park constitutive model, (b) uniaxial bilinear model

As shown in Figure 5.3, each beam was discretized in 5 parts and the loads were applied as concentrated according to this discretization. A parametric study was carried out and the results highlighted that the increase in the number of model elements didn't increase computational accuracy. Dead loads and live loads were applied under the design gravity load combination according to UFC guidelines [30], according to equation (7) of section 2.5.2, with dead loads D and live loads L set equal to 3 kN/m^2 and 2 kN/m^2 , respectively.

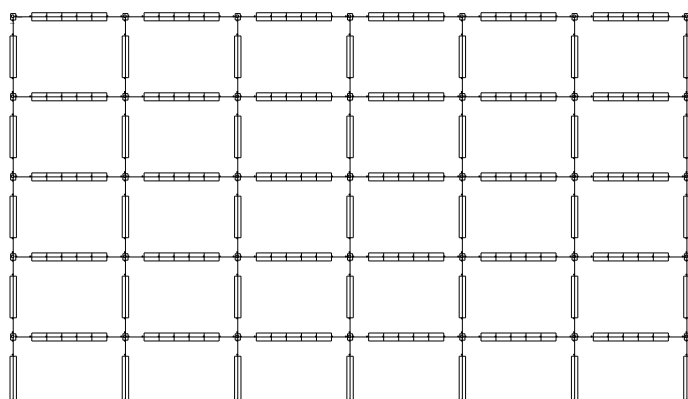


Figure 5.3 : Discretization of structural elements

5.1.2 Assessment of dynamic amplification factor

In a progressive collapse analysis, as discussed in section 2.6, the amplification of gravity loads on beams/floor areas above the removed column(s) must be considered. This allows to consider in an implicit way the vertical inertia forces generated in the portion of the structure involved in the progressive collapse. So that the next step of the study provided the assessment of the Dynamic Amplification Factor (DAF). There are no specific Equations for DAF prediction in case of European frame buildings complying with Eurocodes. Table 3-5 of UFC guidelines [30] provides an Equation for nonlinear static analysis of RC frame structures, as described by equation (5).

In this study, the DAF was specifically assessed for the case-study structure by comparing the gravity load capacity resulting from Pushdown Analysis (PDA) to that predicted via Incremental Dynamic Analysis (IDA) in a previous study [106], under increasing vertical deformation induced by the sudden removal of a ground-floor column. Indeed, the structure under study was already investigated in another study [106], where it was modelled through the FE code SeismoStruct [73]. The model used in this study was compared to the last one revealing a good agreement in terms of modal properties (*i.e.*, vibration periods and mode shapes as well as corresponding participating

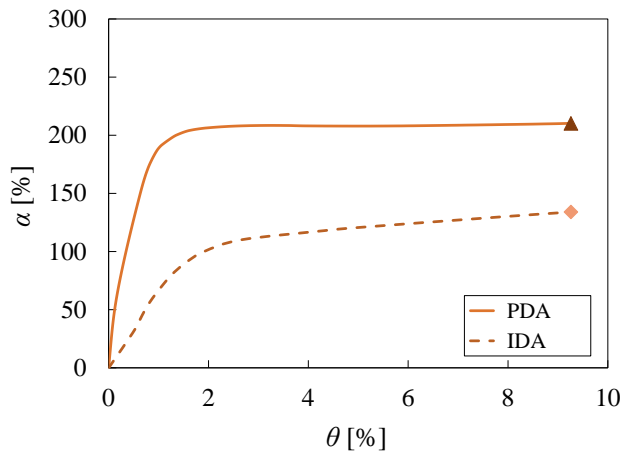
mass ratios). The vertical deformation was described in terms of beam drift, indicated with θ , that is a common variable of PDA and IDA; it can be associated with a load multiplier, α , defined by Parisi and Augenti [40] as the ratio between the sum of vertical reaction forces R_i of base restraints during progressive collapse analysis and the sum of vertical reaction forces of base restraints $R_i(Q_b)$ corresponding to the design gravity loads. The numerator and the denominator measure the gravity load capacity of the structure and the vertical resistance demand on the structure, respectively. On the other hand, θ can be defined as the ratio between the vertical displacement of the control point (assumed to be the upper joint of the removed column) and the beam length (equal to 5 m). The results of PDA and IDA were plotted in α - θ plane, to obtain dimensionless capacity curves. From another point of view, this illustration of results allowed to verify the structural robustness through α_{max} value; indeed, if the last one is higher than unit, it means that the structure is robust, and it is able to redistribute loads after the damaging event.

In this study two different column removal scenarios were defined, according to Figure 5.1. The comparison between analysis results are illustrated in Figure 5.4; it is of simple intuition that PDA with uniform gravity loads led to an overestimation of the gravity load capacity, due to the lack of consideration of the dynamic load amplification on beams above the removed column. The triangle and rhombus-shaped indicators show the points of peak load capacity in PDA and IDA, respectively. By the ratio of the load multiplier obtained through pushdown and incremental dynamic analysis, the DAF was obtained as follows:

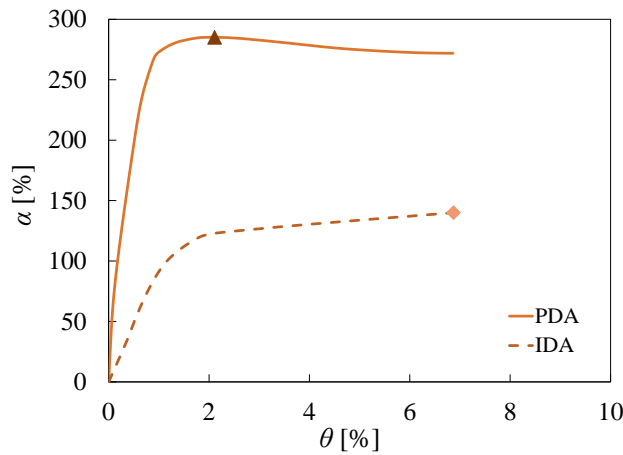
$$DAF = \frac{\alpha_{PDA}}{\alpha_{IDA}} \quad (18)$$

Figure 5.5 shows DAF- θ curves for both column-removal scenarios, evidencing a realistic estimation of dynamic load amplification for the Eurocode-conforming structure under study. Its value was always higher than unity up to large vertical drifts. In addition, this demonstrated that the DAF value found according to UFC guidelines, equal to 1.16, was lower than that directly computed through PDA-IDA comparison.

This further remarks the need for additional and comprehensive studies aimed at the DAF evaluation for building structures designed in accordance with the Eurocodes, particularly to Eurocode 2 [71] and Eurocode 8 [115] for gravity-load designed and earthquake-resistant structures, respectively.



(a)



(b)

Figure 5.4: Comparison between pushdown analysis (PDA) and incremental dynamic analysis (IDA): (a) Scenario A1; (b) Scenario A2

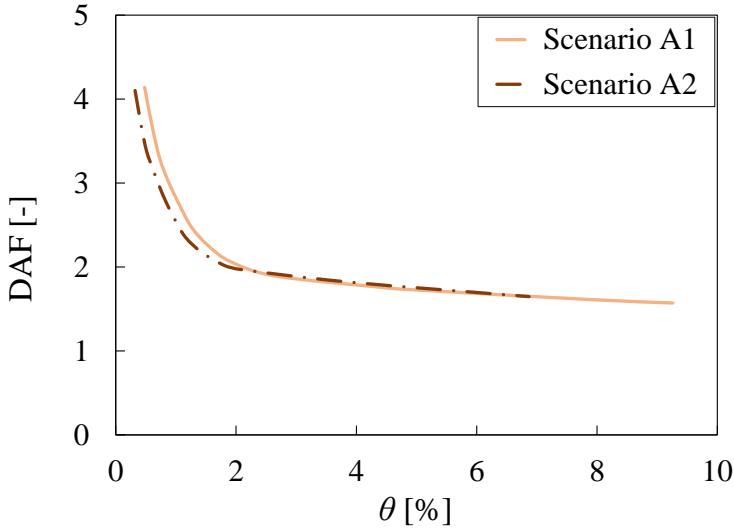


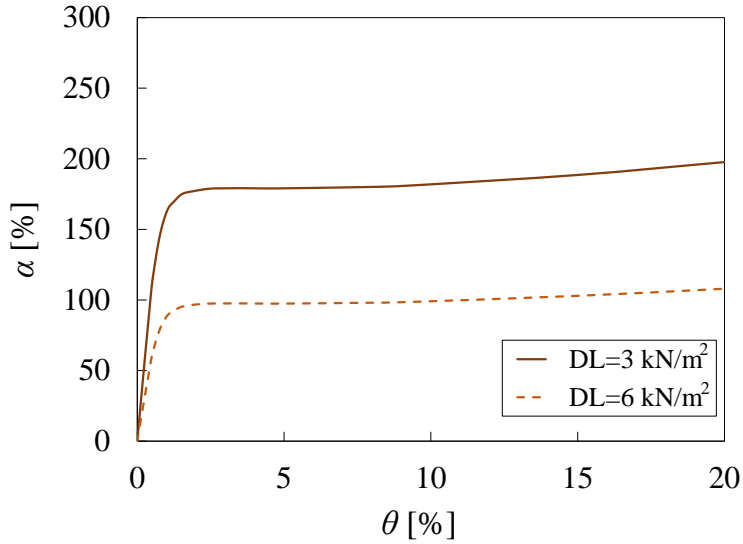
Figure 5.5 : Structure-specific DAF assessment for the case-study frame system

5.2 Progressive collapse capacity evaluation

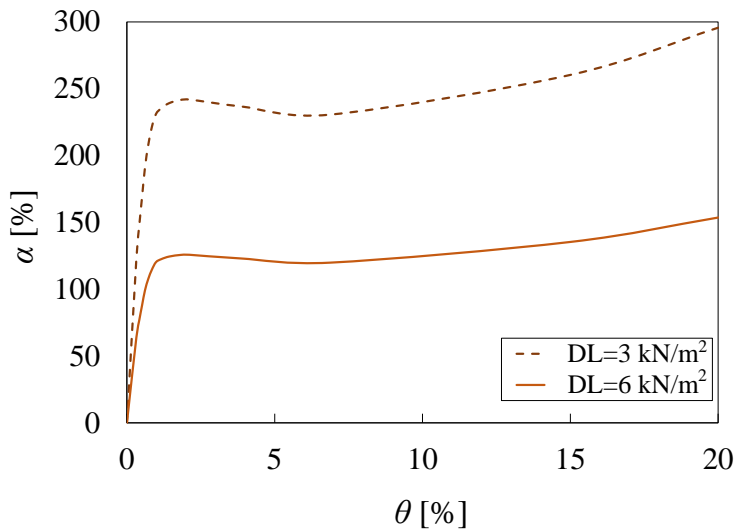
5.2.1 Influence of design loads and ultimate steel strain on progressive collapse capacity

As discussed above, two different column removal scenarios were defined and the progressive collapse capacity of the structure under these was assessed. Pushdown analyses were performed for scenario A1 and A2, coincident with the worst cases of column loss for the structure under investigation in the previous study [107]. In this phase of the study, two different variables were taken into account, *i.e.* the design gravity loads and the ultimate steel strain. To evaluate the influence of the first one, live loads were increased to 6 kN/m². Figure 5.6 shows the dimensionless pushdown capacity curves, which indicate that this increase had an important effect on structural robustness. A reduction from 181% to 99% was found for scenario involving the corner column (scenario A1) and this underlined an insufficient level of robustness to design gravity loads. The progressive collapse capacity reduced by 92% when the central column was

removed (scenario A2) even though the maximum load multiplier was still found to be higher than unity.



(a)

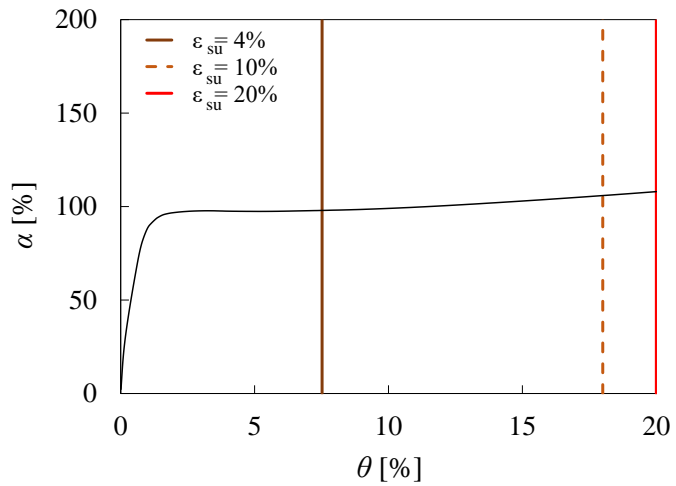


(b)

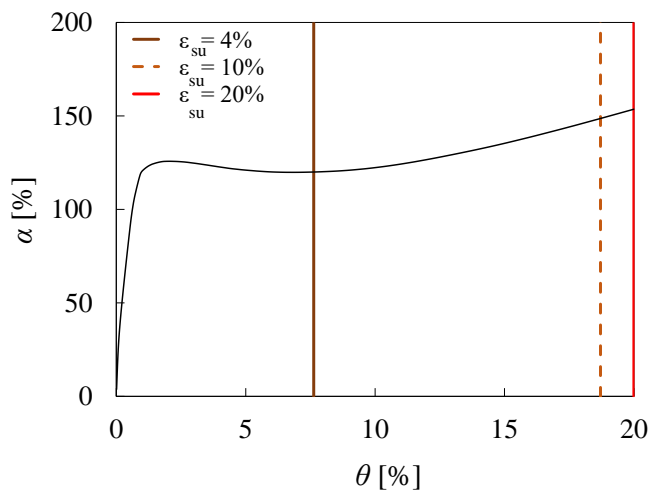
Figure 5.6: Influence of design gravity loads on progressive collapse capacity: (a) scenario A1, (b) scenario A2

Subsequently, the influence of ultimate steel strain, ε_{su} , on progressive collapse capacity was assessed. Three different values of ε_{su} were considered, *i.e.* 4%, 10% and 20%. The reason of this choice is the same as discussed in section 3.3.1.

In Figure 5.7 the vertical drifts corresponding to the selected values of ε_{su} are identified for each scenario. Different lines identify the residual part of capacity curves after the attainment of each strain threshold; in this way the influence of ε_{su} on structural robustness in terms of peak load capacity (measured through α_{max}) and maximum vertical drift (*i.e.*, θ_{max}) can be evaluated. The progressive collapse of RC frames of RC is actually related to an ultimate drift θ_u ranging between 15% and 20%, according to previous studies [5, 90]. If ε_{su} is set to 4%, a vertical drift around 8% was reached for both scenarios. If it increases to 10% or 20%, the beams can develop both compressive arch action and tensile catenary action, allowing the RC frame to reach $\theta_{max} = 18\%$ and $\theta_{max} = \theta_u$, respectively. These results underline that the compressive arch action and tensile catenary action allow an increase in maximum load multiplier at drifts larger than approximately 7%; Figure 5.7 shows a sort of global hardening behaviour, especially in scenario A2. This is outlined also by axial forces in beams (denoted as N) under varying drift. Figure 5.8b and Figure 5.9 b illustrate their trend for both scenarios with near-collapse deformed shapes in Figure 5.8a and Figure 5.9a. The graphs show that the beams above the removed column at floor levels 1 and 5 were subjected to the largest variations in axial force. This turns out to be more marked for the scenario A2, in which the beams at those floor levels experienced in first instance a compressive axial loading, arch action, up to a vertical drift $\theta_{max} \approx 8\%$ and then a tensile axial loading, catenary action, till collapse. When the maximum axial strain in longitudinal steel bars exceeded 4%, reaching 10% and 20% the tensile catenary action was mobilised. As regards the other beams at central floor levels, the forces gradually vanish under increasing drift.



(a)



(b)

Figure 5.7: Influence of ultimate steel strain on pushdown capacity curves: (a) scenario A1, (b) scenario A2

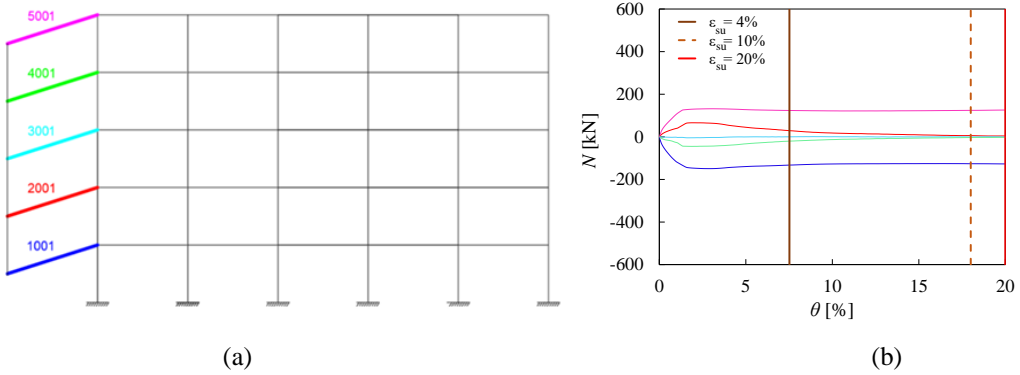


Figure 5.8: Beam behaviour under scenario A1: (a) beams denomination, (b) axial force under varying drift and ultimate steel strain.

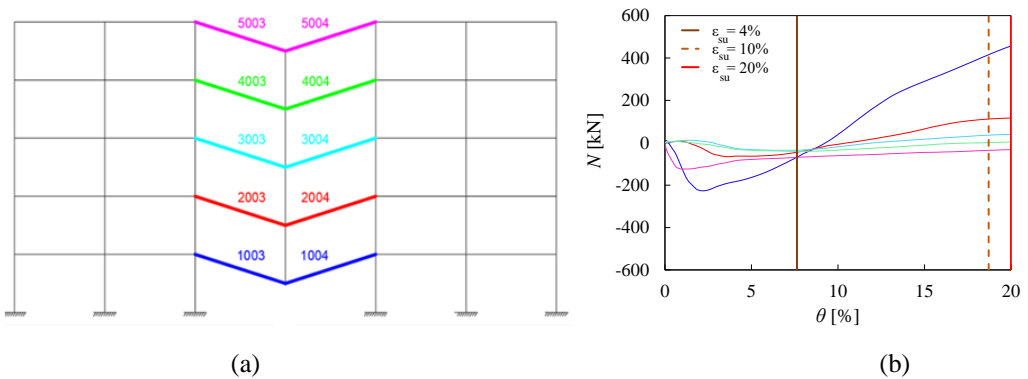


Figure 5.9: Beams behaviour under scenario A2: (a) beams denomination, (b) axial force under varying drift and ultimate steel strain.

5.2.2 Shear safety checks

The structure under study, as mentioned above, was designed only to gravity loads, according to previous code [71]. The latter did not provide for a strategy relating to the strength hierarchy, which was later introduced in subsequent codes. For this reason the next step of the research led to shear checks, due to the possibility of shear failure in structural elements that can occur and affect the progressive collapse capacity, according to previous studies on RC frame buildings not designed for earthquake resistance [e.g. 40]. Shear failure mechanisms were not modelled in the FE model implemented in OpenSees [110]; to this aim, in order to identify the analysis step related to the first

occurrence of shear failure, previous shear safety checks were carried out on the structure. The shear resisting force of frame members was assessed through the capacity model proposed by Biskinis and Fardis [114], according to the following Equation:

$$V_{RD} = V_N + V_C + V_W \quad (19)$$

where V_N , V_C and V_W denote the contributions to shear strength from the axial load (in the form of an inclined internal strut resisting mechanism), the concrete, and the transverse reinforcement (according to the Ritter-Mörsch truss resisting mechanism analogy), respectively. A step-by-step evaluation of shear demand on frame members during the pushdown analysis was carried out in order to obtain demand-to-capacity ratios (DCRs). The results are listed in Table 5.2 and Table 5.3, collected by varying scenario, column line or beam span and floor level. The beam span are labelled in alphabetical order from the left- to the right-hand side, according to Figure 5.10. On the other side, the columns were labelled from 1 to 7 from the left- to the right-hand side. As the results show, premature failures occurred in the beams span A in the third step of progressive collapse analysis with DCR ranging from 1.01 (floor level 5) to 1.49 (floor level 1). For the scenario involving the central column, the beams belonging to the spans C and D were subjected to this type of failure, with a DCR between 1.39 and 1.44. For the vertical elements, the DCRs were less than unit, so that shear failure did not affect them. Figure 5.11a and b show graphically the localization of shear failures in structural elements.

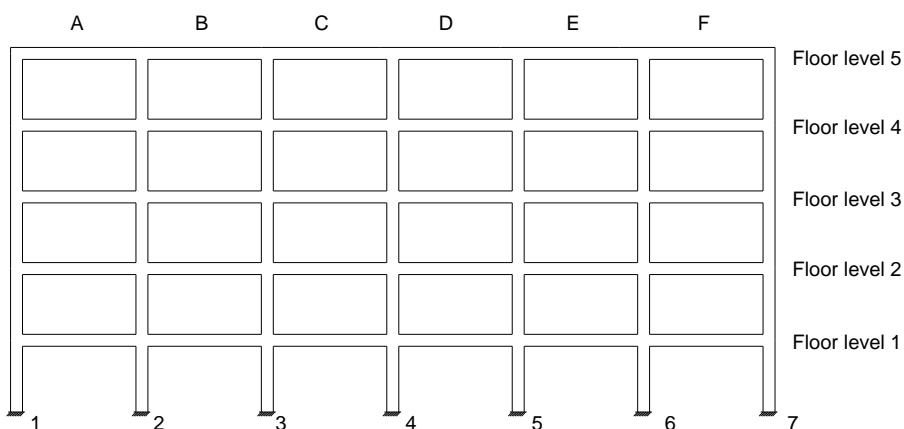


Figure 5.10: Denomination of columns line and beams span

Floor level	Scenario A1					
	Beam span					
	A	B	C	D	E	F
1	1.49	0.74	0.59	0.60	0.60	0.63
2	1.15	0.55	0.50	0.49	0.49	0.50
3	1.15	0.52	0.49	0.49	0.49	0.50
4	1.16	0.53	0.51	0.50	0.50	0.49
5	1.01	0.54	0.44	0.44	0.44	0.47

Floor level	Column line						
	1	2	3	4	5	6	7
1	0.00	0.22	0.07	0.06	0.08	0.09	0.01
2	0.89	0.31	0.32	0.26	0.25	0.24	0.02
3	0.57	0.41	0.24	0.23	0.24	0.24	0.00
4	0.58	0.43	0.23	0.25	0.25	0.25	0.01
5	0.79	0.59	0.41	0.35	0.33	0.32	0.03

Table 5.2: Demand-to-capacity ratios corresponding to the first occurrence of shear failure in structural elements for scenario A1*

*Red values indicate DCRs > 1 , *i.e.*, failed elements.

Floor level	Scenario A2					
	Beam span					
	A	B	C	D	E	F
1	0.54	0.56	1.44	1.44	0.56	0.54
2	0.52	0.56	1.42	1.42	0.56	0.52
3	0.51	0.55	1.40	1.40	0.55	0.51
4	0.52	0.53	1.40	1.40	0.53	0.52
5	0.55	0.66	1.39	1.39	0.66	0.55

Floor level	Column line						
	1	2	3	4	5	6	7
1	0.24	0.13	0.32	0.00	0.32	0.13	0.24
2	0.16	0.05	0.46	0.00	0.46	0.05	0.16
3	0.19	0.01	0.50	0.00	0.50	0.01	0.19
4	0.20	0.05	0.54	0.00	0.54	0.05	0.20
5	0.25	0.13	0.84	0.00	0.84	0.13	0.25

Table 5.3: Demand-to-capacity ratios corresponding to the first occurrence of shear failure in structural elements for scenario A2

*Red values indicate DCRs > 1 , *i.e.*, failed elements.

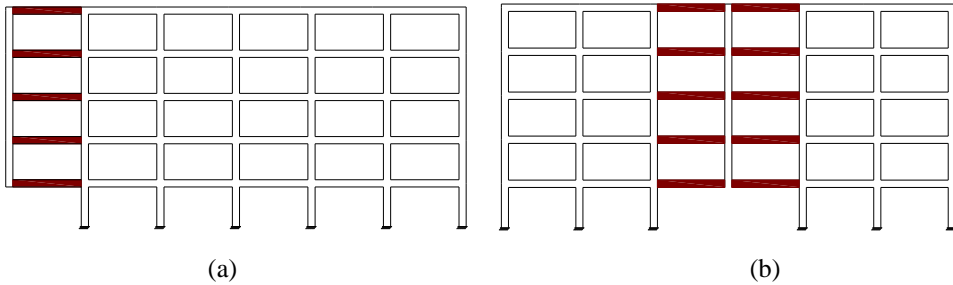


Figure 5.11: Shear failures location: (a) scenario A1, (b) scenario A2

5.3 Seismic safety assessment

The next step of the study involved the seismic assessment of the structure that was assumed to be located in L'Aquila, Italy; this falls in an high-seismicity area and was subjected to several damage produced by the earthquake of 2009 [13]. Nonlinear incremental static analysis were carried out, according to Eurocode 8-Part 3 [115]. A site-dependent seismic hazard assessment was carried out according to the Italian building code NTC2018 [2] and the seismic parameters shown in Table 5.4 were

considered. Two different load patterns were taken into account to assess the seismic capacity of the structure:

- Mass profile, with lateral forces proportional to inertia masses, assuming a uniform acceleration pattern along with the height of the structure.
- Mode profile, with lateral forces proportional to inertia masses times first mode displacements.

Pushover analysis were carried out with displacement control and the control point of these analysis was set to a beam-column joint at the roof level. The output was a capacity curve, that was first scaled down according to the first-mode participating factor and then approximated through a bilinear diagram according to Eurocode 8 – Part 3 [115]. Seismic capacity and demand were then transformed in the acceleration-displacement plane, resulting in capacity and demand spectra, respectively. Seismic capacity and demand were then transformed in the acceleration-displacement plane, resulting in capacity and demand spectra, respectively. The comparison between the inelastic displacement demand, S_{di} , and the displacement capacity, d^*_u , allowed the seismic assessment. The performance point (PP) was defined by the intersection between the demand and capacity spectra and this allowed the seismic safety assessment in terms of displacement DCR.

Figure 5.12 shows the outcome of seismic performance assessment, where:

- S_a and S_d are the spectral accelerations and displacements, respectively.
- S_{ay} is the yield spectral acceleration of the structure.
- S_{de} is the elastic displacement demand (corresponding to point D and elastic acceleration demand S_{ae}).

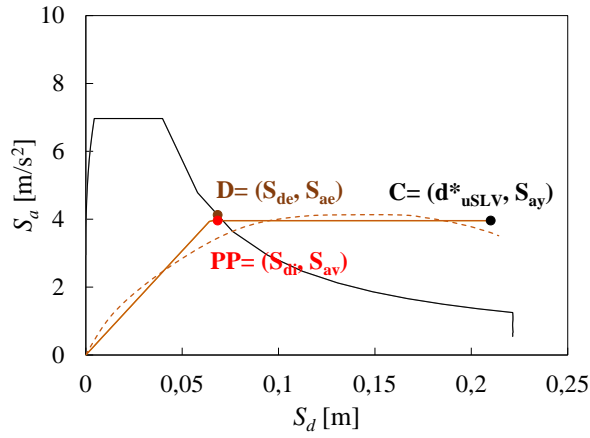
The point C is defined by the displacement capacity and yield spectral acceleration. A satisfactory global performance of the structure was found, under mode and mass force profiles with DCR equal to 33% and 43%, respectively.

Subsequently, seismic safety of the case-study structure was locally assessed against brittle shear failures in structural elements, in line with what was done previously for the progressive collapse analysis. The same capacity model used in Section 5.2.2 was taken

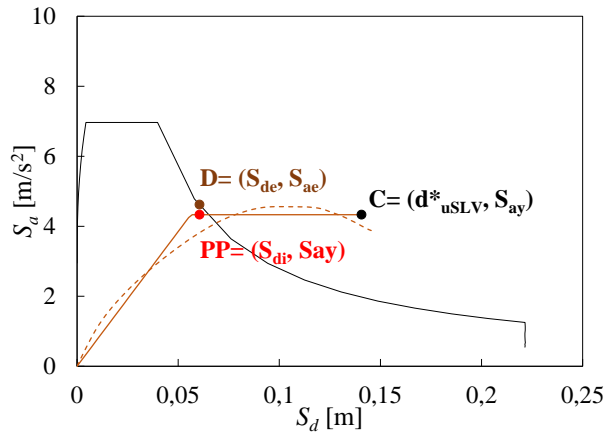
into account to perform these checks. According to Eurocode 8 – Part 3 [115] and NTC2018 [2], those local checks were performed at the global performance point, identified by red circle identified in Figure 5.12. The procedure was different from that used for progressive collapse analysis, where local safety checks were carried out step by step to identify the first occurrence of shear failure. This because local checks for seismic assessment do not indicate the first occurrence nor the sequence of shear failures throughout the analysis because demand-to-capacity ratios are directly associated with displacement demand on the structure. Table 5.5 and Table 5.6 show shear strength DCRs evaluated for structural elements and the ratios outline that most of frame members were expected to fail in shear under the design earthquake. The results shown in table are graphically illustrated in Figure 5.13, in which are identified the unsafe members for each orientation of lateral forces.

Seismic hazard parameter	Value
Nominal Lifetime (V_N)	50 years
Occupancy Factor (C_U)	1
Reference Period (V_R)	50 years
Topographic Category	T_I
Return Period of design earthquake (T_R)	475 years
Horizontal Peak Ground Acceleration (a_g)	0.26 g
Upper Bound Period (T_C^*)	0.350 s
Stratigraphic Amplification Factor (S_s)	1.154
Topographic Amplification Factor (S_T)	1
Ground Type	B
Peak Ground Acceleration (PGA)	0.3 g
Maximum Amplification Factor of horizontal spectral acceleration (F_0)	2.36

Table 5.4: Seismic hazard parameters for the case-study structure



(a)



(b)

Figure 5.12: Global seismic performance assessment of case-study structure: (a) mode force profile; (b) mass force profile

Floor level	Mass profile					
	Beam span					
	A	B	C	D	E	F
1	2.36	2.24	2.25	2.25	2.24	2.28
2	2.20	2.06	2.02	1.97	1.92	1.89
3	1.82	1.70	1.66	1.61	1.56	1.53
4	1.36	1.33	1.29	1.26	1.23	1.19
5	1.36	1.33	1.29	1.26	1.23	1.19

Floor level	Column line						
	1	2	3	4	5	6	7
1	2.03	2.07	2.14	2.19	2.25	2.32	2.04
2	1.60	2.20	2.14	2.09	2.04	1.98	0.90
3	1.15	1.86	1.77	1.68	1.58	1.48	1.02
4	0.70	1.39	1.32	1.25	1.19	1.13	0.74
5	0.02	0.81	0.79	0.75	0.71	0.63	0.60

Table 5.5: Beams and columns shear checks: demand-to-capacity ratios corresponding to mass profile

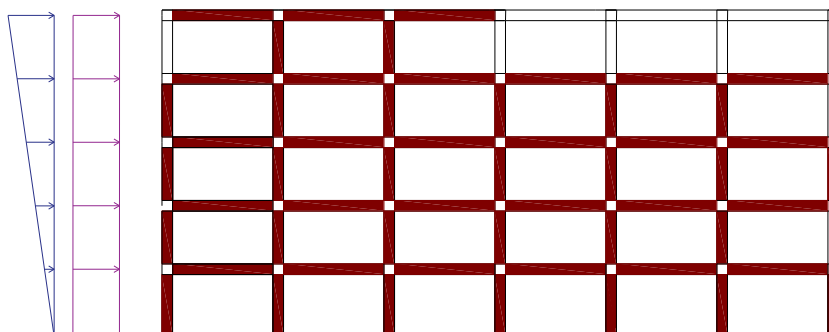
*Red values: DCRs > 1, i.e., failed elements.

Floor level	Mode profile					
	Beam span					
	A	B	C	D	E	F
1	2.24	2.18	2.21	2.23	2.25	2.28
2	2.32	2.18	2.14	2.10	2.06	2.03
3	2.05	1.90	1.85	1.80	1.74	1.72
4	1.58	1.51	1.46	1.42	1.37	1.32
5	1.13	1.01	1.00	0.98	0.98	0.89

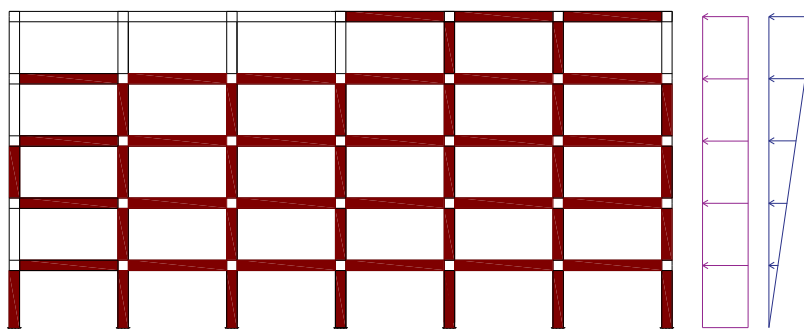
Floor level	Column line						
	1	2	3	4	5	6	7
1	1.59	1.81	1.93	2.03	2.12	2.21	1.89
2	1.80	2.25	2.24	2.20	2.16	2.12	0.98
3	1.46	2.16	2.07	1.98	1.88	1.78	1.17
4	1.04	1.76	1.67	1.58	1.50	1.42	0.91
5	0.18	1.12	1.05	0.99	0.93	0.81	0.65

Table 5.6: Beams and columns shear checks: demand-to-capacity ratios corresponding to mode profile

*Red values: DCRs > 1, i.e., failed elements.



(a)



(b)

Figure 5. 13: Identification of frame members failing in shear for each orientation of lateral forces

5.4 Structural retrofitting with carbon fibre-reinforced polymers

5.4.1 Design of FRP systems

From the analyses carried out in the previous sections, it has been inferred that the safety of the structure is undermined by the potential occurrence of local failures. In the structural engineering field, to date, many retrofit measures that can improve the structural behaviour are known. Among the possible interventions there is the use of

fibre reinforced polymers (FRPs), which consist of a polymeric matrix and continuous fibre reinforcement with high mechanical properties. They are the most widely used material today for structural improvements to existing buildings. FRPs have an anisotropic and heterogeneous behaviour, showing a predominantly linear elastic behaviour until collapse. These materials have several peculiarities, which vary according to the type of the single FRP and which determine their field of application. However, all fibre-reinforced products have common characteristics such as: (i) high lightness, (ii) high mechanical resistance, (iii) high resistance to corrosion, (iv) high thermal insulation, (v) high dielectric and non-magnetic properties. The fibres have a high tensile strength and therefore represent the resistant elements of the fibre-reinforced material. When a fibre-reinforced material undergoes an axial tensile stress, the real stresses are absorbed by the fibres, while the polymer matrix has only the task of distributing them among the fibres, thus determining a uniformity of stress among them. The resin has also the function of protecting the fibres from wear, as well as to ensure their good alignment. FRP materials are characterized by a perfectly linear elastic behaviour until failure. The fibres used for production of FRP must have either high mechanical strength or high elastic modulus, depending on the problem to be addressed. The geometric configuration of the fibres can be distinguished in:

- Uniaxial fabrics, consisting of fibres or bundles of fibres all arranged in parallel (warp) and held together by a weft of filaments that can be the same material of the fibres of the warp or, more often, from a different material (*e.g.*, nylon or polyester).
- Biaxial fabrics, obtained by weaving fibre bundles in two orthogonal directions. They can be made using both fibres of the same type in the two directions and fibres of a different nature (*e.g.*, carbon in one direction and aramid in the other).
- Multiaxial fabrics, obtained by arranging the fibres according to several directions, variously inclined to each other. There are commercially available triaxial fabrics, with bundles of fibres woven along three directions inclined at

120° to each other, and quadriaxial fabrics characterized by the presence of four different orders of fibres inclined at 135° to each other.

In this study carbon fibres were chosen and the frame members prone to shear failure were supposed to be strengthened with CFRP sheets with single or multiple plies depending on the type and location of the member to be retrofitted. The properties of the selected CFRP are shown in Table 5.7; they were designed according to CNR-DT 200R1/2013 guidelines [116]. A single-ply CFRP wraps was used for beams and multiply confinement systems for columns. More specifically, CFRP sheets around columns consisted of 5 plies at the ground floor, 3 plies at the second floor, 2 plies at the third floor, and a single ply at the last two floors.

Weight per unit area, w_f	Equivalent thickness of dry fabric, t_f	Effective area per unit width, A_f	Tensile strength, f_f	Ultimate tensile force per unit width, F_f	Young's modulus, E_f	Ultimate strain, ε_{fu}
[g/m ²]	[mm]	[mm ² /mm]	[GPa]	[kN/m]	[GPa]	[%]
1200	0.666	666.4	4.9	3265	252	2

Table 5.7: Properties of selected CFRPs

5.4.2 Impact of FRPs on seismic retrofitting and structural robustness

Once the reinforcement scheme was designed, its influence on seismic capacity and structural robustness was evaluated. In the light of this, the previous analyses were repeated for the reinforced structure, in order to understand the effective contribution given by this retrofit measure. During these analysis the capacity changes while the demand calculation was the same as in the previous section. Table 5.8 and Table 5.9 show the shear demand-to-capacity ratios obtained for the retrofit structure; these were found to be lower than unity in all frame members. This means that the retrofitting system was able to solve the issue of shear failure in beams and columns.

Floor level	Mass profile					
	Beam span					
	A	B	C	D	E	F
1	0.83	0.79	0.80	0.80	0.79	0.80
2	0.68	0.64	0.63	0.62	0.60	0.60
3	0.64	0.60	0.59	0.57	0.55	0.54
4	0.48	0.47	0.46	0.45	0.43	0.42
5	0.35	0.33	0.33	0.32	0.32	0.29

Floor level	Column line						
	1	2	3	4	5	6	7
	1	0.54	0.91	0.92	0.95	0.97	0.99
2	0.48	0.97	0.93	0.91	0.89	0.87	0.39
3	0.39	0.82	0.77	0.73	0.69	0.65	0.43
4	0.28	0.65	0.62	0.59	0.56	0.53	0.33
5	0.01	0.34	0.33	0.31	0.30	0.26	0.24

Table 5.8: Shear demand-to-capacity ratios of structural elements after retrofitting for mass profile

Floor level	Mode profile					
	Beam span					
	A	B	C	D	E	F
1	0.79	0.77	0.78	0.79	0.79	0.81
2	0.82	0.77	0.76	0.74	0.73	0.72
3	0.73	0.67	0.65	0.64	0.62	0.61
4	0.56	0.53	0.52	0.50	0.48	0.47
5	0.40	0.36	0.35	0.35	0.35	0.32

Floor level	Column line						
	1	2	3	4	5	6	7
	1	0.41	0.80	0.84	0.88	0.92	0.96
2	0.52	0.99	0.98	0.96	0.94	0.93	0.44
3	0.47	0.95	0.90	0.86	0.82	0.78	0.51
4	0.41	0.83	0.79	0.74	0.70	0.67	0.41
5	0.07	0.47	0.44	0.41	0.39	0.34	0.26

Table 5.9: Shear demand-to-capacity ratios of structural elements after retrofitting for mode profile

Subsequently, pushdown analysis were carried out for the retrofit structure under the two column removal scenarios, in order to assess the impact of the CFRP. The results, shown in Figure 5.12, underline that the seismic retrofitting allowed the structure to develop a satisfactory level of robustness to both corner and central column-removal scenarios. When the corner column was removed (scenario A1) the first shear failure was reached at a vertical drift $\theta = 13.6\%$, corresponding to a peak load multiplier higher than unity, *i.e.* $\alpha_{max} = 1.02$. This underlines the beneficial effect of the CFRP; indeed, the as-built structure suffered the first shear failure at $\theta = 0.03\%$, corresponding to $\alpha_{max} = 0.33$. When the removal column scenario involved a central element, it was found an higher robustness level of the structure after seismic retrofitting. The first shear failure occurred at $\theta = 1.0\%$ and $\alpha_{max} = 1.18$, indicating again an increase in both displacement and load capacity of the retrofitted structure. In as-built conditions, PDA under scenario A2 highlighted the first shear failure at $\theta = 0.3\%$ and $\alpha_{max} = 0.48$.

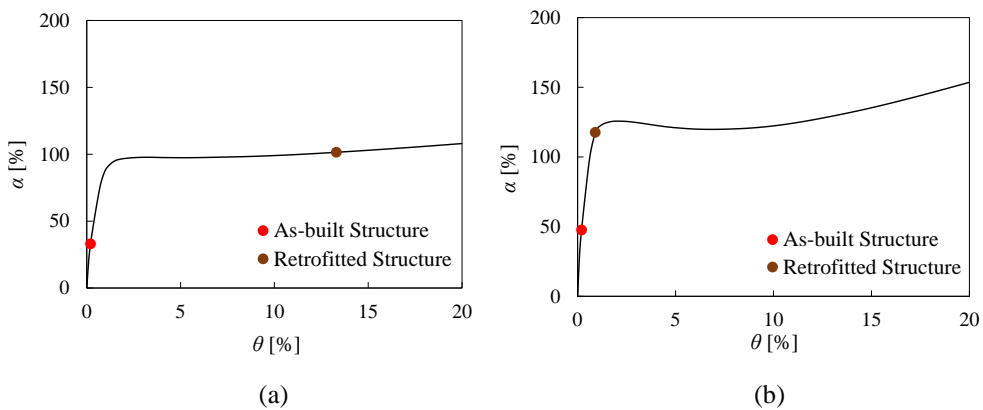


Figure 5. 14: Impact of retrofit measure on structural robustness (a) scenario A1, (b) scenario A2

5.4.3 Sensitivity of joint seismic-robustness performance to beam span length and shear strength of strengthening system

In order to evaluate the impact of geometric and material parameters on progressive collapse resistance, a parametric analysis was carried out. The parameters considered include the beam span length, L_b , of the case study structure, and the CFRP shear

resistance. These analyses involved the corner column removal scenario (A1) due to its higher vulnerability. Five values of L_b were considered, from 4 m to 6 m with an variation range of 0.5m. The results of the PDA are shown in Figure 5.15 and outline that an increase in the beam span length produces a decrease in terms of robustness. The values of load multiplier and vertical drift corresponding to the achievement of the first brittle failure are collected in Table 5.10; these show that as the beam span length the failure is reached for lower and lower load multiplier values, even if the variation between the different values is minimal.

The seismic capacity was evaluated through the pushover analysis, and the outcome is shown in Figure 5. 16a and b for mode and mass force profile, respectively.

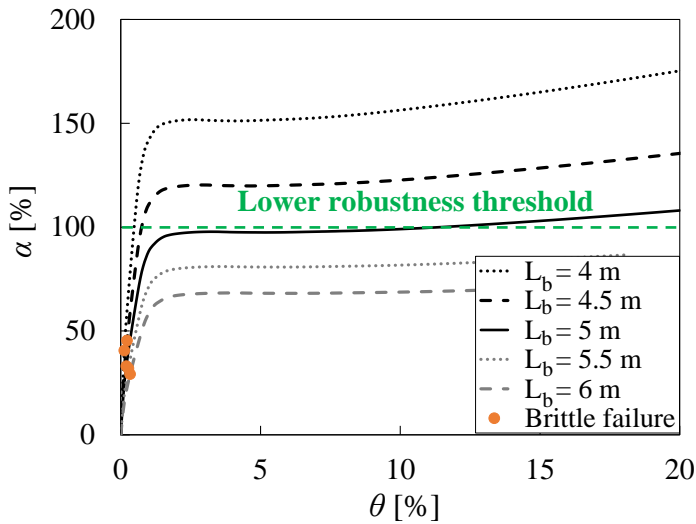


Figure 5. 15: Impact of beam span length variation on structural robustness

Beam span length [m]	4	4.5	5	5.5	6
α [%]	45.38	40.54	33.05	31.9	29.2
θ [%]	0.13	0.22	0.20	0.27	0.33

Table 5.10: Load multiplier and vertical drift values corresponding to the achievement of the first brittle failure

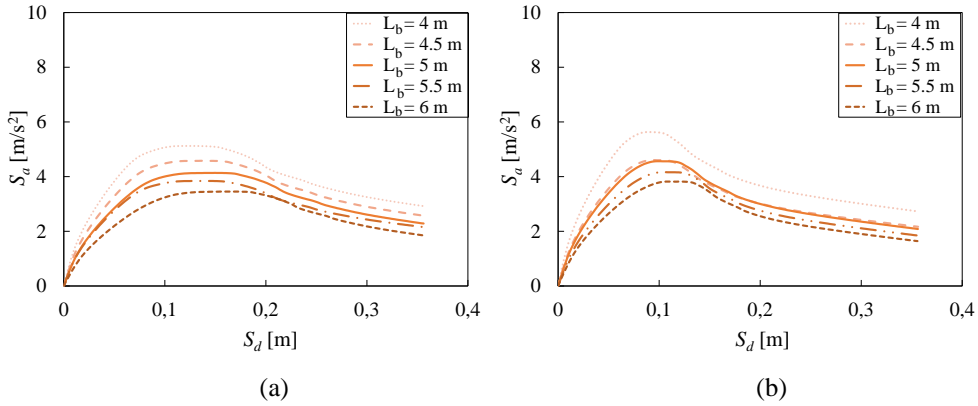


Figure 5.16: Pushover of case study structure under variation of beam span length: (a) mode force profile, (b) mass force profile

The variation of the beam span length led to the necessity of a new FRP strengthening systems design, according to CNR-DT 200R1/2013 guidelines [116]. A single-ply CFRP was sufficient for beams belonging to all floor levels, except when $L_b = 6$ m; in this case, CFRP sheets consisted of two plies at each floor level. The arrangement of composite materials for the columns is described in Table 5.11. Specifically, for a variation of L_b between 4 and 5 m, the same configuration of CFRP sheets was found: it consisted of 5 plies at the ground floor, 3 plies at the second floor, 2 plies at the third floor and a single-ply at the last two floors. For $L_b = 5.5$ m a similar result was found, with the exception of the ground floor in which 4 plies were used. When the beam span length was 6 m, a larger number of CFRP sheets than the code limits were required, so their design was not possible.

Beam span length [m]	4	4.5	5	5.5	6
Level 1	5	5	5	4	>6
Level 2	3	3	3	3	>6
Level 3	2	2	2	2	-
Level 4	1	1	1	1	-
Level 5	1	1	1	1	-

Table 5.11: Arrangement of CFRP along columns: plies distribution for structure levels

Later PDAs were carried out in order to assess the influence and effectiveness of the seismic retrofit measure on the progressive collapse resistance. The impact of the retrofit measure is evidenced in Figure 5. 17. For the cases of $L_b=4$ m and 4.5 m, it was found that the first brittle failures were obtained for higher α values equal to 1.2 and 1.15 times of design load, respectively. In these cases it is highlighted the positive impact of the CFRP. When L_b is equal to 5.5 m and 6 m, the local retrofit strategies aiming at the increase of the section's ductility do not allow reaching the required progressive collapse resistance. From here we can conclude that if a retrofit measure is effective in terms of seismicity, it is not necessarily the same in terms of progressive collapse resistance.

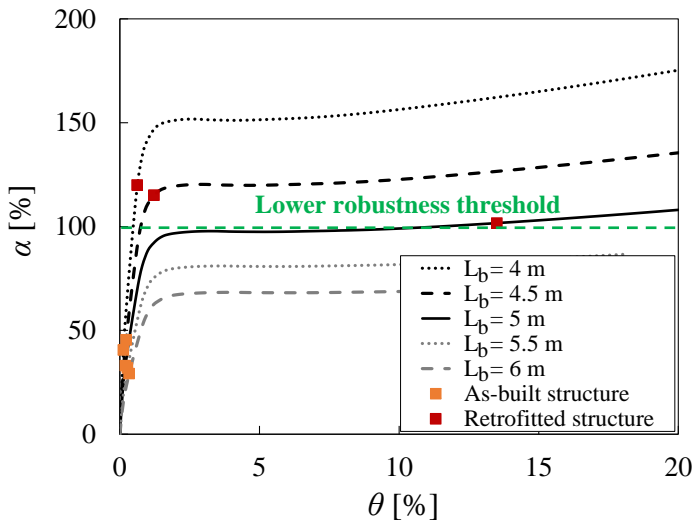


Figure 5. 17: Influence of retrofit measure under varying beam span length

Successively, the impact of CFRP shear strength variation, V_{rdf} , was investigated. The analyses were performed for L_b values between 4 m and 5 m due to the lack of structural robustness of the other two cases and varying V_{rdf} between -20% and 20%. Figure 5. 18 shows the results of this parametric analysis. The red squares refer to the brittle failures reached by the retrofitted structure, analysed first. In addition, other two types of markers are used in figure: (i) the light red and green triangles are related to the

achievement of the first brittle failure after a reduction of V_{rdf} of 10% and 20%, respectively, while (ii) the light blue and grey dots indicate the first brittle failure reached at 10 and 20% increases in V_{rdf} , respectively. The results are collected in Table 5.12, as beam span length and CFRP shear strength vary. For the case with L_b equal to 4m and 5 m, similar results were found after reducing the CFRP shear strength. In fact, a reduction of this parameter of -10% and -20% produced similar results, as demonstrated by the overlapping of the red and green triangle. For $L_b = 4$ m and 5 m, the brittle failure occurred for $\alpha = 1.03$ and $\alpha = 0.9$ times the design load, respectively. A more significant difference can be observed for the case with $L_b = 4.5$ m where, for a reduction in V_{rdf} of -10% and -20%, the brittle failure occurs for $\alpha = 1.08$ and $\alpha = 0.9$ times the design load, respectively. An increase of CFRP shear strength led to an increase of load multiplier corresponding to the achievement of the first brittle failure; specifically, for a 10% increase of V_{rdf} , it was found for $\alpha = 1.3$, $\alpha = 1.16$ and $\alpha = 1.06$ when $L_b = 4$ m, 4.5 m and 5 m, respectively. For an increase of 20% of the shear, the value of α corresponding to the first brittle failure was 1.42 and 1.23 for $L_b = 4$ m, 4.5 m, respectively.

Beam span length [m]	4		4.5		5	
	α [%]	θ [%]	α [%]	θ [%]	α [%]	θ [%]
$\Delta V_{rdf} = -10\%$	103	0.5	108	0.9	91	1.1
$\Delta V_{rdf} = -20\%$	103	0.5	95	0.7	91	1.1
$\Delta V_{rdf} = 0$	120	0.6	115	1.2	102	13.5
$\Delta V_{rdf} = +10\%$	131	0.7	123	9.9	106	18
$\Delta V_{rdf} = +20\%$	142	1	127	14	-	-

Table 5.12: Influence of CFRP shear strength variation on the achievement of first brittle failure

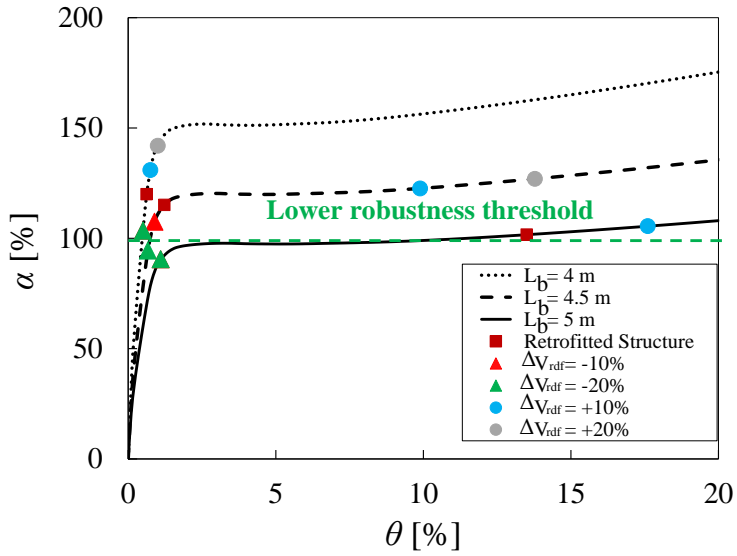


Figure 5. 18: Influence of CFRP shear strength variation on brittle failures

CHAPTER 6 – PROBABILISTIC ROBUSTNESS ASSESSMENT OF PRECAST RC BUILDINGS

6.1 Objectives of the work

The last step of this work involved the study of the progressive collapse resistance of Precast Reinforced Concrete (PRC) frame structures, representative of low-rise commercial buildings. This choice is due to the fact that in Europe, PRC buildings designed according to past codes are usually characterized by dry beam-column connections, with the addition of threaded dowels in case of modern structures designed for earthquake resistance [117,118]. Concerning robustness-oriented design of PC buildings, two fib guidelines were published: the fib Bulletin 63 [119] providing principles for the mitigation of progressive collapse risk, and fib Bulletin 43 [120] focused on structural detailing. Nonetheless, no specifications on joint design for earthquake resistance and robustness are available yet. In previous study [121], PC structural systems were compared to their monolithic counterparts, demonstrating that European PC buildings are prone to progressive collapse. In this respect, mechanical properties of beam-column connections and tying reinforcement were found to significantly affect the structural response of PC buildings under different column removal scenarios. Nevertheless, those preliminary investigations evidenced the need for a probabilistic robustness assessment to evaluate the influence of seismic detailing, peripheral tying reinforcement, and related uncertainties. In this study, a fragility-based robustness assessment of a precast RC frame structure representative of low-rise commercial buildings located in Europe is presented. Different column loss scenarios

were considered, namely, the sudden failure of a single column located in the corner, edge, or centre of the building, as they can produce the partial or total collapse of the structural system. The following types of beam-column connections were considered: (i) a simple frictional connection designed only to gravity loads according past codes; (ii) a threaded-dowel connection designed for earthquake resistance; and (iii) a robustness-targeted connection including a tying reinforcing system according to current provisions for mitigating the progressive collapse risk of precast concrete structures. In this study two building classes are considered, *i.e.* buildings designed only to gravity loads and those designed for earthquake resistance. After that the characteristics of the case-study structure, structural modelling and analysis procedures, and performance limit states are described, the paper focuses on progressive collapse simulation based on large-displacement incremental dynamic analysis (IDA) of three-dimensional (3D) fiber-based finite element (FE) models with nonlinear links simulating connections. Due to the lack in the current literature, the study aims to provide a quantitative evaluation for the risk assessment of substandard and earthquake-resistant precast reinforced concrete buildings through fragility analysis by considering (i) relative simplified modelling technique based on nonlinear time history analyses, (ii) practical performance limit states for damage assessment, (iii) the role of tying reinforcing system according to current code provisions to improve the progressive collapse resistance of such structural typology.

6.2 Case-study structure

Two classes of low-rise, commercial, European PC buildings, were considered:

- Substandard existing buildings designed to sustain only gravity loads, where beam-column connections resistance relies only on frictional behaviour of their interface.
- Earthquake-resistant buildings, where beam-column connections resistance relies on frictional behaviour and threaded dowels. In the last case it was

considered also a variant of the structure, obtained with the presence of tying reinforcement designed according to current robustness-oriented guidelines.

6.2.1 Material and geometric properties

Based on previous studies of European PC frame structures, the mean value and the CoV of both concrete and steel properties (the latter related to both rebar and threaded dowels) were summarised in Table 6. 1 for both types of structures considered. In case of substandard PC buildings, the beam-column connection resistance relies only on frictional behaviour of its beam-column interface, considering a pinned connection without any flexural resistance. Although detailed statistics of friction coefficient between bearing pads and PC members are not available, in this study mechanical properties experimentally derived by Brunesi et al. [122] were used. Accordingly, the beam-column behaviour was characterized via an elastic-perfectly plastic shear force–displacement relationship, assuming deterministic values of the friction coefficient m , initial stiffness K_0 , ultimate shear V_f (computed as a function of m) and ultimate displacement Δ_f .

According to previous studies by Ravasini et al. [121], a three-storey PC building with both primary and secondary beams, as well as one-way floor slabs oriented along the short span direction, was assumed (Figure 6.1). The building plan consisted of six bays in the x -direction (with equal span length $L_x = 7.2$ m) and three bays in the y -direction (with span length L_y equal to either 10.8 or 7.2 m). The inter-storey height was set to 3.3 m at the first floor and 3.6 m at upper floors. Columns and beams were characterized by a square and a rectangular cross section, respectively. At the first and second floor levels the columns were 600×600 mm² in size while the beams were 500×700 mm²; those located at the third floor were characterized by a square cross section (500×500 mm² in size). Columns and beams were equipped with 22-mm longitudinal reinforcing bars and 12-mm stirrups with 60 mm spacing. Design gravity loads in the accidental loading conditions were defined in accordance with UFC 4-023-03 guidelines (DoD, 2016) [30] through Equation (7) of section 2.5.2 with dead and live loads

respectively set to 6.4 and 4 kN/m², resulting in $Q_{bd} = 9.68$ kN/m² at the first and second floors and $Q_{bd} = 5.28$ kN/m² at the third.

Building Class	Item	Property	Mean	CoV
Gravity-load designed	Concrete	f_c	36.00 MPa	15%
			[123,124]	[125,126]
	Reinforcing steel	f_y	322.50 MPa	8%
			[125,126]	[125,126]
			29.30%	12%
	Beam-column dry connection	ε_{su}	[125,126]	[125,126]
			m	0.2
K_0			2 kN/mm	–
V_f			6 kN	–
		D_f	3 mm	–
Earthquake- resistant	Concrete	f_c	59.75 MPa	15%
			[127]	[127]
	Reinforcing steel	f_y	490.30 MPa	5%
			[127]	[127]
			25.90%	13%
		ε_{su}	[127,128]	[127,128]
Dowel steel	$f_{y,d}$	580.00 MPa	5%	
			[129]	

Table 6. 1: Mechanical properties of concrete, steel, and beam-column connections*

*[]: indicates reference studies

As shown in Figure 6.1a, three column removal scenarios at ground level were considered as follows:

- Corner column loss scenario (involving column A-1).
- Edge columns loss scenario (involving column B-1).
- Interior column loss scenario (involving column B-4).

In the study three types of beam column connections were considered, as shown in Figure 6.2. These are coincident with:

- Type 1 (T1), substandard PC connection: frictional beam-column connection with bearing pad, representative of existing substandard PC buildings.
- Type 2 (T2), earthquake-resistant PC connection: beam-column connection with threaded steel dowels, representative of those used in seismically-designed PC buildings.
- Type 3 (T3), improved connection with tying reinforcement: beam-column connection with dowels and tying reinforcement to provide integrity and continuity between precast members.

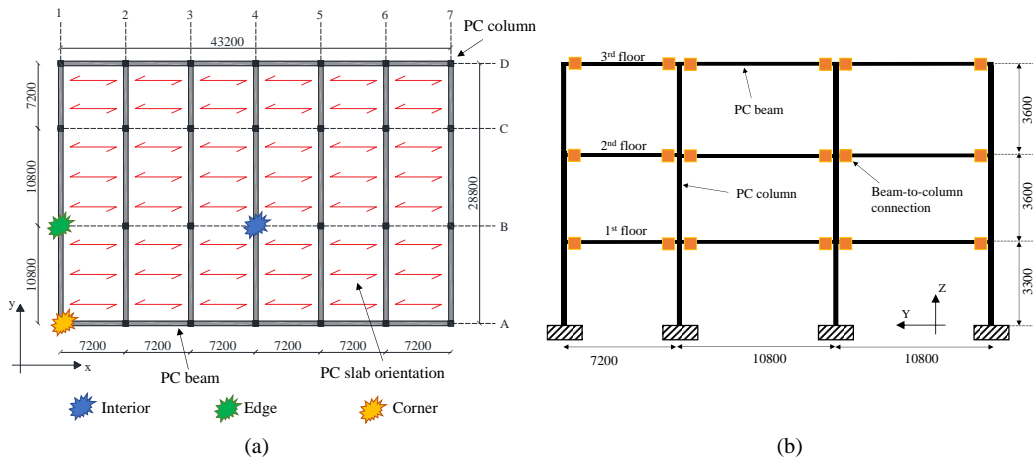


Figure 6.1: Geometry of case-study PC building: (a) plan and orientation of one-way floor slabs with identification of column removal scenarios; (b) elevation (dimensions in mm).

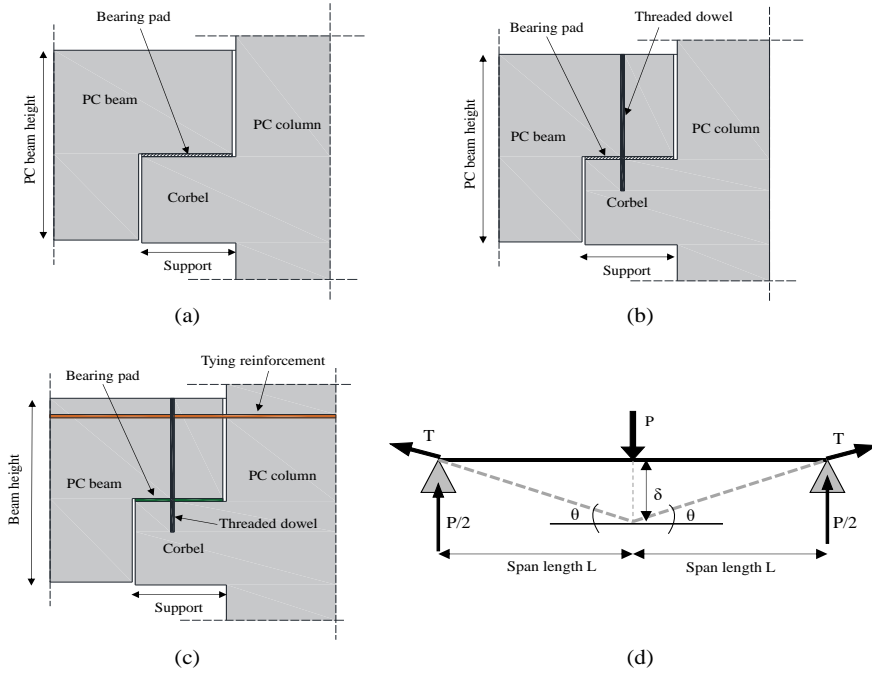


Figure 6.2: Beam-column connections: (a) Type 1, (b) Type 2, (c) Type 3 and (d) simplified structural model to design tying reinforcement.

To mitigate progressive collapse risk, international codes and guidelines provide prescriptive rules to design such tying reinforcement to sustain and redistribute gravity loads after the loss of a load-bearing element. Belletti et al. [130] demonstrated that tie force (TF) demand calculations using current codes and analytical methods provide a considerable scatter. In this study, TF demand was calculated through the simplified two-span beam model in Figure 6.2d, where force equilibrium at catenary stage under equivalent gravity load P was solved through the following equation:

$$T = \frac{P}{2\text{sen}\theta} \approx \frac{P}{2\theta} \quad (20)$$

The magnitude of P is based on the tributary floor area of the removed column, according to the building layout. The parameter ϑ is the beam chord rotation achieved at catenary stage, namely, $\theta = \tan^{-1}(\delta/L) \approx \delta/L$. According to recent studies, $\vartheta = 0.2$ was usually adopted to design tying reinforcement in beam systems. This value derived from experimental tests on cast-in-situ RC frame structures available in literature by [131- 134]. Analytical investigations were also performed based on similar values of

chord rotation [106, 135, 136]. In the current version of UFC 4-023-03 guidelines [30], ties are not recommended to be placed in RC beams unless a rotational capacity of 0.2 rad can be achieved. Based on a simulated design according to UFC 4-023-03 guidelines (DoD, 2016) [30], tying reinforcement was sized according to different column removal scenarios. For the edge and corner column removal scenarios it was characterised by $3\text{Ø}30$ with an area equal to 2119.50 mm^2 ; for the interior column removal scenario it was characterised by $5\text{Ø}32$ with an area equal to 4019.20 mm^2 (Figure 6.3).

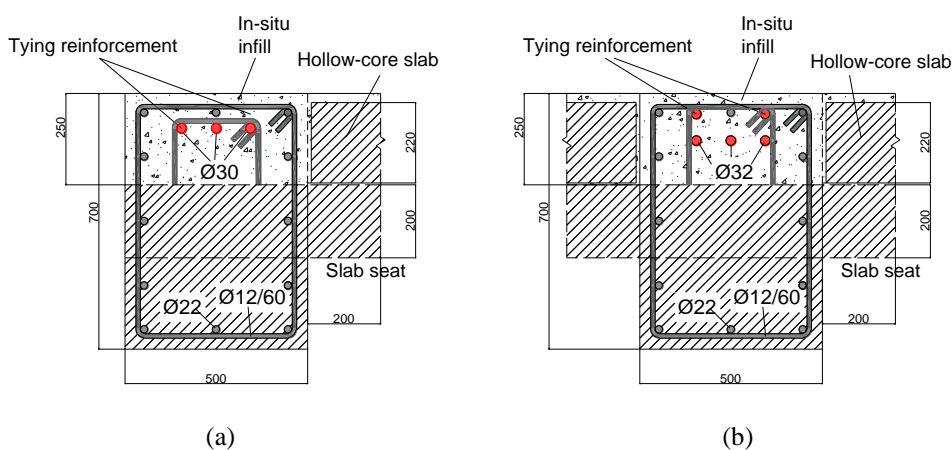


Figure 6.3: Tying reinforcement size: (a) edge and corner column removal scenarios; (b) interior column removal scenario

6.2.2 Structural modelling

The case study structure was modelled through the finite element code Seismostruct [73] that was used to carry out nonlinear time history analyses (NLTHAs) for progressive collapse simulation. Force-based fiber modelling approach [101,102] with spread inelasticity was used for frame elements, whereas connections were modelled using nonlinear link elements. To minimise computational work, links were used in the bays directly affected by column removal. The nonlinear constitutive model by Mander [76] was assigned to concrete, whereas a bilinear relationship was used for steel reinforcement according to past studies [106, 107, 137]. Geometric and mechanical nonlinearities were included, while neglecting strain rate effects. Concrete and steel properties were assumed according to Table 6. 1, depending on the model considered,

i.e. gravity load designed and earthquake-resistant models. Floors were considered only as loads without capacity contribution, according to their construction features in European PC buildings. As mentioned for the previous studies, a special-purpose death element routine was used in SeismoStruct [73], which allowed sudden removal of a column after gravity loads are applied and equilibrium is achieved. Each selected column to remove was deleted by assigning a deactivation time of 0.01 s. The total target time of NLTHA was set to 3 s, iteratively solving equations through Newton-Raphson algorithm and convergence criteria based on displacements and rotations. A tangent stiffness-proportional Rayleigh damping equal to 5% was assigned to the 3D model (Figure 6.4a).

6.2.3 Beam-column connection modelling

In previous works by Ravasini et al. [121], beam-column connections were modelled using uncoupled link elements available in SeismoStruct [73]. Nonlinearities were assigned through the following relations: (i) a shear (V) – displacement (Δ) relationship to simulate the connection resistance in case of pure frictional behaviour and/or threaded dowels and (ii) moment (M) – rotation (θ) relationship to simulate the flexural connection resistance to negative and positive relative rotations. The different connections were modelled as described by Figure 6.4. Specifically:

- Type 1 connection (Figure 6.4b) was modelled with a $V - \Delta$ relation based on frictional properties according to Table 6. 1, and zero flexural resistance according to assumption of pinned connection;
- Type 2 connection (Figure 6.4c) was obtained through $V - \Delta$ relation based on the resistance of threaded dowel according to test data by Psycharis et al. [129] for two $\varnothing 25$ dowels, and $M - \theta$ relation with positive and negative resisting moments calculated via equations by El Delbs et al. [138] and Elliott et al. [139].
- Type 3 connection (Figure 6.4d) was modelled through a $V - \Delta$ and $M - \theta$ relations similar to those of Type 2 connection, and tying reinforcement

modelled as a truss element connecting nodes of column and beam, with bilinear stress–strain law for steel based on properties in Table 6. 1.

A rigid element between the precast column and beam was used to account for support eccentricity. The removal of the column left the beam-to-column joint intact. The model of Type 2 connection used in this study was a significant improvement of that assumed in previous studies [121] where shear resistance was neglected. That modelling updating including the $V - \Delta$ relation is further supported by fib Bulletin 43 [120], which states that past analytical provisions led to underestimate both resistance and lateral displacements at failure for threaded dowel connections. Indeed, Eq. (21) for prediction of shear resistance V_{Rd} of dowel connections was derived for unconfined concrete:

$$V_{RD} = \alpha_d n_d \phi_d \sqrt{f_c} f_y \quad (21)$$

where: α_d is a coefficient varying from 0.7 to 1.3 [129], n_d is the number of dowels; and ϕ_d is the dowel diameter. Conversely, experimental tests by Psycharis et al. [129] evidenced higher values of V_{Rd} , hence motivating the assumption of their data associated with two $\text{Ø}25$ dowels. However, due to the different concrete compressive strength used in the experimental test compared to the mean value reported in Table 6. 1, V_{Rd} was upscaled according to Eq. (21).

Table 6.2 outlines the values assigned to nonlinear link properties for modelling of different beam column connections under edge (peripheral) column removal scenario, assumed here as an example. In case of Type 2 connection, it is worth mentioning that failure is associated with the achievement of steel dowel resistance, assuming a sufficient concrete cover to avoid concrete spalling. This assumption is considered reasonable for recent earthquake-resistant PC structures in Europe. For further details refer to Psycharis et al. [129]. Concerning Type 3 connection, the same $V - \Delta$ relationship of Type 2 was used, but the negative branch of $M - \theta$ relationship was calculated based on the tying reinforcement, using formulations provided by El Delbs et al. [138|139] and Elliott et al. [139]. Details concerning the calculation of moment–rotation relationship are reported in Ravasini et al. [121].

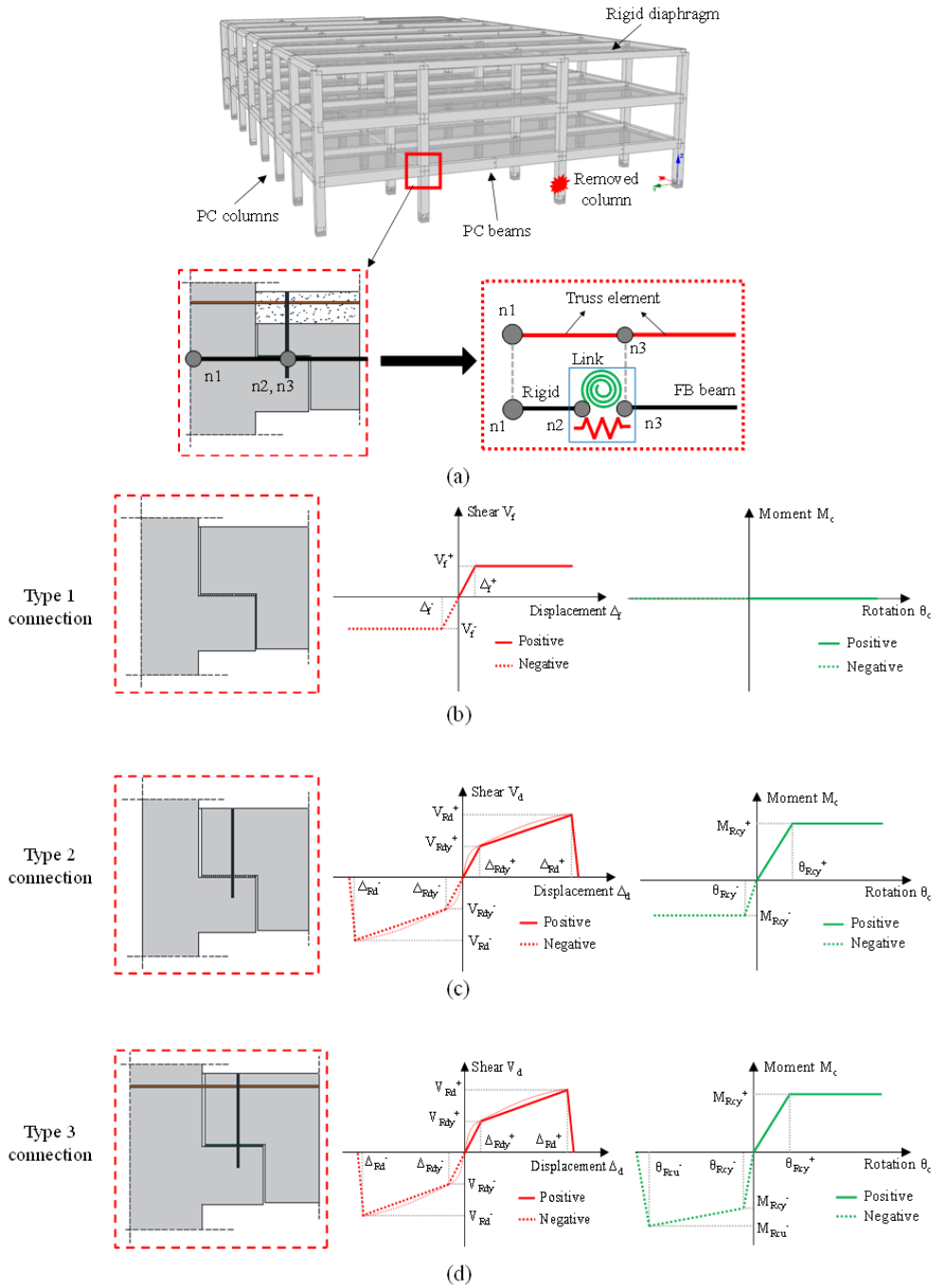


Figure 6.4: Modelling of case-study PC building: (a) 3D FE model and connections; (b) Type 1 connection; (c) Type 2 connection; (d) Type 3 connection.

Connection		$V - \Delta$ relationship							
Type									
1	V_f^+ [kN]		Δ_f^+ [mm]		V_f^- [kN]		Δ_f^- [mm]		
	6.00		3.00		6.00		3.00		
2	V_{Rd}^+	Δ_{Rd}^+	V_{Rdy}^+	Δ_{Rdy}^+	V_{Rd}^-	Δ_{Rd}^-	V_{Rdy}^-	Δ_{Rdy}^-	
	[kN]	[mm]	[kN]	[mm]	[kN]	[mm]	[kN]	[mm]	
2	663.29	90.00	289.31	10.00	663.29	90.00	289.31	10.00	
3	663.29	90.00	289.31	10.00	663.29	90.00	289.31	10.00	
		$M - \theta$ relationship							
2	M_{Rc}^+	θ_{Rc}^+	M_{Rcy}^+	θ_{Rcy}^+	M_{Rcu}^-	θ_{Rcu}^-	M_{Rcy}^-	θ_{Rcy}^-	
	[kN·m]	[rad]	[kN·m]	[rad]	[kN·m]	[rad]	[kN·m]	[rad]	
2	–	291.11	–	0.0057	–	154.83	–	0.0105	
3	–	291.11	–	0.0057	788.37	0.239	630.70	0.00205	

Table 6.2: Nonlinear links properties for different types of beam-column connections

6.3 Definition of performance limit states

After the structure modelling, a set of Performance Limit States (PLSs) was considered for progressive collapse analysis of the case-study PC frame structures. Ravasini et al. [121] demonstrated that the progressive collapse resistance of case-study buildings mostly depends on the nonlinear behaviour and failure modes of beam-column connections. Thus, different sets of PLSs were assumed for the case-study buildings, depending on their type of connection.

In case of substandard existing PC buildings, a single collapse PLS was considered and associated with the loss of beam support at the location of column corbels. Collapse is thus a consequence of excessive lateral displacement at the beam-column interface.

Three different PLSs were assumed in case of earthquake-resistant PC buildings with Type 2 and 3 connections, according to Figure 6.5a and b. In line with the previous studies, the loss of the support was associated with a lateral displacement equal to 200 mm. A schematic representation of initial and collapse conditions is shown in Figures 6.6 **Figure 6.a** and **b**, considering a Type 2 connection as an example.

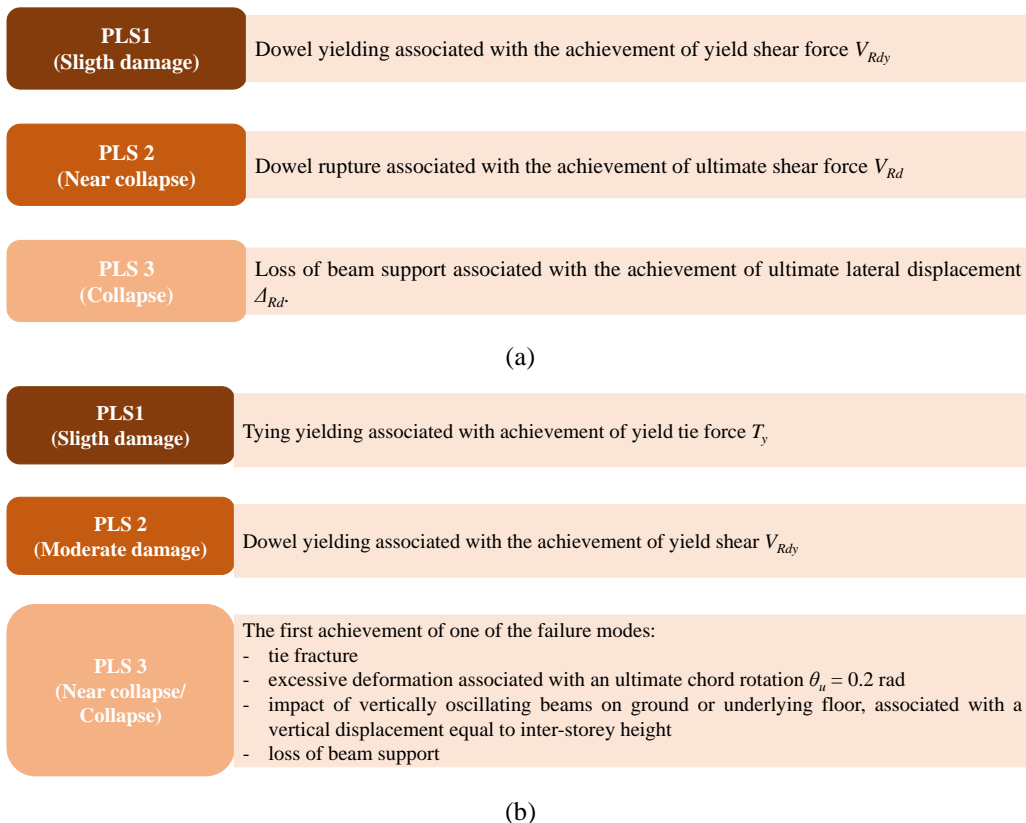


Figure 6.5: Performance limit states definition: (a) PC buildings with Type 2 connection and (b) PC buildings with Type 3 connection

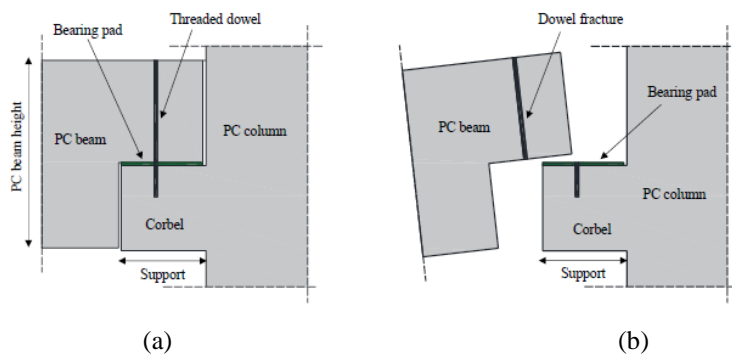


Figure 6.6: Type 2 connection: (a) initial configuration; (b) collapse due to loss of support

6.4 Progressive collapse analysis of PC buildings with mean values of properties

In first instance, IDA was carried out on structural models with mean mechanical properties according to Table 6. 1. For each structural model and scenario, the achievement of each PLS during NLTHA was identified through the vertical displacement δ of the beam-column joint located on top of the removed column. That displacement was converted into the corresponding chord rotation θ (or equivalently, vertical beam drift; *see, e.g.*, Parisi et al. [106]), which was then assumed as engineering demand parameter (EDP). Each NLTHA run of IDA was performed by assigning a load factor α to gravity loads and inertia masses, and subsequently recording the time history of vertical displacements. The results of this first step on analyses are shown in Figure 6.7, Figure 6.8, **Figure 6.** and Figure 6.9 in terms of drift time histories under varying α and column loss scenario, associated with the three types of connection under investigation and corresponding building structures (*i.e.*, substandard existing building and earthquake-resistant building).

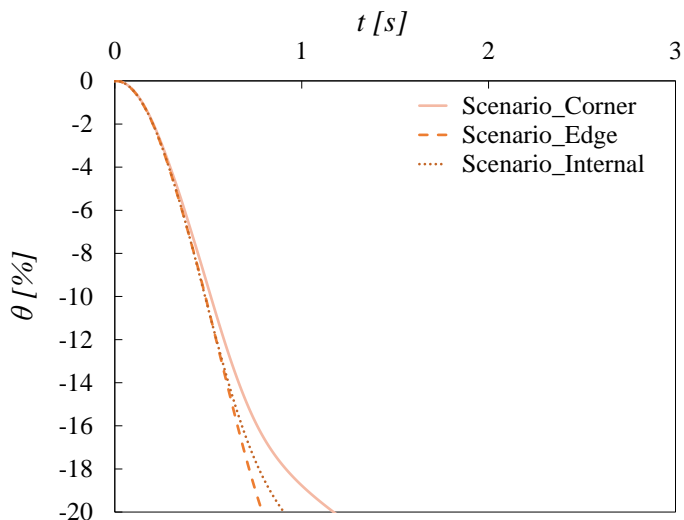


Figure 6.7: Drift time histories of substandard building with Type 1 connection under varying column loss scenario.

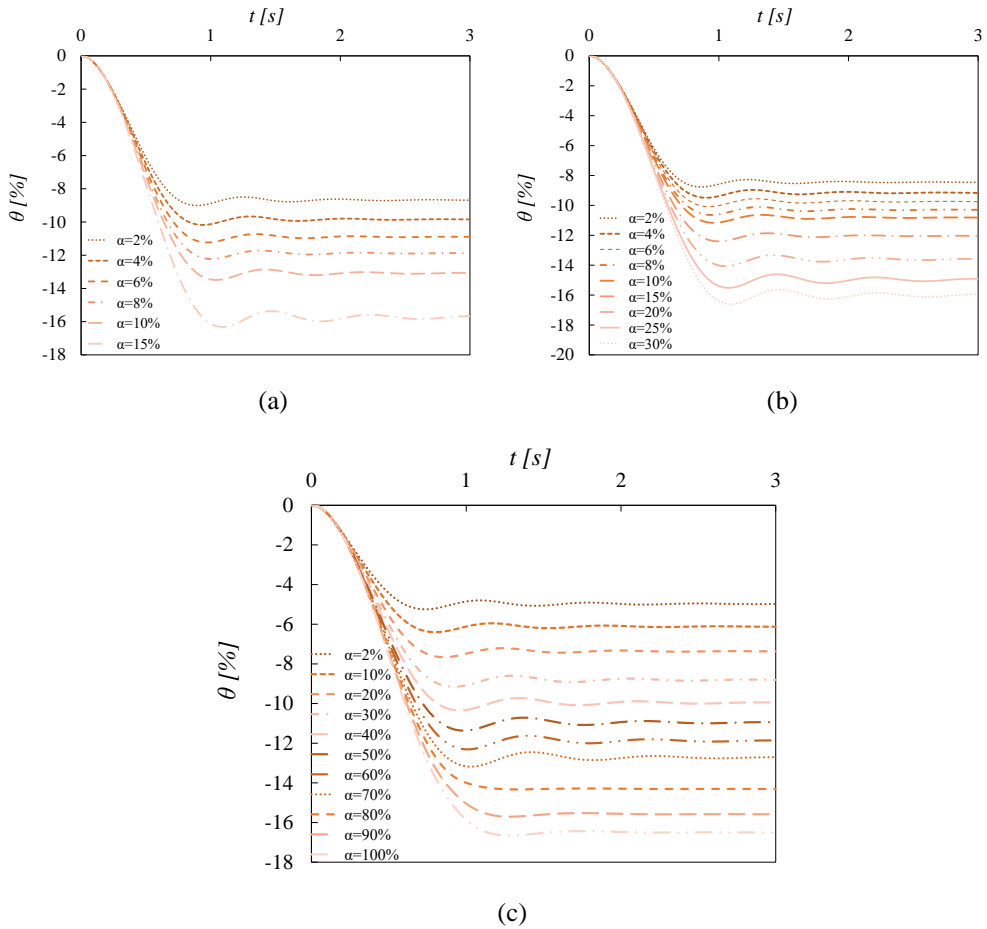


Figure 6.8: Drift time histories under varying load factor for earthquake-resistant building with Type 2 connection: (a) internal scenario; (b) edge scenario; (c) corner scenario.

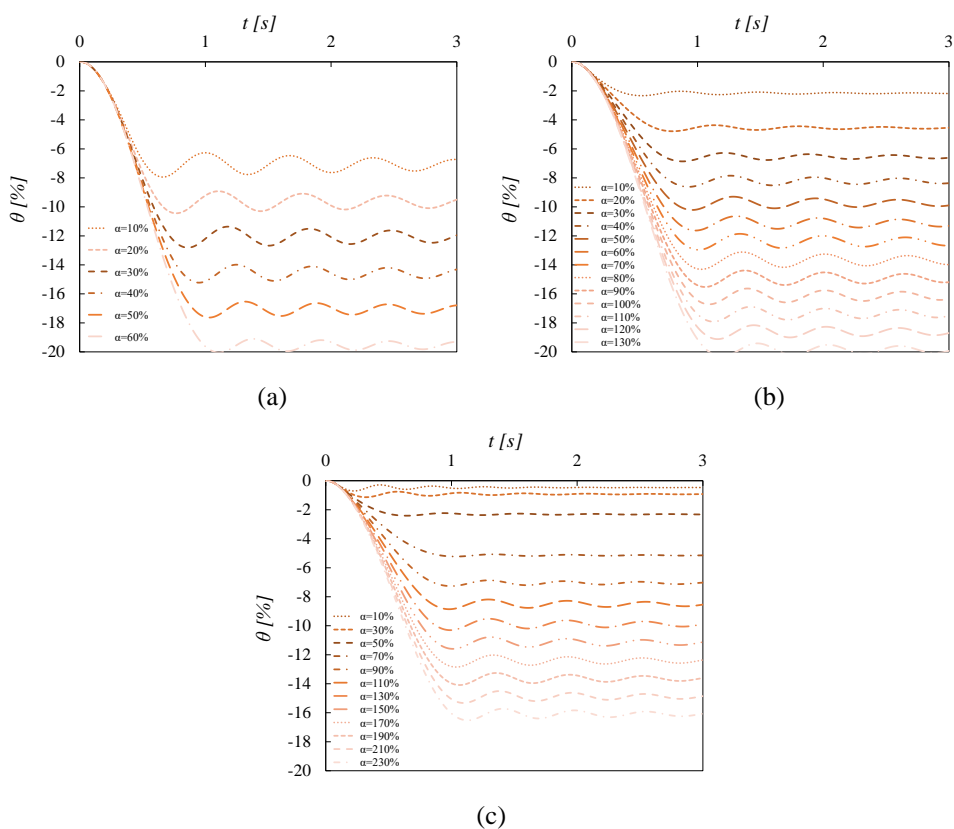


Figure 6.9: Drift time histories under varying load factor for earthquake-resistant building with Type 3 connection: (a) internal scenario; (b) edge scenario; (c) corner scenario.

Firstly, the purpose of these analyses was to assess the α value at which the PLSs were reached, varying the structural type and the scenario considered. It is possible to denote this value as α_{PLS} . The values of α_{PLS} predicted for each performance limit state, column loss scenario, and type of beam-column connection were collected in Table 6.3. From the results, it is possible to underline that for the substandard PC building, the Type 1 connections (characterized by only frictional behaviour) produce the loss of beam support at very low levels of gravity loads, *i.e.* $\alpha_{PLS} = 2\%$ for every column loss scenario considered. This is due to the negligible resistance of pinned beam-column connections to sustain local deformations produced by column loss. This implies that Type 1 connections are not able to avoid progressive collapse of substandard PC buildings when a single column fails.

Performance	Corner Scenario			Edge Scenario			Internal Scenario		
Limit State	T1	T2	T3	T1	T2	T3	T1	T2	T3
PLS1		2%	80%		2%	20%		2%	30%
PLS2	2%	100%	230%	2%	30%	130%	2%	15%	60%
PLS3		100%	230%		30%	130%		15%	60%

Table 6.3: Value of load multiplier corresponding to the achievement of PLSs under different column removal scenarios*

*T: indicates the connection type

In the other cases, the results outline that a sequential occurrence of PLS1 and PLS2, whereas PLS3 was found under the same gravity loads of PLS2. For the edge and internal column loss scenarios lower levels of gravity load capacity were obtained, demonstrating that these are more critical than the corner scenario. Regardless of the column removal location, the load capacity at PLS1 was the same of the pinned connection, as highlighted by the value of α_{PLS} . The progressive collapse capacity considerably increased in case of Type 3 connection, as a result of tie yielding under a load factor equal to 80%, 20%, and 30% in case of corner, edge, and internal column loss scenario, respectively. This shows that tie yielding produced a beneficial increase of beam-column connection resistance, resulting into a higher load redistribution capacity compared to other (single-hazard-oriented) types of connection.

When PLS2 and PLS3 were considered the progressive collapse capacity of the earthquake-resistant building with Type 2 connection reached the resistance demand in case of corner scenario ($\alpha_{PLS} = 100\%$), while showing insufficient levels of robustness in case of both edge and internal scenarios, as respectively indicated by limit state load factors equal to 30% and 15%. In all cases, PLS3 was associated with the attainment of $\theta_u = 20\%$.

Considering the Type 3 connection, the addition of horizontal steel ties within beams of the earthquake-resistant led to a further increase in progressive collapse capacity, with values of α_{PLS} equal to 230% and 130% in the corner and edge scenarios, respectively. By contrast, the loss of internal column was a critical scenario for the PC frame structure, as evidenced by $\alpha_{PLS} = 60\%$. This indicates that horizontal ties within beams are not a

sufficient measure to prevent progressive collapse in case of internal column loss, highlighting the need for alternative options to mitigate the risk of collapse (e.g., horizontal ties within floor systems, vertical ties, protective design of internal columns). An overall view of the sensitivity of progressive collapse capacity to the location of the removed column is provided by IDA curves. Each IDA curve provides a graphical representation of the relationship between α , which is assumed to be an intensity measure (IM) for gravity loads, and θ , which is considered a structural response parameter. These are shown in Figure 6.10: in case of Type 2 connection, the IDA curve has approximately a trilinear shape that further remarks the sequence of performance limit states, as well as their corresponding values of load factor and chord rotation. In other words, the intermediate corner points between approximately linear α - θ branches are associated with the attainment of PLS1 and PLS2.

The IDA curves related to Type 3 connection showed that the interaction between frictional resistance of bearing pads, shear-flexural resistance associated with dowels, and tensile resistance of steel ties results in a more nonlinearity, particularly in case of corner scenario.

Figures 6.11a, b and c show near-collapse deformed shapes of the earthquake-resistant building with Type 2 connection subjected to corner, edge, and internal scenarios, respectively. Displacements were scaled by a factor equal to 2 to ensure a good visualization of deformations experienced by PC beams and beam-column connections (modelled via nonlinear links) during progressive collapse.

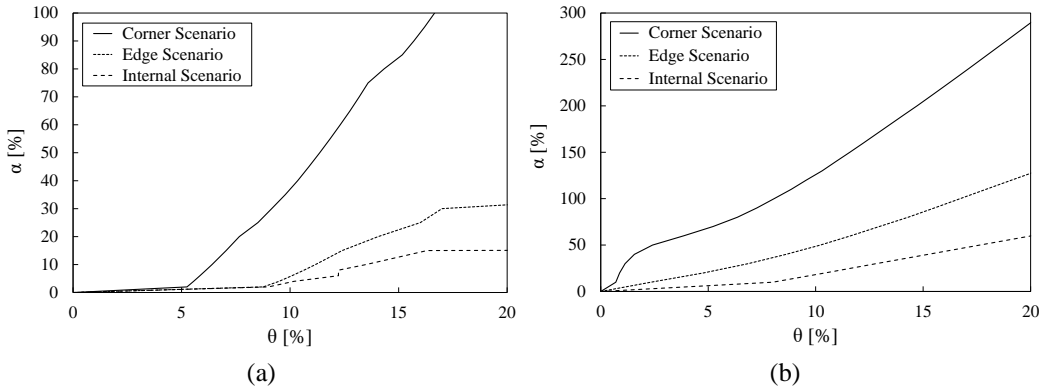


Figure 6.10: IDA curves under varying column removal scenario: (a) earthquake-resistant building with Type 2 connection; (b) earthquake-resistant building with Type 3 connection.

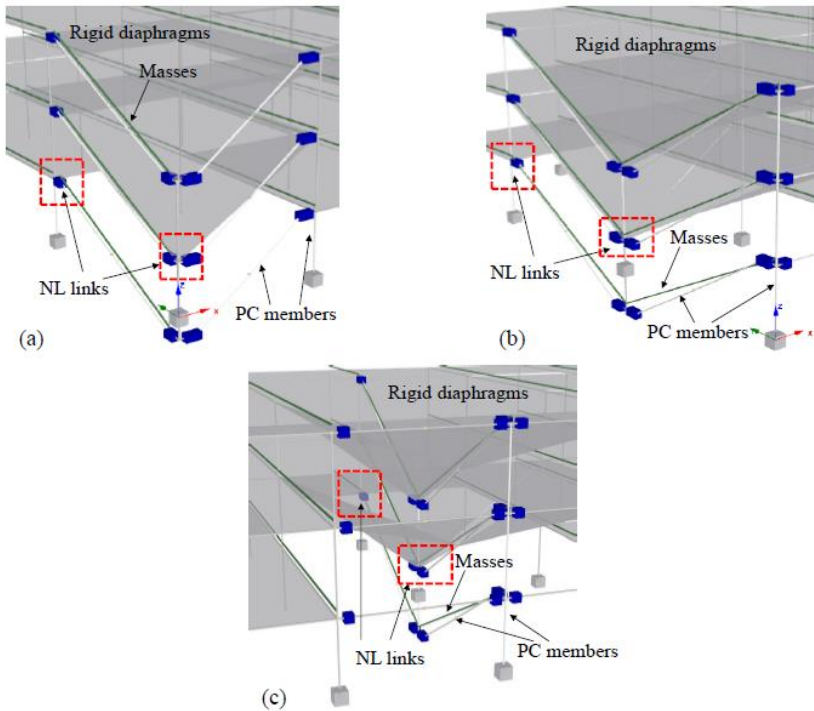


Figure 6.11: Near-collapse deformed shapes of earthquake-resistant building with Type 2 connection: (a) corner scenario, (b) edge scenario, (c) internal scenario

6.5 Fragility analysis

The results of the previous analyses showed that the substandard building designed only to gravity loads does not prevent progressive collapse under any location of column loss. Furthermore, seismic detailing and horizontal ties within PC beams were not able to produce a sufficient level of robustness under internal column loss. The internal column loss was the most critical scenario but it is easy to recognize that the external columns of buildings may be more exposed to hazardous events than their internal counterparts, particularly if blast and localised fire are effectively prevented through non-structural risk mitigation measures (e.g., sprinkler or early warning systems). For these reasons and to specifically characterise robustness against hazardous events occurring outside buildings, progressive collapse fragility analysis described in next section was carried out under the assumption of edge column loss. This is motivated by the fact that the edge scenario was found to be the worst case compared to its corner counterpart.

6.5.1 Random variables

Fragility analysis was undertaken by means of Monte Carlo simulation, the latter being implemented to propagate the effect of uncertainties in capacity model properties, which were treated as random variables (*RVs*). According to previous studies [140-142] building portfolios consisted of one hundred realizations per structural model case, implying that IDA-based multi-damage state lognormal fragility models were derived through a few thousands NLTHAs, whereby the intensity of gravity loads was monotonically sequenced so that the occurrence or exceedance of each damage state condition was tracked.

The material properties selected as random variables are the following:

- Concrete compressive strength, f_c .
- Yield strength of steel reinforcement, f_y .
- Yield strength of steel dowel, f_{yd}
- Ultimate strain of reinforcing steel, ϵ_{su} .

The Latin Hypercube algorithm was considered for complete Monte Carlo sampling of RVs with Lognormal distribution and statistics reported in Table 6. 1, as discussed by Brunesi et al. [33]. IDA was carried out to characterize the nonlinear response of each randomly generated building sample, assuming the edge column loss scenario. The output of each IDA consisted in a dynamic capacity curve, so that values of α_{PLS} were recorded to track the occurrence of each damage state using the previously defined criteria. In that way, the fractions of sampled buildings that reached or exceeded each damage state of interest given α were computed, allowing the computation of progressive collapse fragility under increasing intensity of gravity loads. The fragility data set associated with each PLS was then fitted using a Lognormal cumulative distribution function, which is here defined via the median value $\alpha_{PLS,m}$ and logarithmic standard deviation (dispersion β) of α_{PLS} . This procedure allowed the development of two set of analytical fragility models at multiple damage conditions, thus producing two effects to be singled out: (i) the impact of seismic detailing on robustness, and (ii) the influence of peripheral tying reinforcement.

6.5.2 Discussion of results

6.5.2.1 Earthquake-resistant building with Type 2 connection

The results obtained for this kind of building are plotted in Figure 6.12. It shows that lateral displacement Δ_{Rdy} and shear force V_{Rdy} (PLS1) were reached in early analysis stages corresponding to $\alpha \approx 2\%$, as remarked by an initial low slope till $\theta \approx 10\%$. In the second stage, the hardening response of dowel beam-column connection increased the slope of the second branch till α ranging in the interval [25%,40%] and $\theta \approx 16\%$. In that stage, threaded steel dowels fractured (PLS2, Δ_{Rd} and load V_{Rd} were achieved) and consequently, support loss (PLS3) occurred, as shown by a low slope similar to that of the first branch. These considerations for IDA curves were reflected in the probability occurrence of PLSs shown in the fragility curve. That corresponding to PLS1 is characterized by a jump function due to the occurrence of dowel yielding at the same

α -level, so α_{PLS} was deterministically equal to 2% with no need to fit a Lognormal distribution function. Sequential occurrence of PLS2 and PLS3 was evident: the achievement of steel dowel fracture (due to absence of lateral load resistance) was soon followed by the loss of support. It is worth to mention that such fragility curves do not highlight a considerable dependence on statistical uncertainty.

In addition, the parameters of fragility functions and coefficient of determination (R^2) resulting from their fitting to data are shown in Table 6.4. These outlined that seismic detailing produced a positive effect on the increase of structural robustness, essentially shifting the collapse load factor from 2% to approximately 36%.

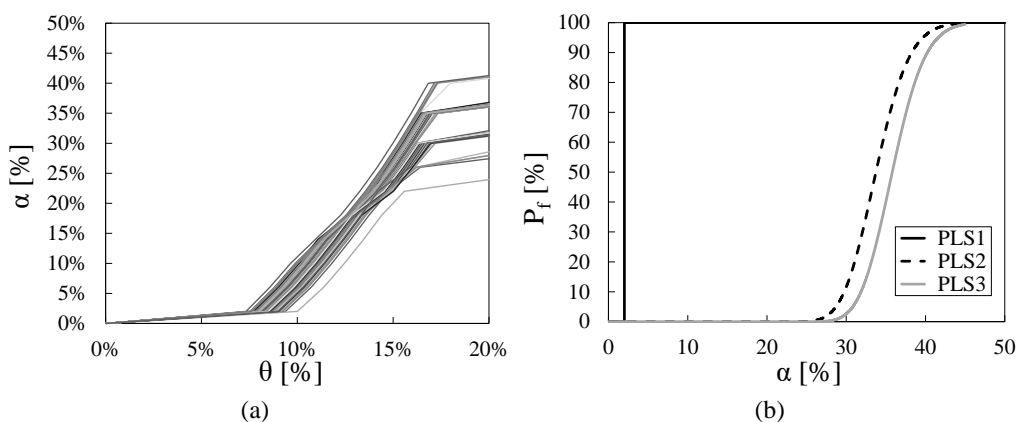


Figure 6.12: Earthquake-resistant building with Type 2 connection: (a) IDA curves; (b) fragility curves.

Performance Limit State	$a_{PLS,m}$	β	R^2
PLS1	2%	–	–
PLS2	33.74%	0.0983	0.9999
PLS3	35.80%	0.0910	0.9989

Table 6.4: Median, dispersion and coefficient of determination of fragility curves for earthquake-resistant building with Type 2 connection

6.5.2.2 Earthquake-resistant building with Type 3 connection

Conversely to the previous case, it is not evident a sequential occurrence of PLSs by the Figure 6.13. This was attributed to the achievement of tie yielding (PLS1) in early IDA

stages corresponding to $\alpha \approx 20\%$ and $\theta \approx 5\%$. Following that stage, the steel dowel connection contributed together with ties to resist gravity loads. PLS2 and PLS3 occurred sequentially, with the former related to the achievement of yield displacement Δ_{Rdy} and yield force V_{Rdy} of steel dowel. In this case, PLS3 was related to the achievement of the chord rotation limit equal to 0.2. Also in this case the parameters and coefficient of determination related to the fragility functions of the structure with steel ties are listed in Table 6.5. The beneficial effects of tying reinforcement are very high, as evidenced by median load capacities that were 3.45–5.35 times those related to the Type 2 connection. The dispersion of fragility curves related to Type 3 connection was significantly lower than that associated with Type 2 connection.

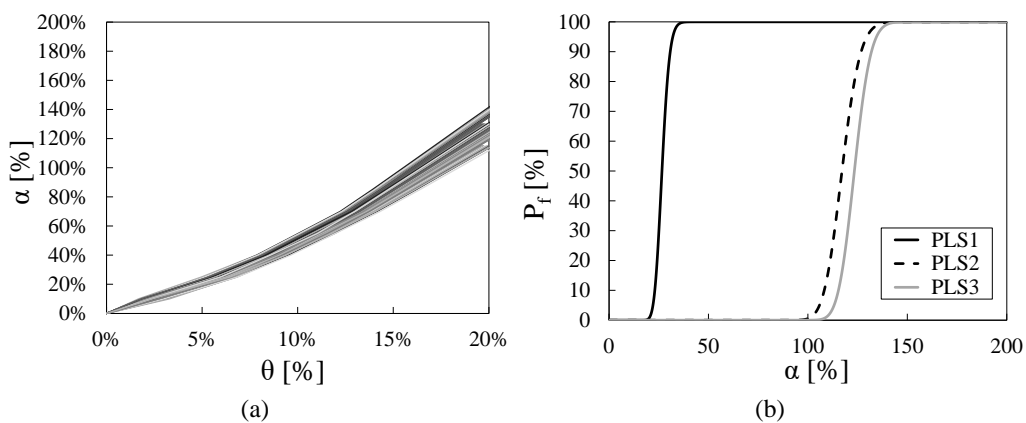


Figure 6.13: Earthquake-resistant building with Type 3 connection: (a) IDA curves; (b) fragility curves

Performance Limit State	$a_{PLS,m}$	β	R^2	$a_{PLS,mT3}/a_{PLS,mT2}$	b_{T3}/b_{T2}
PLS1	26.62%	0.1134	1.0000	5.35	0.11
PLS2	117.15%	0.0618	0.9929	3.47	0.63
PLS3	123.39%	0.0525	1.0000	3.45	0.58

Table 6.5: Median, dispersion and coefficient of determination of fragility curves for earthquake-resistant building with Type 3 connection

CHAPTER 7 - CONCLUSIONS AND POTENTIAL FUTURE DEVELOPMENTS

This thesis deals with the issue of structural robustness and progressive collapse, specifically investigating the variables that should most influence these phenomena. In this context there are still many aspects to be investigated and that can guide the structural design. To this aim, in first instance, the sensitivity of the structural performance of a modern class of European RC framed systems subjected to single-column removal was investigated through several sets of Non Linear Time History Analyses (NLTHA). The influence of a set of five properties on progressive collapse resistance of the structure was evaluated, in order assess which of these had the greatest impact. The analyses results led to the conclusions that the reduction of yield strength of steel reinforcement and of longitudinal reinforcement ratio of primary beams span length may have a fatal effect, consisting in the progressive collapse of the framed structure. Also the reduction of span length of primary and secondary beams had an important impact on drift demand. The sensitivity of the load capacity corresponding to five performance limit states for both corner and central column-removal scenarios at the ground floor was investigated too. All nonlinear analyses evidenced a sequential occurrence of the performance limit states proposed in this research. Tornado diagrams indicated that the span length of primary and secondary beams and the yield strength of steel reinforcement were the capacity model properties that mostly influence the limit state load capacity. By contrast, the compressive strength of concrete had an impact on load capacity associated with significant or extensive damage levels, that is, when the compressive arch action of beams was mobilized. If performance levels corresponding to extensive damage or progressive collapse were considered, the load capacity turned out to be influenced by both strength of steel reinforcement and longitudinal reinforcement ratio of primary beams, because the catenary action of beams was exploited.

Since extreme events can induce a spatially-distributed initial damage to multiple components of the structure, there was a need to simulate the removal of several structural elements. Nonlinear dynamic analyses were carried out under two types of multi-column loss scenarios at the ground floor of a RC framed structure, involving several couples of columns. It was obtained that the sudden removal of consecutive columns produced the lowest levels of load capacity against progressive collapse, which was found to be 30% and 61–63% of design gravity load for scenarios involving columns located in the corner and inside the structure, respectively. On the other side, a maximum load capacity equal to 1.4 times the design gravity load was predicted when opposite corner columns were removed, whereas slightly lower capacity levels were induced by the loss of opposite inner columns. As regards the sequential removal of columns, that involved a corner column and nearby columns, when the deactivation time for the second removed column was set one order of magnitude higher than that of the first column, the peak load capacity reduced by up to 13%. This occurred because the removal of a nearby column caused a further dynamic amplification of structural response. The opposite outcome was found when the deactivation time of the second removed column was set two orders of magnitude higher. In almost all scenarios, a sequential removal of columns caused drift capacity levels significantly lower than those associated with simultaneous scenarios.

As discussed above, the progressive collapse can be due to extreme actions, but it is clear that errors in the design phase or incorrect structural retrofitting measures could also be the causes. In this perspective, the progressive collapse capacity of a real RC framed building that suffered partial collapse during structural retrofitting was studied. Eighteen scenarios of structural retrofitting operations were simulated, in order to reproduce the conditions that caused the collapse at that time. These scenarios were obtained by varying location and number of ground-floor columns subjected to concrete cover removal and soil excavation around column bases. Pushdown analysis outlined that the removal of concrete cover from an internal column resulted in a collapse capacity drop greater than that predicted for the same scenario involving a perimeter or corner column. The maximum load multiplier of the structure under retrofitting operations decreased

further as the number of involved columns was increased. The maximum reduction of progressive collapse capacity was predicted in the case of simultaneous soil excavation at the base of three columns.

Some buildings can also suffer additional hazards that may be either triggered by earthquakes (e.g., landslides, soil liquefaction, tsunamis) or associated with other natural or anthropogenic events, such as floods, vehicle collision, blast, and fire. Therefore, a multi-hazard performance assessment of building structures is thus of paramount importance to implement integrated retrofit strategies, which otherwise would not be economically sustainable if oriented to structural risk mitigation against a single hazard. To this aim the next phase of the work involved the assessment of a benchmark RC frame structure and the influence on structural robustness of a retrofit measure through the use of Carbon Fibre Reinforced Polymers (CFRP). Seismic and progressive collapse assessments were based on nonlinear incremental static analyses with displacement control, *i.e.* pushover and pushdown analysis procedures. Robustness enhancement can be effectively driven by seismic retrofitting based on strengthening, highlighting the importance of multi-hazard approaches for design, assessment and retrofit of structures. A parametric analysis allowed to conclude that a variation in beam span length can produce significantly different effectiveness levels for CFRP strengthening, evidencing insufficient levels of robustness in some cases. In those situations, local seismic strengthening may be ineffective to significantly improve robustness, hence calling for other retrofitting options that, for instance, can provide alternative load paths. Significant beneficial effects of local seismic strengthening on robustness can result from 10%–20% amplifications in shear strength at beam ends, significantly delaying the occurrence of brittle failures. In case of shorter beams with span length between 4 m and 4.5 m, a shear strength reduction of the local seismic strengthening system can still ensure a sufficient level of robustness.

Since the structural feature of disaster resilience was investigated only partially in case of precast RC buildings to date, the robustness of typical European precast concrete frame buildings was assessed using a mean-centred IDA-based procedure and fragility analysis. The probabilistic approach led to the conclusion that the estimation of

progressive collapse capacity was found to be characterized by low levels of uncertainty, even degenerating into a deterministically predicted value of load capacity associated with the attainment of slight damage to the earthquake-resistant building. The presence of tying reinforcement limited the dispersion of fragility curves corresponding to moderate damage and collapse, which ranged approximately from 0.05 to 0.11 over all buildings. Seismic detailing increased the median load factor at collapse from 2% to approximately 36%, demonstrating some effectiveness in the mitigation of progressive collapse. Beneficial effects were produced by peripheral tying reinforcement, as evidenced by median load capacities that were 3.45–5.35 times those related to the building with dowel connections. The mean-centred robustness assessment provided conservative estimates of progressive collapse capacity in case of earthquake-resistant building, while producing opposite effects for the building with tying reinforcement and, consequently, the need for a probabilistic assessment.

These studies are aimed at supporting future codification activities on structural design and assessment against progressive collapse, either at national or European level. Nonetheless, this is still a major challenge because of the large variety of structural types to be studied. Future developments of these studies could include: (i) the beneficial contribution by secondary beams, floor systems and connections in 3D capacity models, particularly in case of precast RC buildings; (ii) the influence of aging and deterioration processes, as well as the extension of this kind of safety assessments in case of historical constructions that are often subjected to restoration and structural retrofitting; and (iii) the impact of other seismic retrofit methods (e.g., steel braces, RC walls, steel caging) on progressive collapse resistance.

REFERENCES

1. EN 1990 (2002): Eurocode - Basis of structural design [Authority: The European Union Per Regulation 305/2011, Directive 98/34/EC, Directive 2004/18/EC.
2. NTC (2018). DM 17.01.2018: Norme Tecniche per le Costruzioni. Rome: Ministry of Infrastructures and Transportation. [In Italian].
3. ASCE/SEI 7-05, ASCE Standard, 2006. Minimum design loads for buildings and other structures. American Society of Civil Engineers, Reston, Virginia .
4. General Service Administration (GSA), 2013. "Alternate path analysis & design guidelines for progressive collapse resistance", Washington, DC.
5. Adam J.M., Parisi F., Sagaseta J., Lu X.. Research and practice on progressive collapse and robustness of building structures in the 21st century. *Engineering Structures*. 2018; 173: 122-149.
6. Kunnath S.K., Bao Y., El-Tawil S.. Advances in computational simulation of gravity-induced disproportionate collapse of RC frame buildings. *J Struct Eng*. 2018;144:03117003.
7. Khorsandnia N., Valipour H., Foster S., Amin A.. Experimental study of progressive collapse resistance of reinforced concrete framed structures. *ACI Struct J*. 2017;114:1385–1396.
8. Li S., Shan S., Zhai C., Xie L.. Experimental and numerical study on progressive collapse process of RC frames with full-height infill walls. *Eng Fail Anal.* 2016;59:57–68.
9. Ren P., Li Y., Lu X., Guan H., Zhou Y.. Experimental investigation of progressive collapse resistance of one-way reinforced concrete beam-slab substructures under a middle-column removal scenario. *Eng Struct*. 2016;118:28–40
10. Xiao Y., Kunnath S.K., Li F.W., Zhao Y.B., Lew H.S., Bao Y.. Collapse test of three-story half-scale reinforced concrete frame building. *ACI Struct J*. 2015;112:429–438.
11. Yu J., Tan K.. Structural behavior of RC beam-column subassemblages under a middle column removal scenario. *J Struct Eng*. 2013; 139:233–250.
12. Adam J.M., Buitrago M., Bertolesi E., Sagaseta J., Moragues J.J.. Dynamic performance of a real-scale reinforced concrete building test under a corner-column failure scenario. *Engineering Structures*. 2020; 210, 110414.
13. Augenti N, Parisi F. Learning from construction failures due to the 2009 L'Aquila, Italy, earthquake. *Journal of Performance of Constructed Facilities*. 2010; 24(6): 536–555.
14. Ghosh J., Sood P.. Consideration of time-evolving capacity distributions and improved degradation models for seismic fragility assessment of aging highway bridges, *Reliability engineering System Safety*. 2016; 154: 197–218.
15. Gioiella L., Tubaldi E., Gara F., Dezi L., DallAsta A.. Modal properties and seismic behaviour of buildings equipped with external dissipative pinned rocking braced frames, *Engineering Structures*. 2018; 172: 807–819.
16. Kim Y., Lim S.A., Park H.S.. Optimal seismic retrofit method for reinforced concrete columns with wing walls. *Engineering Structures*. 2020; 210: 110390.
17. Maheri M.R., Sahebi A.. Use of steel bracing in reinforced concrete frames. *Engineering Structures*. 1997; 19 (12): 1018–1024.
18. Pampanin S., Bolognini D., Pavese A.. Performance-based seismic retrofit strategy for existing reinforced concrete frame systems using fiber-reinforced polymer composites. *Journal of Composite for Construction*. 2007; 11 (2): 211–226.

19. Pohoryles D.A., Melo J., Rossetto T., Varum H., Bisby L.. Seismic retrofit schemes with FRP for deficient RC beam-column joints: State-of-the-art review. *Journal of Composite for Construction*. 2019; 23 (4): 03119001.
20. Ozcan O., Binici B., Ozecebe G.. Seismic strengthening of rectangular reinforced concrete columns using fiber reinforced polymers. *Engineering Structures*. 2010; 32 (4): 964–973.
21. Li S., Shan S., Zhang H., Li Y.. Rapid retrofit of reinforced concrete frames after progressive collapse to increase sustainability. *Sustainability*. 2019; 11: 4195.
22. Shayanfar M., Bigonah M., Sobhani D., Zabihi-Samani M.. The effectiveness investigation of new retrofitting techniques for RC frame against progressive collapse. *Civil Engineering Journal*. 2018; 4 (9): 2132–2142.
23. Orton S., Jirsa J.O., Bayrak O.. Carbon fiber-reinforced polymer for continuity in existing reinforced concrete buildings vulnerable to collapse, *ACI Structural Journal*. 2009; 106 (5): 608–616.
24. Qian K., Li B.. Strengthening and retrofitting precast concrete buildings to mitigate progressive collapse using externally bonded GFRP strips. *Journal of Composite for Construction*. 2019; 23 (3): 04019018
25. Qin W., Liu X., Xi Z., Huang Z., Al-Mansour A., Fernand M.. Experimental research on the progressive collapse resistance of concrete beam-column sub-assemblages reinforced with steel-FRP composite bar. *Engineering Structure*. 2021; 233: 111776
26. Lin K., Li Y., Lu X., Guan H.. Effects of seismic and progressive collapse designs on the vulnerability of RC frame structures. *Journal of Performance of Constructed Facilities*. 2017; 31 (1): 04016079.
27. Stewart, M. G.. Acceptable risk criteria for infrastructure protection. *International Journal of Protective Structures*. 2010; 1(1): 23-40.
28. EN 1991-1-7, 2006. Eurocode 1: Actions on structures - Part 1-7: General actions - Accidental actions [Authority: The European Union Per Regulation 305/2011, Directive 98/34/EC, Directive 2004/18/EC].
29. Fib Model Code for Concrete Structures 2010, 2012. Fédération Internationale du Béton, Lausanne.
30. Department of Defense (DoD) Unified Facilities Criteria (UFC-04-023-03), 2016. Design Building to Resist Progressive Collapse. Washington, D.C.
31. International Code Council, 2009. International Building Code (IBC 2009). International Code Council.
32. American Society of Civil Engineers (ASCE), 2016. Minimum design loads and associated criteria for buildings and other structures (ASCE/SEI 7-16). Structural Engineering Institute of the ASCE.
33. Brunesi E, Nascimbene R, Parisi F, Augenti N. Progressive collapse fragility of reinforced concrete framed structures through incremental dynamic analysis. *Engineering Structures*. 2015; 104:65–79.
34. Brunesi E, Parisi F. Progressive collapse fragility models of European reinforced concrete framed buildings based on pushdown analysis. *Engineering Structures*. 2017;152:579–596.
35. Parisi F. Blast fragility and performance-based pressure–impulse diagrams of European reinforced concrete columns. *Engineering Structures*. 2015;103:285–297.
36. Jian H., Zheng Y.. Simplified Models of Progressive Collapse Response and Progressive Collapse-Resisting Capacity Curve of RC Beam-Column Substructures. *Journal of performance constructed facilities*. 2014; 28(4): 04014008
37. Qian K, Li B, Ma J-X.. Load-carrying mechanism to resist progressive collapse of RC buildings. *ASCE Journal of Structural Engineering*. 2014; 04014107
38. Baker, J.W., Schubert, M., Faber, M.H.. On the assessment of robustness. *Structural Safety*. 2008 ; 30(3): 253-267.

39. Frangopol, D.M., Curley, J.P.. Effects of damage and redundancy on structural reliability. *Journal of Structural Engineering*. 1987 ; 113: 1533-1549.
40. Parisi, F., Augenti, N.. Influence of seismic design criteria on blast resistance of RC framed buildings: A case study. *Engineering Structures*. 2012; 44: 78-93.
41. Starossek U., Haberland M.. Approaches to measures of structural robustness. *Structure & Infrastructure Engineering*. 2011; 7:625–31.
42. Bozza, A., Asprone, D., Manfredi, G.. Developing an integrated framework to quantify resilience of urban systems against disasters. *Natural Hazards*. 2012; 78: 1729–1748.
43. Bruneau, M., Chang, S., Eguchi, R., Lee, G., O'Rourke, T., Reinhorn, A., Shinozuka, M., Tierney, K., Wallace, W., von Winterfeldt, D.. A framework to quantitatively assess and enhance seismic resilience of communities. *Earthquake Spectra*. 2003; 19: 733–752.
44. Chang, S.E., Shinozuka, M.. Measuring improvements in the disaster resilience of communities. *Earthquake Spectra*. 2004; 20: 739–755.
45. Cimellaro, G.P., Reinhorn, A.M., Bruneau, M.. Framework for analytical quantification of disaster resilience. *Engineering Structure*. 2010; 32(11): 3639–3649.
46. Ouyang, M., Dueñas-Osorio, L.. Multi-dimensional hurricane resilience assessment of electric power systems. *Structural Safety*. 201; 48: 15–24.
47. Cardona, O.D., Ordaz, M.G., Marulanda, M.C., Barbat, A.H.. Estimation of probabilistic seismic losses and the public economic resilience—an approach for a macroeconomic impact evaluation. *Journal Earthquake Engineering*. 2008; 12: 60–70.
48. Gotangco, C.K., See, J., Dalupang, J.P., Ortiz, M., Porio, E., Narisma, G., Dator-Bercilla, J.. Quantifying resilience to flooding among households and local government units using system dynamics: a case study in Metro Manila. *Journal Flood Risk Management*. 2015; 9(3): 196–207.
49. Kimhi, S., Shamai, M.. Community resilience and the impact of stress: adult response to Israel's withdrawal from Lebanon. *Journal of Community Psychology*. 2004; 32: 439–451.
50. Miles, S.B.. Foundations of community disaster resilience: well-being, identity, services, and capitals. *Environmental Hazards*. 2015; 14(2): 103–121.
51. Rose, A.. Defining and measuring economic resilience to disasters. *Disaster Prevention and Management*. 2004; 13: 307–314.
52. Zeng, X., Lu, X.Z., Yang, T., Xu, Z.. Application of the FEMA-P58 methodology for regional earthquake loss prediction. *Natural Hazards*. 2016; 83(1): 177–192.
53. Federal Emergency Management Agency (FEMA), 2012a. Seismic performance assessment of buildings: 1 – Methodology (FEMA P-58-1), Washington, D.C., USA.
54. Federal Emergency Management Agency (FEMA), 2012b. Seismic performance assessment of buildings: 2 – Implementation guide (FEMA P-58-2), Washington, D.C., USA.
55. Xiong, C., Huang, J., Lu, X.Z.. Framework for city-scale building seismic resilience simulation and repair scheduling with labor constraints driven by time–history analysis. *Computer.-Aided Civil and Infrastructure Engineering*. 2019
56. Cimellaro, G.P., Renschler, C., Reinhorn, A.M., Arendt, L.. Peoples: a framework for evaluating resilience. *Journal Structural Engineering*. 2016; 142(10): 04016063.
57. Bozza, A., Asprone, D., Fabbrocino, F.. Urban resilience: a civil engineering perspective. *Sustainability* 9. 2017a; 103.
58. Burby, R.J., Deyle, R.E., Godschalk, D.R., Olshansky, R.B.. Creating hazard resilient communities through land-use planning. *Natural Hazards Review*. 2000; 1(2): 99–106.
59. Opricovic, S., Tzeng, G.. Multicriteria planning of post-earthquake sustainable reconstruction, *Computer.-Aided Civil and Infrastructure Engineering*. 2002; 17(3): 211–220.

60. Chang, S.E., Miles, S.B.. Resilient community recovery: improving recovery through comprehensive modeling. MCEER Research Progress and Accomplishments. 2003; 3: 139–148.
61. Nejat, A., Damjanovic, I.. Agent-based modeling of behavioral housing recovery following disasters. *Computer-Aided Civil and Infrastructure Engineering*. 2012; 27(10): 748–763.
62. Marjanishvili S. and Katz B.. A Performance-Based Framework for Structural Resilience to Blast-Induced Damage. 10th International Conference of the International Institute for Infrastructure Resilience and Reconstruction (I3R2). 2014. Purdue University, West Lafayette, Indiana, USA
63. Ning A. and Zheng H.. A Framework of Seismic Design Based on Structural Resilience. *Proceedings of the 2nd International Conference on Civil, Structural and Transportation Engineering (ICCSTE'16)*. 2016
64. Mebarki A. , Jerez S., Prodhomme G. & Reimeringer M.. Natural hazards, vulnerability and structural resilience: tsunamis and industrial tanks, *Geomatics, Natural Hazards and Risk*. 2016; 7:sup1: 5-17,
65. Alarco'n E., Recuero A., Perera R., Lo'pez C., Gutie'rrez J.P., De Diego A., Pico'n R., Lo'pez J.F.. A reparability index for reinforced concrete members based on fracture mechanics; *Engineering Structures* 2001; 23: 687–697.
66. Park Y, Ang A.. Mechanistic seismic damage model for reinforced concrete. *J Struct Div ASCE*. 1985; 111: 722–39.
67. Chancellor B., Eatherton M., Roke D., and Akbař T.. Self-Centering Seismic Lateral Force Resisting Systems: High Performance Structures for the City of Tomorrow. *Buildings*. 2014.
68. Grigorian M., Grigorian C.. An introduction to the structural design of rocking wall-frames with a view to collapse prevention, self-alignment and reparability. *Structural Design of Tall and Special Buildings*. 2016.
69. Grigorian M, Grigorian C.. Performance control: a new elastic–plastic design procedure for earthquake resisting moment frames. *Journal of the Structural Division; ASCE*. 2012; 6 (138): 473–483.
70. Grigorian M, Grigorian C.. Recent developments in plastic design analysis of steel moment frames. *Journal of Constructional Steel Research*. 2012; 76: 83–92
71. CEN. EN 1992-1-1Eurocode 2: Design of concrete structuresPart 1.1: General rules and rules for buildings. Brussels, Belgium: Comité Européen de Normalisation, 2004.
72. Parisi F, Augenti N. Influence of seismic design criteria on blast resistance of RC framed buildings: A case study. *Engineering Structures*. 2012; 44: 78–93.
73. Seissoft. SeismoStruct — A computer program for static and dynamic nonlinear analysis of framed structures. 2019.
74. Kunnath SK, Bao Y, El-Tawil S. Advances in computational simulation of gravity-induced disproportionate collapse of RC frame buildings. *Journal of Structural Engineering*. 2018; 144:03117003.
75. Correia AA, Virtuoso FBE. Nonlinear Analysis of Space Frames. In: Mota Soares CA, Martins JAC, Rodrigues HC, Ambrósio JAC, Pina CAB, Mota Soares CM, Pereira EBR, Folgado J (eds.). *Proceedings of the Third European Conference on Computational Mechanics — Solids, Structures and Coupled Problems in Engineering*, Lisbon, Portugal; 2006.
76. Mander JB, Priestley MJN, Park R. Theoretical stress–strain model for confined concrete. *J Struct Eng*. 1988;114:1804–1826.
77. CEN. EN 1991-1-7Eurocode 1: Actions on structuresPart 1.7: General actions—Accidental actions. Brussels, Belgium: Comité Européen de Normalisation, 2006.
78. CEN. EN 1990—Eurocode 0: Basis of structural design. Brussels, Belgium: Comité Européen de Normalisation, 2005.

79. Arshian AH, Morgenthal G, Narayanan S. Influence of modelling strategies on uncertainty propagation in the alternate path mechanism of reinforced concrete framed structures. *Engineering Structures*. 2016; 110: 36–47.
80. Sasani M. Response of a reinforced concrete infilled-frame structure to removal of two adjacent columns. *Engineering Structures*. 2008; 30: 2478–2491.
81. Shi Y, Stewart MG. Spatial reliability analysis of explosive blast load damage to reinforced concrete columns. *Structural Safety*. 2015; 53:13–25.
82. Galasso C, Maddaloni G, Cosenza E. Uncertainty analysis of flexural overstrength for capacity design of RC beams. *Journal of Structural Engineering*. 2014; 140:04014037.
83. Priestley MJN, Seible F, Calvi GM. *Seismic design and retrofit of bridges*. New York: John Wiley & Sons, Inc, 1996.
84. Ellingwood BR, MacGregor JG, Galambos TV, Cornell CA. Probability based load criteria: Loads factor and load combination. *Journal of the Structural Division*. 1982; 108:978–997.
85. Borzi B, Pinho R, Crowley H. Simplified pushover-based vulnerability analysis for large-scale assessment of RC buildings. *Engineering Structures*. 2008; 30: 804–820.
86. Yu X.H., Lu D.G., Qian K., Li B.. Uncertainty and sensitivity analysis of reinforced concrete frame structures subjected to column loss. *Journal of Performance of Constructed Facilities*. 2017; 31: 04016069.
87. Parisi F, Adam JM, Sagaseta J, Lu X. Review of experimental research on progressive collapse of RC structures. In: Augenti N, Jurina L, editors. *Ingegneria Forense, Crolli, Affidabilità Strutturale e Consolidamento—Atti del Convegno IF CRASC '17*; Palermo, Italy: Flaccovio Editore. 2017: 265–276.
88. Tsai MH, Lin BH. Investigation of progressive collapse resistance and inelastic response for an earthquake-resistant RC building subjected to column failure. *Engineering Structures*. 2008; 30: 3619–3628.
89. Shan S, Li S, Xu S, Xie L. Experimental study on the progressive collapse performance of RC frames with infill walls. *Engineering Structures*. 2016; 111:80–92.
90. Yi WJ, He QF, Xiao Y, Kunnath SK. Experimental study on progressive collapse-resistant behavior of reinforced concrete frame structures. *ACI Structural Journal*. 2008; 105:433–439.
91. Porter KA, Beck JL, Shaikhutdinov RV. Sensitivity of building loss estimates to major uncertain variables. *Earthquake Spectra*. 2002; 18: 719–743.
92. Kim J, Park JH, Lee TH. Sensitivity analysis of steel buildings subjected to column loss. *Engineering Structure*. 2011; 33: 421–432.
93. Ellingwood B.. Design and construction error effects on structural reliability, *J. Struct. Eng.* 1987; 113 (2): 409–422.
94. Eldukair Z.A., Ayyub B.M.. Analysis of recent US structural and construction failures, *J. Perform. Constr. Facil.*. 1991; 5: 57–73.
95. Priemus H., Ale B.. Construction safety: An analysis of systems failure. The case of the multifunctional Bos & Lommerplein estate, Amsterdam, *Saf. Sci* 48. 2010; 111–122.
96. Kim J., Shin W.S.. Retrofit of RC frames against progressive collapse using prestressing tendons, *Struct. Design Tall Spec. Build.* 2013; 22: 349–361.
97. Adaros M.S., Smilowitz R.. Challenges and considerations for the retrofit of existing structures for progressive collapse, *J. Perform. Constr. Facil.*. 2015; 29 (5) B4014001.
98. Royal Decree 16.11.1939, n. 2229, Norme per la esecuzione delle opere in conglomerato cementizio semplice ed armato, G.U. n. 92 issued on 18 April 1940 [in Italian].
99. G.M. Verderame, P. Ricci, M. Esposito, F.P. Sansiviero, Le caratteristiche meccaniche degli acciai impiegati nelle strutture in c.a. realizzate dal 1950 al 1980. *Proceedings of XXVI Convegno Nazionale AICAP “Le prospettive di sviluppo delle opere in calcestruzzo strutturale nel terzo millennio”*, Padova, 2011; no. 54 [in Italian].
100. L. Santarella, *Prontuario del cemento armato*, HOEPLI, Milano, 1968 [in Italian].

101. Spacone E., Filippou F. C. and Taucer, F. F.. Fibre beam–column model for non-linear analysis of R/C frames. I: Formulation. *Earthquake Engineering and Structural Dynamics*. 1996a; 25(7): 711–725.
102. Spacone E., Filippou F.C., Taucer F.F.. Fibre beam-column model for non-linear analysis of R/C frames: part II. *Appl Earthquake Engineering and Structural Dynamics*. 1996b; 25(7):727–742.
103. Li S., Zuo Z., Zhai C. et al.. Comparison of static pushover and dynamic analyses using RC building shaking table experiment. *Eng Struct*. 2017; 136:430–440.
104. Mulas M.G., Martinelli P.. Numerical simulation of the partial seismic collapse of a 1960s RC building. *J Perform Constr Facil*.. 2017; 31(6):04017111.
105. Augenti N. Il crollo dell’edificio in Napoli al Rione Arenella. *Proceedings of the III Convegno “Crolli e affidabilità delle strutture civili”*, 2003 [in Italian].
106. Parisi F, Scalvenzi M, Brunesi E. Performance limit states for progressive collapse analysis of reinforced concrete framed buildings. *Structural Concrete* 2019; 20: 68–84
107. Parisi F, Scalvenzi M. Progressive collapse assessment of gravity-load designed European RC buildings under multi-column loss scenarios. *Engineering Structures*. 2020; 209: 110001.
108. Monti G, Nuti C, Santini S. CYRUS – Cyclic response of upgraded sections. 96-2, University of Chieti, Italy; 1996.
109. Masi A, Digrisolo A, Santarsiero G. Concrete strength variability in Italian RC buildings: Analysis of a large database of core tests. *Applied Mechanics and Materials*. 2014; 597: 283–290.
110. McKenna F, Fenves GL, Scott MH. OpenSees — Open system for earthquake engineering simulation. Berkeley: Pacific Earthquake Engineering Research (PEER) Center, University of California Berkeley; 2004.
111. Hellesland J., Scordelis A.. Analysis of RC bridge columns under imposed deformations. *IABSE Colloquium*, Delft. 1981: 545-559.
112. Mari A., Scordelis A.. Nonlinear geometric material and time dependent analysis of three dimensional reinforced and prestressed concrete frames. *SESM Report 82-12*, Department of Civil Engineering, University of California, Berkeley. 1984
113. Scott BD, Park R, Priestley MJN. Stress–strain behavior of concrete confined by overlapping hoops at low and high strain rates. *ACI Journal*. 1982; 79(1): 13–27.
114. Biskinis DE, Roupakias GK, Fardis MN. Degradation of shear strength of reinforced concrete members with inelastic cyclic displacement. *ACI Struct Journal*. 2004; 101(6): 773–783.
115. CEN. EN 1998-1:2004: Eurocode 8 – Design of structures for earthquake resistance. Part 1: General rules, seismic actions and rules for buildings. Brussels: Comité Européen de Normalisation; 2004.
116. CNR. CNR-DT 200R1/2013: Guide for the design and construction of externally bonded FRP systems for strengthening existing structures. Rome: National Research Council of Italy; 2013.
117. Belleri, A., Brunesi, E., Nascimbene, R., Pagani, M., & Riva, P.. Seismic performance of precast industrial facilities following major earthquakes in the Italian territory. *Journal of Performance of Constructed Facilities*. 2015; 29(5): 1–10.
118. Clementi, F., Scalbi, A., & Lenci, S.. Seismic performance of precast reinforced concrete buildings with dowel pin connections. *Journal of Building Engineering*. 2016; 7, 224–238.
119. *Fib Bulletin* 63. (2012). Design of precast concrete structures against accidental actions.
120. *Fib Bulletin* 43. (2008). Structural connections for precast concrete buildings.

121. Ravasini S., Belletti B., Brunesi E., Nascimbene R., & Parisi F.. Nonlinear Dynamic Response of a Precast Concrete Building to Sudden Column Removal. *Applied Sciences*. 2021; 11(2): 1–22.
122. Brunesi E., Peloso S., Pinho R., & Nascimbene R.. Friction characterization testing of fabric felt material used in precast structures. *Structural Concrete*; 2020: 21(2), 735–746.
123. Magliulo G., Fabbrocino G. & Manfredi, G.. Seismic assessment of existing precast industrial buildings using static and dynamic nonlinear analyses. *Engineering Structures*. 2008; 30(9): 2580–2588
124. Belleri A. & Riva P.. Seismic performance and retrofit of precast concrete grouted sleeve connections. *PCI Journal*. 2012; 57(1): 97–109.
125. Bolognini D., Borzi B. & Pinho R.. 2008. Simplified pushover-based vulnerability analysis of traditional Italian RC precast structures. *The 14 Th World Conference on Earthquake Engineering*.
126. Casotto C., Silva V., Crowley H., Nascimbene R. & Pinho R.. Seismic fragility of Italian RC precast industrial structures. *Engineering Structures*. 2015; 94: 122–136.
127. Ercolino M., Bellotti D., Magliulo G. & Nascimbene R.. Vulnerability analysis of industrial RC precast buildings designed according to modern, seismic codes. *Engineering Structures*. 2018; 158: 67–78.
128. Galasso C., Maddaloni G., & Cosenza E.. Uncertainly Analysis of Flexural Overstrength for Capacity Design of RC Beams. *Journal of Structural Engineering*. 2014; 140(7): 04014037.
129. Psycharis I. N. & Mouzakis H. P.. Shear resistance of pinned connections of precast members to monotonic and cyclic loading. *Engineering Structures*. 2012; 41: 413–427.
130. Belletti B., Franceschini L. & Ravasini, S.. Tie force method for reinforced concrete structures. *Proceedings of the International Fib Symposium on Conceptual Design of Structures*. 2019; 1(1): 57–64.
131. Lim N. S., Tan K. H. & Lee C. K... Effects of rotational capacity and horizontal restraint on development of catenary action in 2-D RC frames. *Engineering Structures*. 2017a; 153: 613–627
132. Lim N. S., Tan K. H. & Lee C. K.. Experimental studies of 3D RC substructures under exterior and corner column removal scenarios. *Engineering Structures*. 2017b; 150: 409–427.
133. Lew H. S., Bao Y., Pujol S. & Sozen M. A.. Experimental study of reinforced concrete assemblies under column removal scenario. *ACI Structural Journal*. 2014; 111(4): 881–892.
134. Yu J. & Tan K. H.. Special detailing techniques to improve structural resistance against progressive collapse. *Journal of Structural Engineering*. 2014; 140(3): 1–15.
135. Li Y., Lu X., Guan H. & Ye L.. An improved tie force method for progressive collapse resistance design of reinforced concrete frame structures. *Engineering Structures*. 2011; 33(10): 2931–2942.
136. Nav F. M., Usefi N. & Abbasnia R.. Analytical investigation of reinforced concrete frames under middle column removal scenario. *Advances in Structural Engineering*. 2018; 21(9): 1388–1401.
137. Mucedero G., Brunesi E. & Parisi F.. Nonlinear material modelling for fibre-based progressive collapse analysis of RC framed buildings. *Engineering Failure Analysis*. 2020; 118:104901
138. El Debs M. K., Miotto A. M. & El Debs A. L. H. C.. Analysis of a semi-rigid connection for precast concrete. *Proceedings of the Institution of Civil Engineers: Structures and Buildings*. 2010; 163(1): 41–51.
139. Elliott K. S., Davies G., Ferreira M., Gorgun H., & Mahdi A. A.. Can precast concrete structures be designed as semi-rigid frames? Part 2 - Analytical equations & column effective length factors. In *Structural Engineer* . 2003; 81: 28–37.

140. Rodríguez D., Brunesi E. & Nascimbene R.. Fragility and sensitivity analysis of steel frames with bolted-angle connections under progressive collapse. *Engineering Structures*. 2021; 228: 111508.
141. Eren N., Brunesi E. & Nascimbene R.. Influence of masonry infills on the progressive collapse resistance of reinforced concrete framed buildings. *Engineering Structures*. 2019; 178: 375–394.
142. Perrone D., Brunesi E., Filiatrault A. & Nascimbene R.. Probabilistic estimation of floor response spectra in masonry infilled reinforced concrete building portfolio. *Engineering Structures*. 2020; 202: 109842